NASA TECHNICAL NOTE

NASA TN D-2380

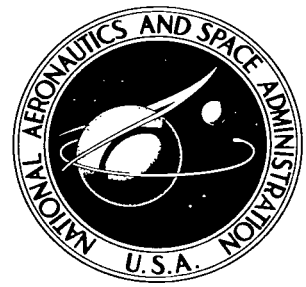

NASA TN D-2380

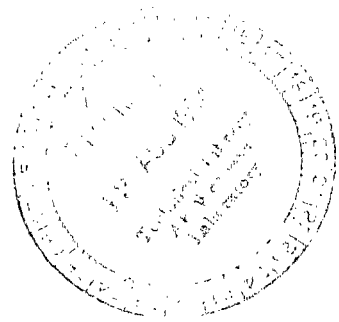

INTERFERENCE EFFECTS OF SINGLE AND MULTIPLE ROUND OR SLOTTED JETS ON A VTOL MODEL IN TRANSITION

by Raymond D. Vogler

Langley Research Center
Langley Station, Hampton, Va.

NATIONAL AERONAUTICS AND SPACE ADMINISTRATION • WASHINGTON, D. C. • AUGUST 1964

INTERFERENCE EFFECTS OF SINGLE AND MULTIPLE ROUND OR SLOTTED JETS ON A VTOL MODEL IN TRANSITION

By Raymond D. Vogler

Langley Research Center
Langley Station, Hampton, Va.

NATIONAL AERONAUTICS AND SPACE ADMINISTRATION

For sale by the Office of Technical Services, Department of Commerce,
Washington, D.C. 20230 -- Price $2.00

INTERFERENCE EFFECTS OF SINGLE AND MULTIPLE ROUND OR SLOTTED JETS ON A VTOL MODEL IN TRANSITION

By Raymond D. Vogler
Langley Research Center

SUMMARY

An investigation at low forward velocities was made to determine some of the interference effects between lifting jets, free-stream velocity, and model surfaces on the longitudinal aerodynamic characteristics of a VTOL model. This model was equipped with various interchangeable arrangements of single and of multiple round or slotted jets, with and without jet deflection. The longitudinal characteristics in ground effect at zero forward velocity were also obtained.

All arrangements showed interference losses that generally increased with velocity ratio (ratio of free-stream velocity to jet velocity), and most arrangements showed nose-up pitching moments that increased with velocity ratio. For the model operating in ground effect, all arrangements showed a loss in lift at some distance closer to the ground than about 7 effective jet diameters. Among the configurations that showed less interference out of ground effect and while hovering in ground effect than the others were the single-jet arrangements with central longitudinal slots and the multiple-jet arrangement with the four-jet diamond pattern.

INTRODUCTION

Considerable research is being done toward the development of vertical take-off and landing (VTOL) airplanes to be used in areas where conventional landing facilities are not available. Jet-supported VTOL configurations are of obvious interest for missions requiring high subsonic or supersonic cruise performance. The lift losses when hovering in ground effect and the jet-induced lift losses and nose-up pitching moments in transition have been the subject of previous investigations (e.g., refs. 1 to 5). Most of these investigations have been restricted to single-jet configurations, even though many proposed VTOL designs use several lift engines or a vectored-thrust engine with several exits. The arrangement of multiple engines has, of course, important effects on the balance, stability and control of the airplane. References 1 and 3 indicate that the arrangement may also have important effects on the forces and moments due to the interference effects.

The purpose of this investigation was to determine the lift and pitching-moment characteristics of a model at transition speeds and hovering near the ground with single jets and various arrangements of multiple jets simulating lift-engine exits in the fuselage. The inlets were not simulated in this investigation and any effects from them on the total force and moment data are not included.

SYMBOLS

The force and moment data are presented about the stability axes and positive directions are indicated in figure 1.

C_D	drag coefficient, $\frac{\text{Drag}}{qS}$
C_L	lift coefficient, $\frac{\text{Lift}}{qS}$
C_m	pitching-moment coefficient, $\frac{\text{Pitching moment}}{qS\bar{c}}$
$\bar{c}$	mean aerodynamic chord, ft
D	drag, including jet force, lb
ΔD	increment in drag due to interference, lb
d_e	effective diameter, diameter of circle equivalent in area to total jet exit area of a given configuration, in.
h	height above ground board measured from lower surface of fuselage, in.
L	lift, including jet force, lb
ΔL	increment in lift due to interference, lb
M	pitching moment, including jet moment, ft-lb
$(M)_{\delta_j, T}$	jet pitching moment for a given jet deflection and given jet thrust at zero tunnel velocity
ΔM	increment in pitching moment due to interference, ft-lb
q	free-stream dynamic pressure, lb/sq ft
S	wing area, 1.67 sq ft
T	resultant measured jet thrust, $\sqrt{L^2 + D^2}$ when $q = 0$, lb

V_j jet velocity, based on isentropic expansion from jet-exit total pressure to atmospheric pressure, fps

V_∞ free-stream velocity, fps

α wing or fuselage angle of attack, deg

δ_j jet deflection angle, positive when measured from vertical axis rearward, $\tan^{-1} D/L$ when $\alpha = 0$ and $q = 0$, deg

MODEL AND APPARATUS

A three-view drawing of the model is shown in figure 1 and a photograph is presented as figure 2. The wing was made of 1/8-inch-thick aluminum plate with rounded leading and trailing edges. When mounted in the high position, the wing was flush with the top flat surface of the fuselage. In the low position, the wing was 1/4 inch above the bottom surface of the fuselage. The nose was of wood and the rear section, of sheet metal. The central section of the fuselage was a steel box with a removable bottom. A more detailed drawing of the steel box and the tubing which supplies the highly pressurized air during testing is shown in figure 3. A separate circular chamber half embedded in the top of the box contained a six-component strain-gage balance on the end of the mounting sting which projected from the floor of the 17-foot test section of the Langley 300-MPH 7- by 10-foot tunnel.

Air entered the model through 1-inch-diameter tubing to a manifold and through two 3/4-inch-diameter tubes from the manifold into the pressure chamber. The tubing from the model to the point where the 1-inch tubing was firmly anchored to the sting (fig. 3) was shielded from the free stream. Experience has shown that the solution to the problem of getting air into the model through piping without reducing data accuracy becomes less difficult when thin-wall metallic tubing is used rather than when the more flexible nonmetallic tubing is used. When the metallic tubing is firmly anchored several feet from the model, the restraints on the balance are small and may be included in the balance constants. The tubing inside the model had many small holes which distributed the air in the upper section of the chamber. The chamber was divided by a perforated plate and screen wire to give a more uniform distribution of the air in the lower part of the chamber. Jet velocities were determined by a single total-pressure probe inserted at the center of the small round jets and at two or three positions in the slotted and large round jets.

The bottom of the pressure chamber containing the nozzles was removable. The ten different nozzle configurations are shown in figure 4. Two sets of inlet fairings, one with jet deflection vanes, and one without, were made for each configuration. (See fig. 4(b).) The fairings were made of wood covered with a glass fabric. The vanes were cut from $1\frac{1}{2}$-inch-diameter brass tubing and the inlet and exit edges shaped as shown in figure 4(b). Nozzles close to each other or near the chamber wall had a part of the fairing removed in order to fit to the wall or adjacent fairing.

TEST CONDITIONS AND ACCURACY

Tests in the tunnel were for an angle-of-attack range from -5° to 25°. All ground-board tests were at zero angle of attack. Tunnel free-stream velocities were usually 30, 60, and 100 fps and jet velocities were about 400 and 600 fps. The ratios of the free-stream velocity to the jet velocity were 0.05, 0.10, 0.17, and 0.25. The main air line had a pressure of 1500 lb/sq in. A control valve between this supply line and the model allowed the pressure to be set in the pressure chamber or jet exit to produce the desired jet velocity with zero tunnel velocity. The corresponding pressures in the manifold were noted so that the jet pressure could be duplicated with the tunnel in operation. With the tunnel operating at the highest test dynamic pressure (12 lb/sq ft) the reduced static pressure in the tunnel would give a larger ratio of total pressure to free-stream-static pressure and hence a greater jet velocity for a given manifold pressure than was obtained at zero tunnel velocity. This increase in jet velocity would be less than 2 percent for the highest tunnel velocity. No correction to the velocity ratio V_{∞}/V_j was made for the increment in velocity caused by reduced static pressure.

The attempt to get uniform velocity through the multiple nozzles by perforating the air tubes and the divider plate in the model was not entirely successful. Usually, higher velocities flowed through the more rearward nozzles than through the forward nozzles. The maximum velocity variation among nozzles of a given configuration was 5 or 6 percent for the round nozzles, less for the opposite ends of the slotted nozzles. The velocity through the largest single round nozzle varied laterally, and was about 15 percent higher on one side than on the other. The nozzle was so large that only the lower jet velocity (400 fps) could be attained. This variation in the velocity of individual jets of a configuration could produce a configuration average jet velocity slightly larger or smaller than the nominal velocity as determined by the pressure ratio of a single jet. Some of the variations in measured static thrust shown in the figures for configurations with the same total nozzle geometric area probably result from the nominal velocity being more or less than the average velocity of the jets. Other possible reasons for the variations in measured static thrust, such as unequal jet-induced losses and the difference between the geometric and effective nozzle area, may be inherent in the configuration.

Installation of vanes in the nozzles reduced the thrust considerably as a result of solid blockage of the vanes which comprised 17 or 18 percent of the nozzle exit area. The vanes reduced the velocity variation among nozzles for some configurations and for the largest round-nozzle configuration reduced the lateral velocity variation from 15 percent to 5 percent. The variations in static thrust of the different configurations are not very significant in the presented data since the measured forces and moments of a configuration are nondimensionalized by the measured static thrust for that particular configuration.

The apparent axes of the jets as determined from static lift and drag forces were usually not perpendicular to the bottom plate of the model but were tilted upstream from approximately 0° to 4° ($\delta_j \approx 0^{\circ}$ to -4°). However, the condition without deflection vanes is referred to as "jets undeflected." The tilt angle was usually 1° to 2° more for the 600-fps than for the 400-fps jet

velocity, probably because of the slightly higher pressure in the rear of the pressure chamber. The jet angle is indicated in the figures for the higher velocity jet. With vanes installed, the downstream deflection of the jet varied from approximately 30° to 40° for the different configurations.

Although the accuracy of the data is not considered as good as most wind-tunnel data, it is believed that the L/T ratios are accurate within ± 0.03. The effects of the Reynolds number on the magnitude of interference forces and moments are unknown at present and, consequently, have not been considered. The Reynolds number of the $3\frac{1}{2}$-inch-diameter jet was about 1.3×10^6 based on the diameter and the maximum jet velocity (600 fps) or about 0.2×10^6 based on the diameter and the maximum free-stream velocity (100 fps).

RESULTS AND DISCUSSION

The data obtained at forward velocity with the jets undeflected have been nondimensionalized by the measured static jet thrust at zero tunnel speed with the wing-off model out of ground effect. Forces and moments obtained with the jets deflected have been nondimensionalized by the measured static jet thrust with the wings in the high position. Static thrust decreased by about 1 percent when wings were added. No attempt has been made to compare the measured static thrusts of the jets issuing from the nozzles of a flat surface with the theoretical thrust from thin-wall converging nozzles with equivalent exit area. Some losses in nozzle thrust may be expected but these are not a part of the interference loss under investigation.

The jet-off aerodynamic characteristics of the model with the wing in the high and the low positions are presented in figure 5. With the jets undeflected, the jet-on data were obtained for all configurations with the wing off and with the wing in the high position (figs. 6 to 15). Data were also obtained with the wing in the low position for configurations 1, 2, and 3. The undeflected jets operating with forward velocity would represent decelerating conditions, or accelerating conditions with auxiliary thrust engines. The basic data with jets deflected are presented in figures 16 to 25. A large part of the data for deflected jets operating in forward flight is in the accelerating range of drag-thrust ratios. The thrust-drag equilibrium for the model, in which inlet-momentum drag is accounted for, would occur at drag-thrust ratios which are the negative of the velocity ratio; that is, $D/T = -V_{\infty}/V_j$. (See ref. 5.) However, inlet effects were not considered as part of this investigation and the inlet was not simulated. With upper surface inlets as on a lift-engine VTOL configuration, some induced lift would be expected which would partly offset the lift losses encountered in the present investigation. The inlet-momentum drag would cause a nose-up moment that would add to the jet-induced moments of the present study.

With the deflected or undeflected jets, the variations in the forces and moments due to changes in angle of attack and velocity ratio are caused by a combination of factors: (1) the vertical and horizontal components of the direct thrust, (2) the aerodynamic forces and moments on the wing-body combination as

would be expected from power-off data, and (3) interference increments due to the action of the jet. These increments are discussed in detail in the following section.

Interference Effects in Transition

In isolating the incremental forces and moments due to interference, it is assumed that the total forces and moments on the model may be expressed by the following equations:

$$L = T\cos(\delta_j - \alpha) + C_L qS + \Delta L \tag{1}$$

$$D = -T\sin(\delta_j - \alpha) + C_D qS + \Delta D \tag{2}$$

$$M = (M)_{\delta_j, T} + C_m qS\bar{c} + \Delta M \tag{3}$$

where the term on the left-hand side of equation (1), (2), or (3) represents the total measured lift, drag, or pitching moment, respectively. The first quantity on the right-hand side of each equation is the jet-thrust effect at static conditions or zero forward velocity, the second term is the measured aerodynamic force or moment as determined from power-off data, and the third term is the interference increment due to the action of the jet. From these equations, the following expressions representing the nondimensional interference increments are obtained:

$$\frac{\Delta L}{T} = \frac{L}{T} - \cos(\delta_j - \alpha) - \frac{C_L qS}{T}$$

$$\frac{\Delta D}{T} = \frac{D}{T} + \sin(\delta_j - \alpha) - \frac{C_D qS}{T}$$

$$\frac{\Delta M}{T\bar{c}} = \frac{M}{T\bar{c}} - \frac{(M)_{\delta_j, T}}{T\bar{c}} - \frac{C_m qS\bar{c}}{T\bar{c}}$$

The interference-increment plots presented in figures 26 and 27 indicate lift losses that generally increase with velocity ratio for all configurations. These lift losses are due to the reduced pressures on the lower surface of the wing and fuselage induced by the interaction of the free stream and the jets as reported in reference 4. The reduced pressures result from the free-stream acceleration in going around the jet and from the entrainment action of the jet itself. There are random but insignificant variations in lift loss with change in angle of attack. The undeflected multiple round jets show a greater lift loss than the slotted jets as well as an additional loss resulting from jet deflection, whereas the slotted jets (figs. 26(f), (g), and (h)) show little or no effect of deflection on the lift loss. Although the interference losses may be large, they may be partly compensated for by the wing lift in forward speed as shown in the basic data plots of figures 6 to 25.

The drag-thrust ratios presented in the basic data figures are based on the total measured drag of the model and do not include any inlet-momentum drag since the nozzle inlets were not exposed to the free stream. The interference drag increments (figs. 26 and 27) are small at zero angle of attack but the magnitude increases in the negative direction as the angle of attack or the velocity ratio increases. The drag increment is a function of the loss in lift since the reduced pressures on the plate are equivalent to a force normal to the plate, one component of which is thrust at positive angles of attack.

For most configurations, the nose-up pitching-moment increments increase with velocity ratio and for jets deflected are usually greater at the higher angles of attack than at the lower angles, but the magnitude of these differences varies with the configuration. The large nose-up pitching moments are not surprising since the flat-plate pressure investigation of reference 4 for a single jet showed a small area of positive pressures upstream of the jet and a larger area of negative pressures on the plate downstream. Of all configurations tested, the two single-jet configurations with a central longitudinal slot (figs. 26(f) and (g)) and the multiple-jet configurations with the four-jet diamond pattern (fig. 26(b)) show the least effect of interference on the pitching moments. The reduced effect shown by the slotted jets probably results from their more streamlined shape in cross section and the smaller plate area directly behind the jet. The vertical position of the wing is seen to have little, if any, effect on the interference increments.

Hovering in Ground Effect

The longitudinal characteristics of the ten model configurations hovering in ground effect at zero forward speed are shown in figure 28. The jets were operating at the higher of the two thrusts for which out-of-ground-effect data were obtained for each configuration. The lift and pitching-moment data of each configuration have been nondimensionalized by the out-of-ground-effect thrust of the particular configuration. Except for the smallest single round jet configuration (fig. 28(i)), little or no ground effect is indicated for distances greater than 7 effective jet diameters. Near the ground, all jet arrangements show a lift loss ($L/T < 1.0$) except the arrangement with the jet exit consisting of two narrow slots (fig. 28(h)). The gain in lift very near the ground, indicated by this arrangement, is typical of that shown by the perimeter jets in reference 1. Farther from the ground there is a small (3 percent) loss, which is much less, however, than the maximum loss of any other arrangement.

For all arrangements, the lift loss is accompanied by a nose-up pitching moment. Lowering the wing increases the lift loss and the nose-up pitching moment, with the magnitude varying for the different configurations. Three of the better configurations are the two-jet narrow-slot arrangement (fig. 28(h)), the long-central-slot arrangement (fig. 28(g)), and the four-jet diamond-pattern arrangement (fig. 28(b)). The long-central-slot and diamond-pattern arrangements were also two of the better arrangements operating in forward speeds out of ground effect.

SUMMARY OF RESULTS

An investigation at low forward velocities was made to determine some of the interference effects between lifting jets, free-stream velocity, and model surfaces on the longitudinal characteristics of a VTOL model. The model was equipped with various interchangeable arrangements of single and of multiple round or slotted jets, with and without jet deflection. The longitudinal characteristics in ground effect at zero forward velocity were also obtained. Some of the results as indicated by the data are

Out of ground effect: All configurations showed interference lift losses that generally increased with the ratio of free-stream velocity to jet velocity. For most jet arrangements, nose-up pitching moments due to interference occurred and increased with the velocity ratio. The three configurations that suffered the least interference effect on the lift and pitching moment were the two single-jet arrangements with central longitudinal slots and the multiple-jet arrangement with the four-jet diamond pattern.

Hovering in ground effect: All arrangements showed a loss in lift at some distance closer to the ground than about 7 effective nozzle diameters. The arrangement with jets issuing from narrow longitudinal slots on each side of the fuselage gave the least maximum loss and was the only arrangement to show a lift-thrust ratio greater than 1.0. The single-central-longitudinal-slot arrangements also showed better lift characteristics than the multiple-round-jet arrangements. These two single-slot configurations also gave much smaller nose-up pitching moments within ground effect than the other arrangements.

Langley Research Center,
National Aeronautics and Space Administration,
Langley Station, Hampton, Va., May 7, 1964.

REFERENCES

1. Vogler, Raymond D.: Effects of Various Arrangements of Slotted and Round Jet Exits on the Lift and Pitching-Moment Characteristics of a Rectangular-Base Model at Zero Forward Speed. NASA TN D-660, 1961.

2. Spreemann, Kenneth P., and Sherman, Irving R.: Effects of Ground Proximity on the Thrust of a Simple Downward-Directed Jet Beneath a Flat Surface. NACA TN 4407, 1958.

3. Otis, James H., Jr.: Induced Interference Effects on a Four-Jet VTOL Configuration With Various Wing Planforms in the Transition Speed Range. NASA TN D-1400, 1962.

4. Vogler, Raymond D.: Surface Pressure Distributions Induced on a Flat Plate by a Cold Air Jet Issuing Perpendicularly from the Plate and Normal to a Low-Speed Free-Stream Flow. NASA TN D-1629, 1963.

5. Spreemann, Kenneth P.: Investigation of Interference of a Deflected Jet With Free Stream and Ground on Aerodynamic Characteristics of a Semispan Delta-Wing VTOL Model. NASA TN D-915, 1961.

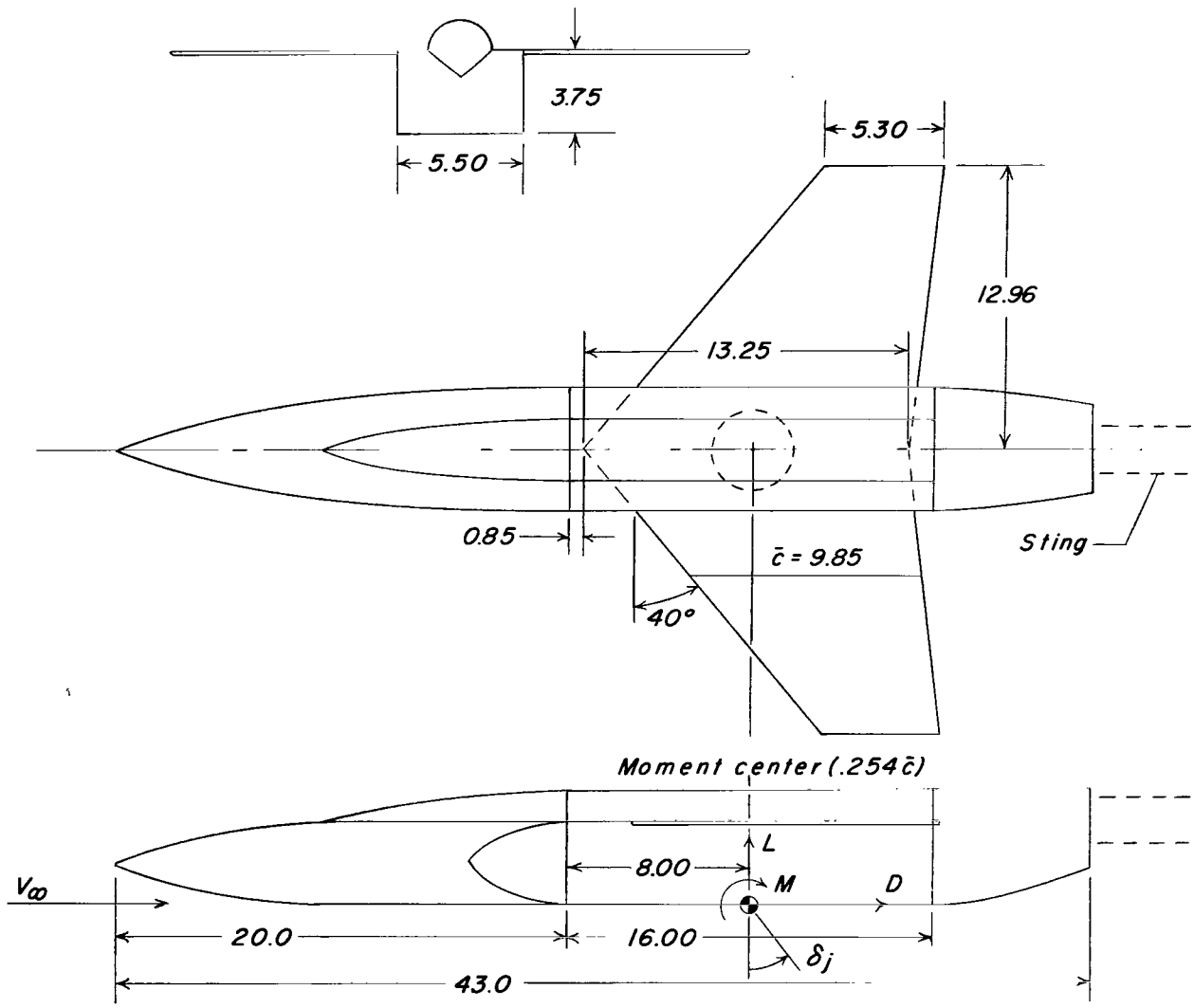

Figure 1.- Three-view drawing of model showing positive direction of forces, moments, and jet deflection angle. Dimensions in inches.

L-62-8680

Figure 2.- Photograph of model showing smallest round jet nozzle (configuration 9).

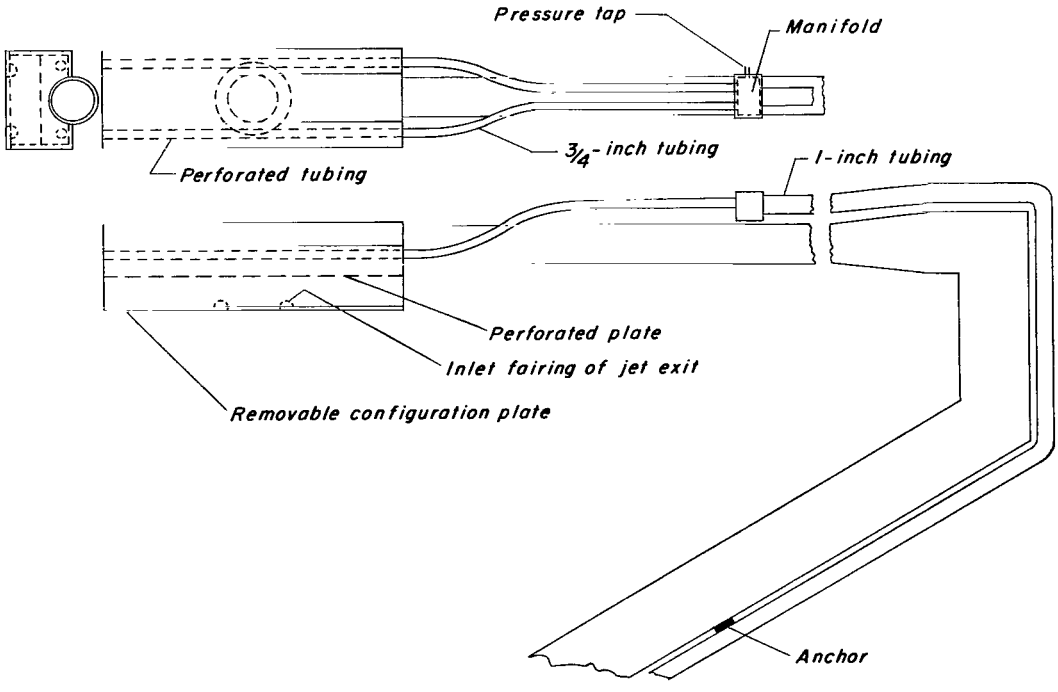

Figure 3.- Sketch showing sting and tubing for getting air to jet nozzles with shield over air line removed.

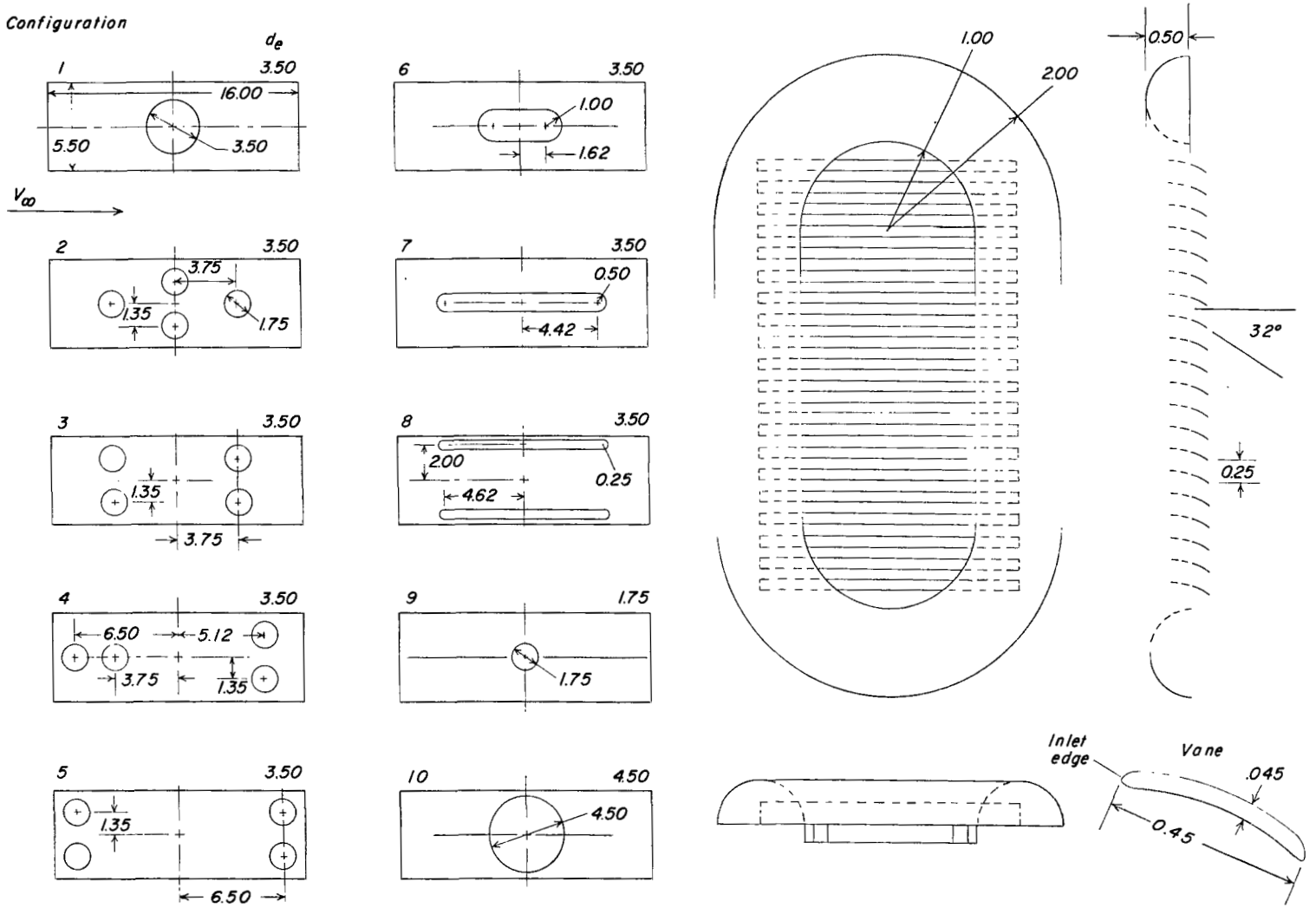

(a) Removable plates for configurations.

(b) Typical inlet fairing of jet nozzle and details of vanes for deflecting the jet.

Figure 4.- Details of nozzle geometry. Dimensions in inches.

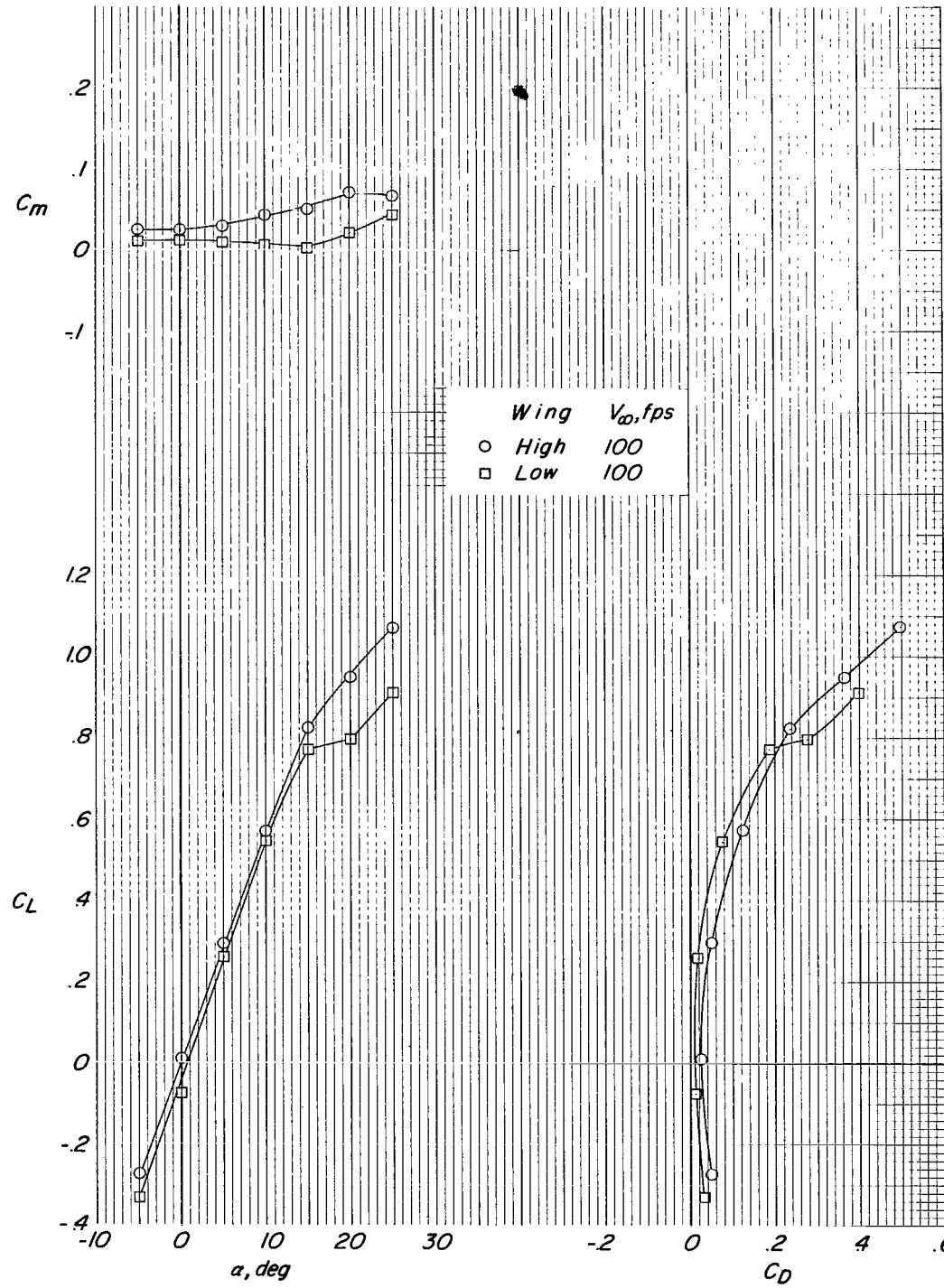

Figure 5.- Jet-off aerodynamic characteristics of the model.

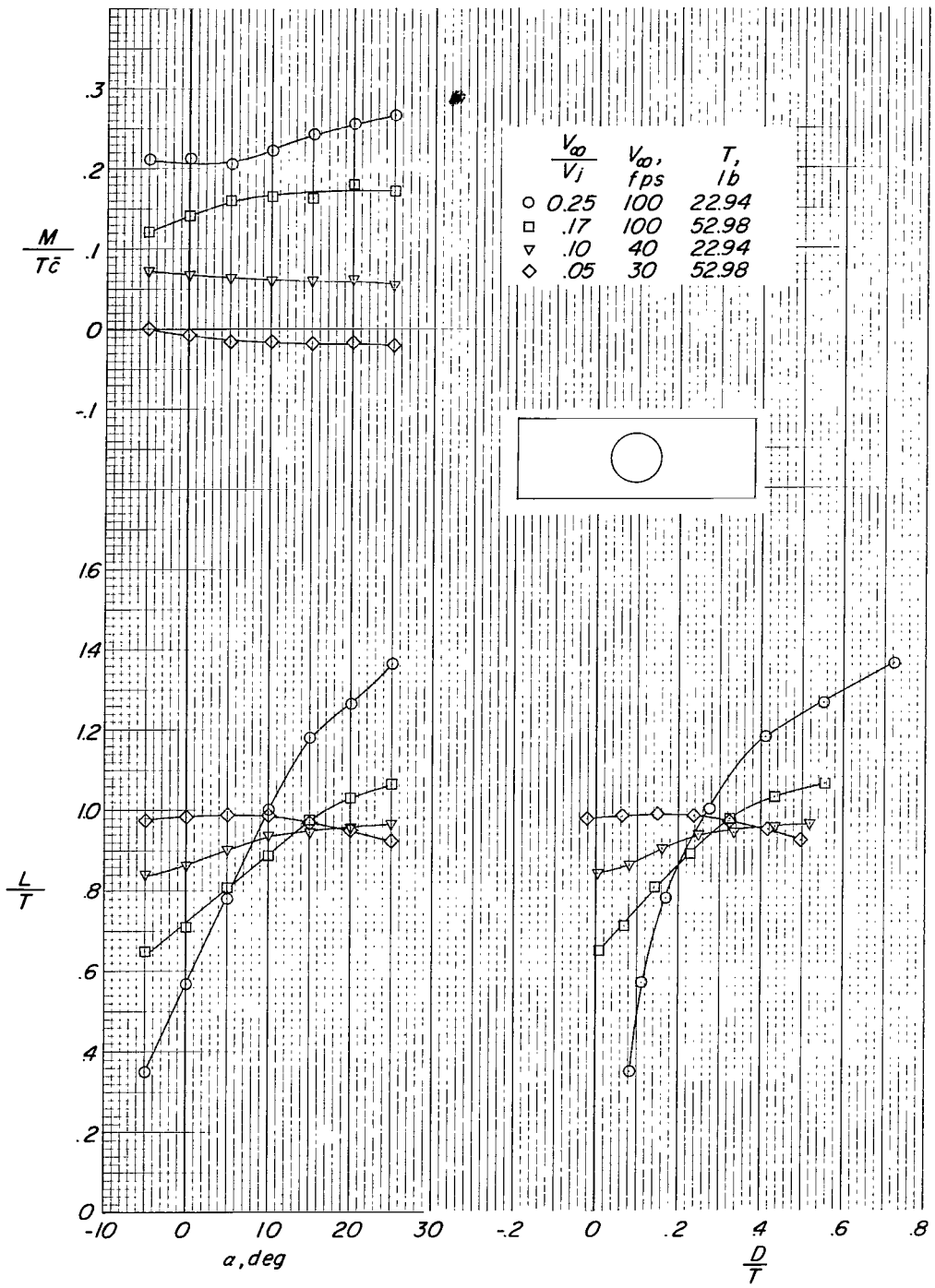

(a) Wing in high position.

Figure 6.- Jet-on aerodynamic characteristics of configuration 1. $\delta_j \approx -4^\circ$.

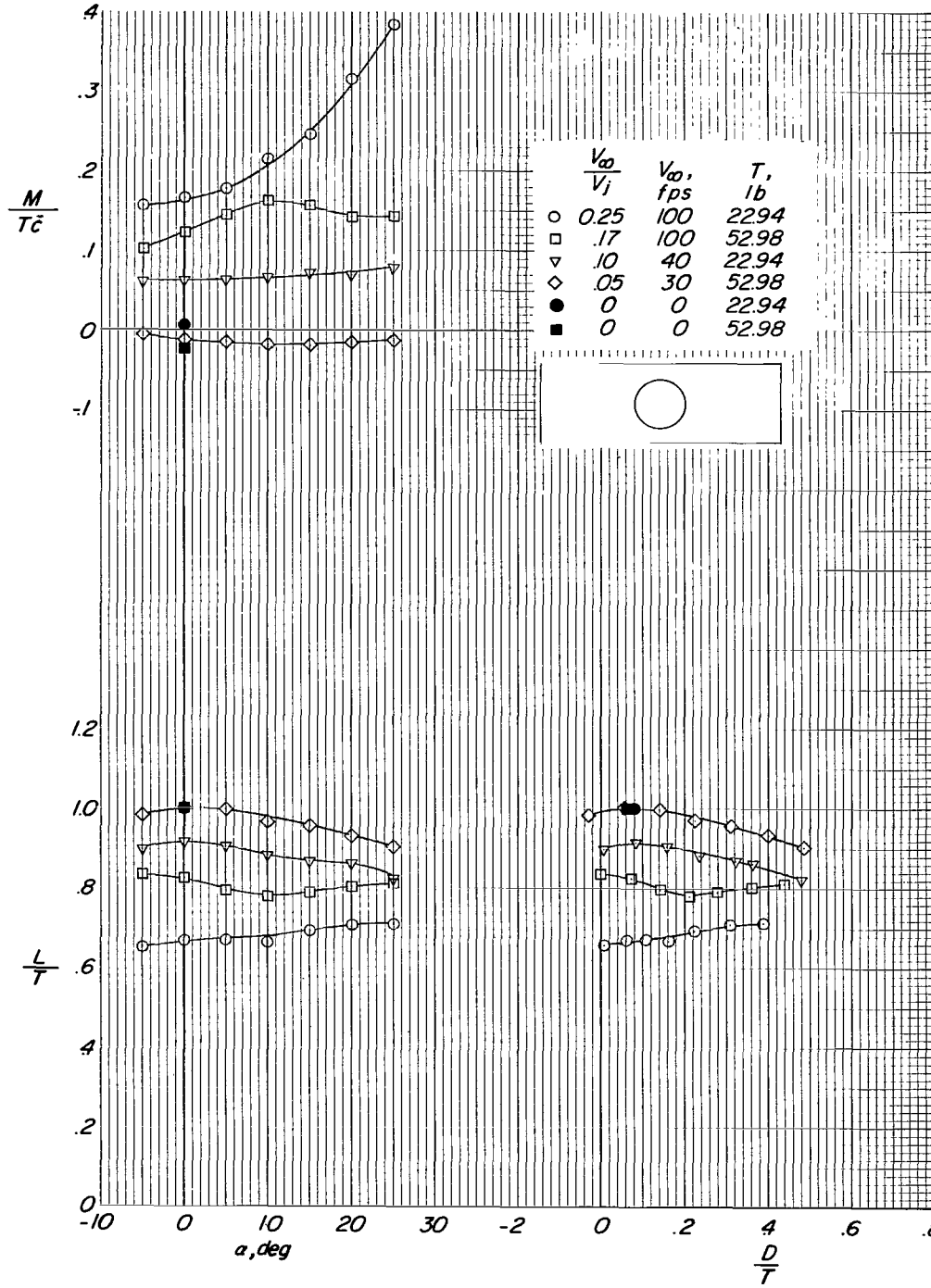

(b) Wing off.

Figure 6.- Continued.

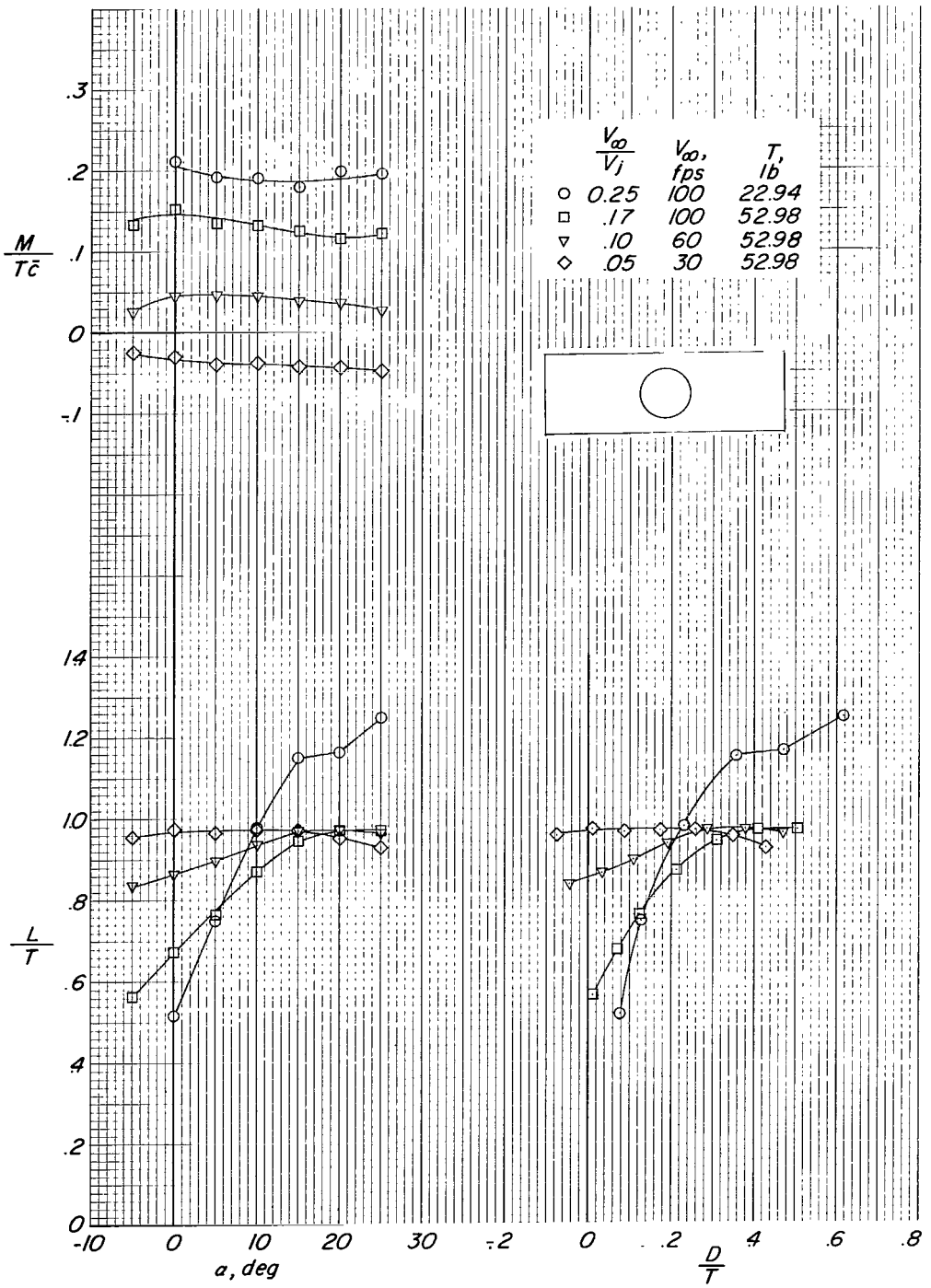

(c) Wing in low position.

Figure 6.- Concluded.

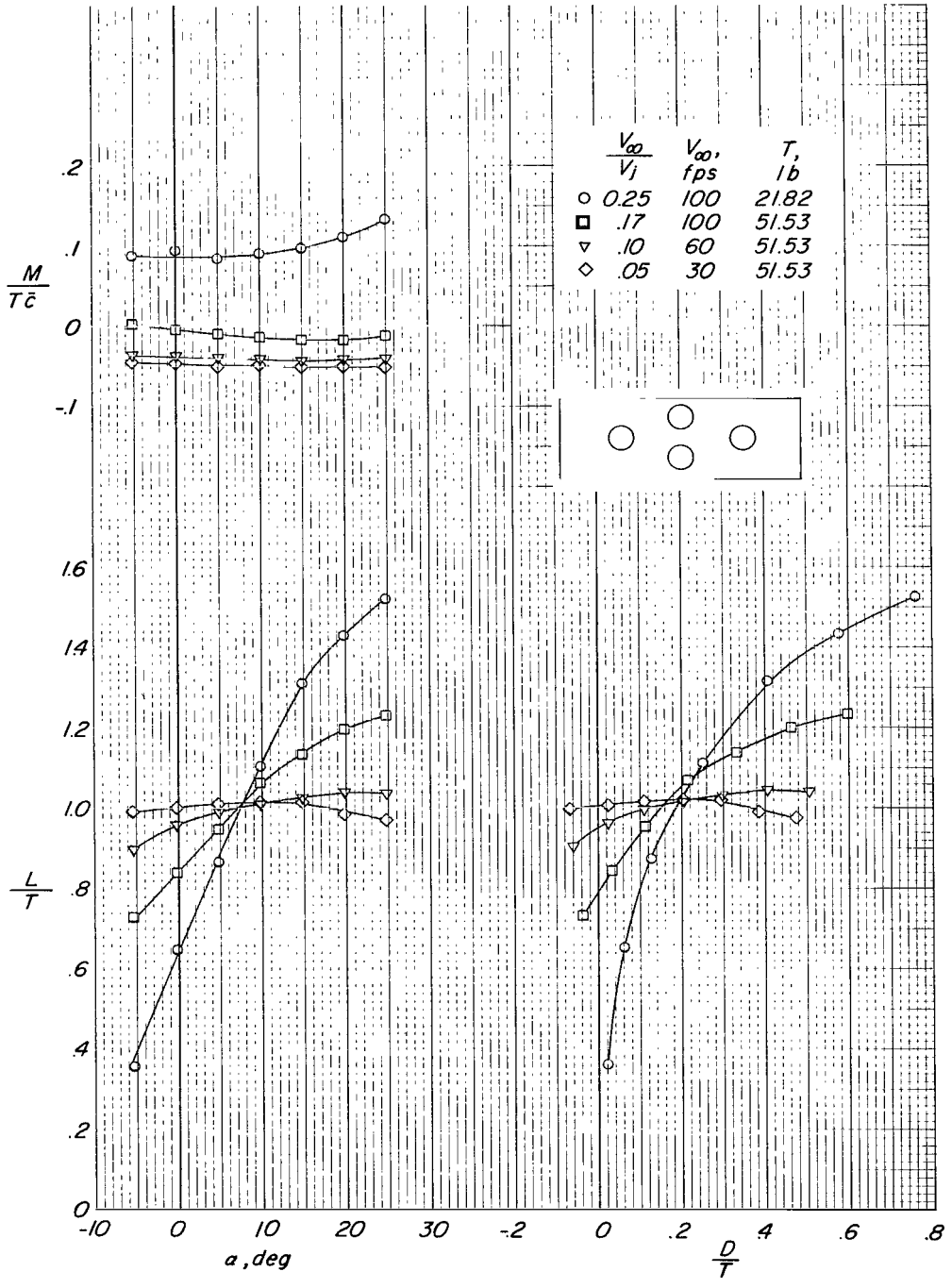

(a) Wing in high position.

Figure 7.- Jet-on aerodynamic characteristics of configuration 2. $\delta_j \approx -2^\circ$.

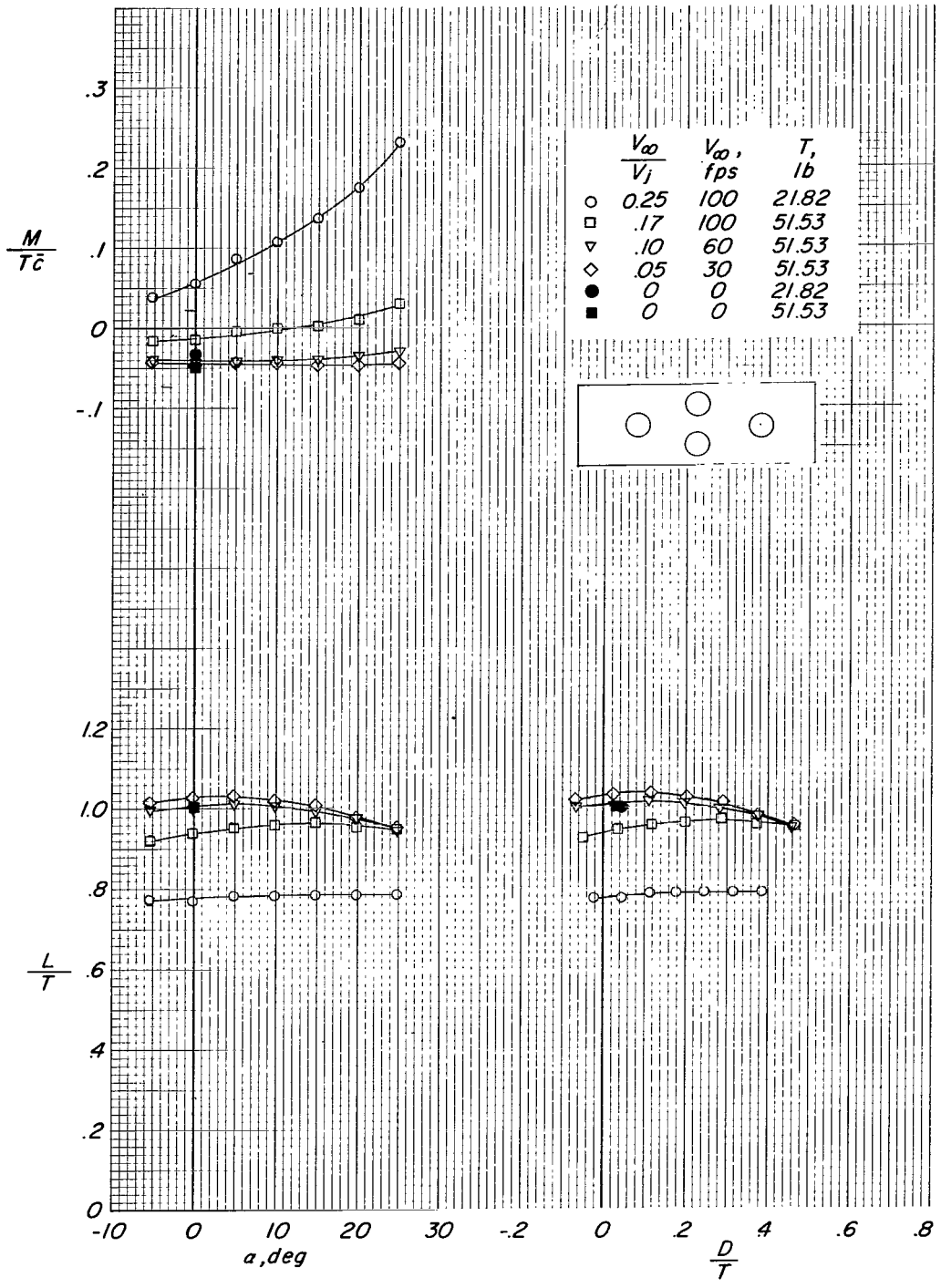

(b) Wing off.

Figure 7.- Continued.

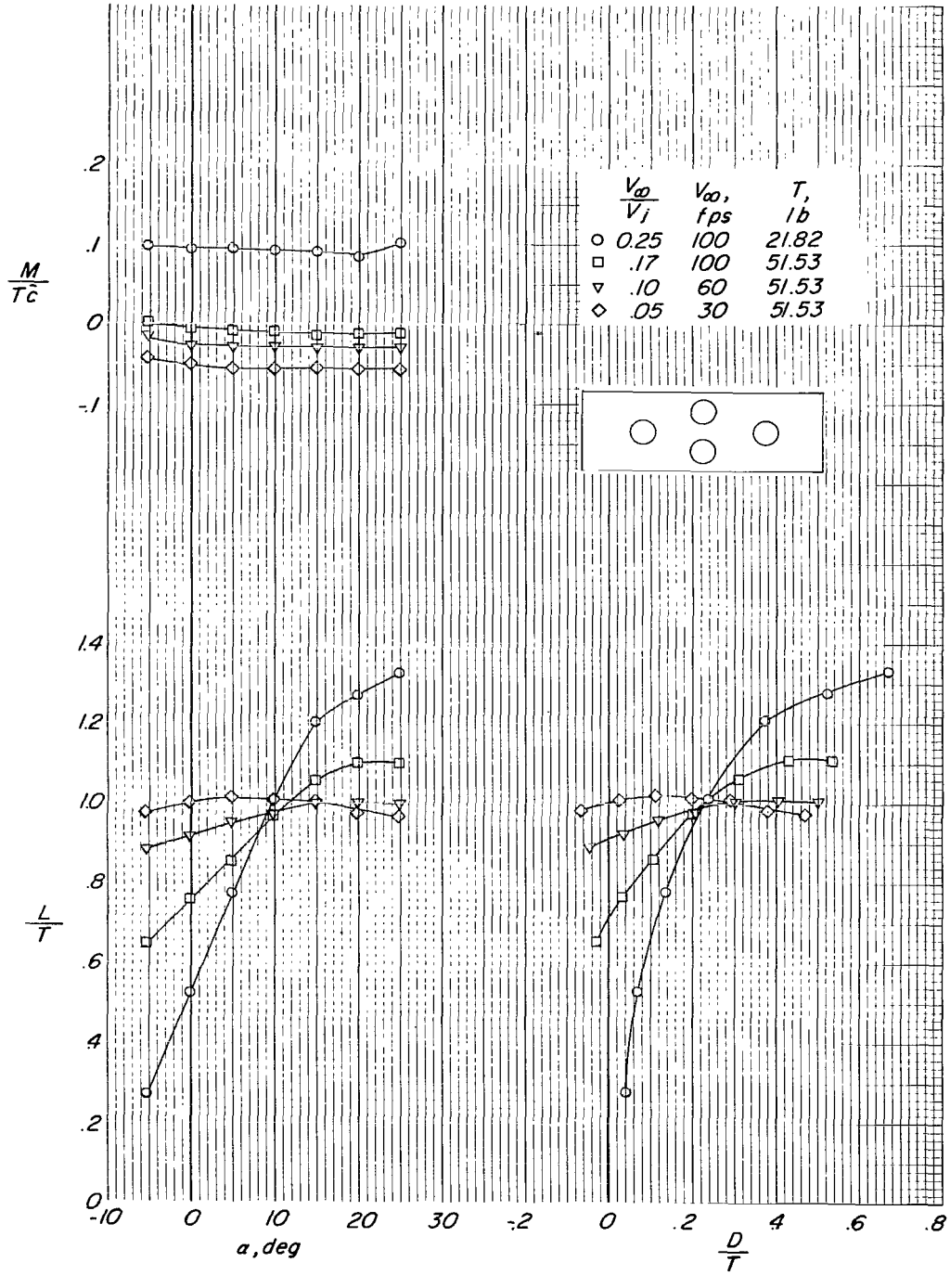

(c) Wing in low position.

Figure 7.- Concluded.

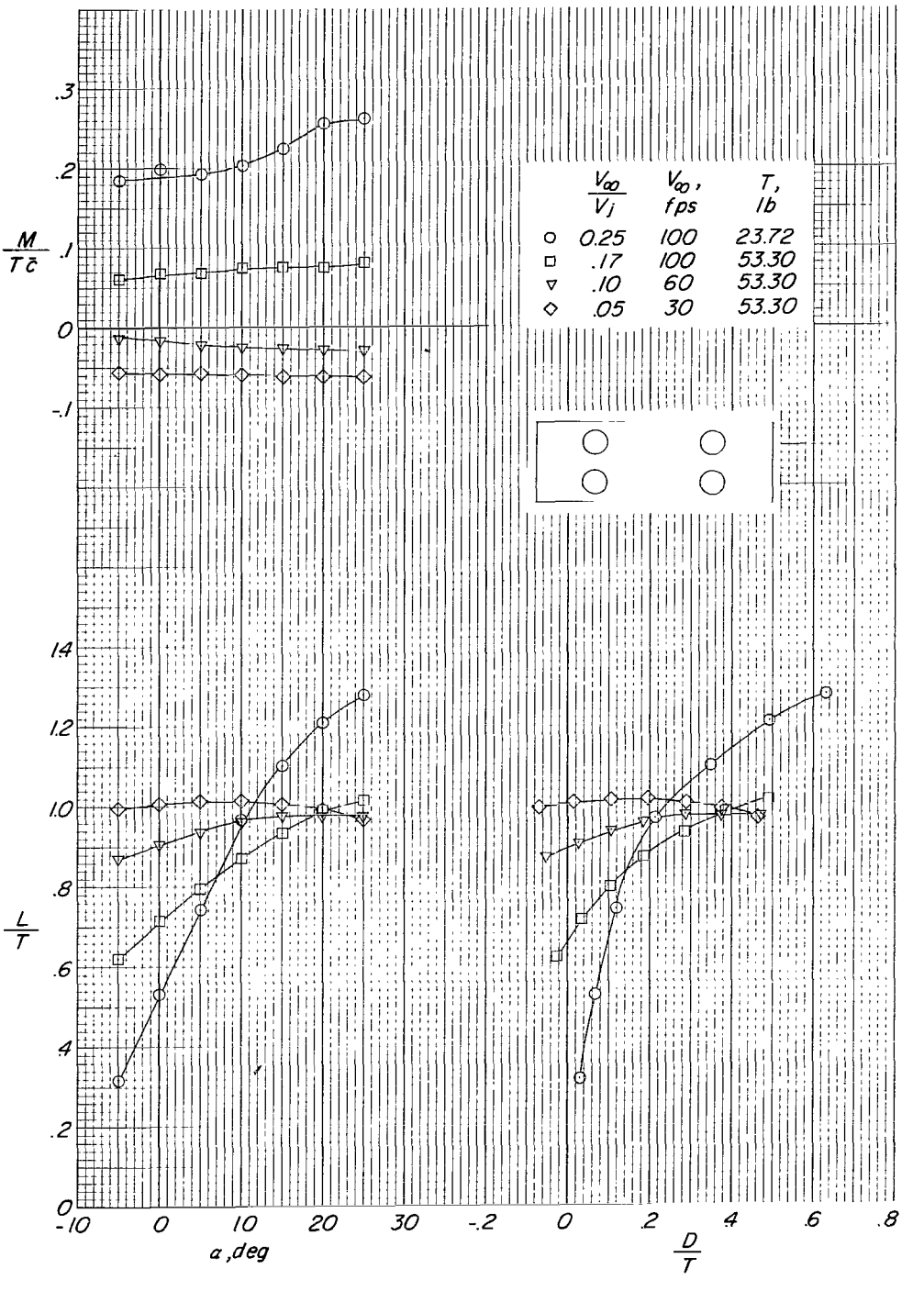

(a) Wing in high position.

Figure 8.- Jet-on aerodynamic characteristics of configuration 3. $\delta_j \approx -2^\circ$.

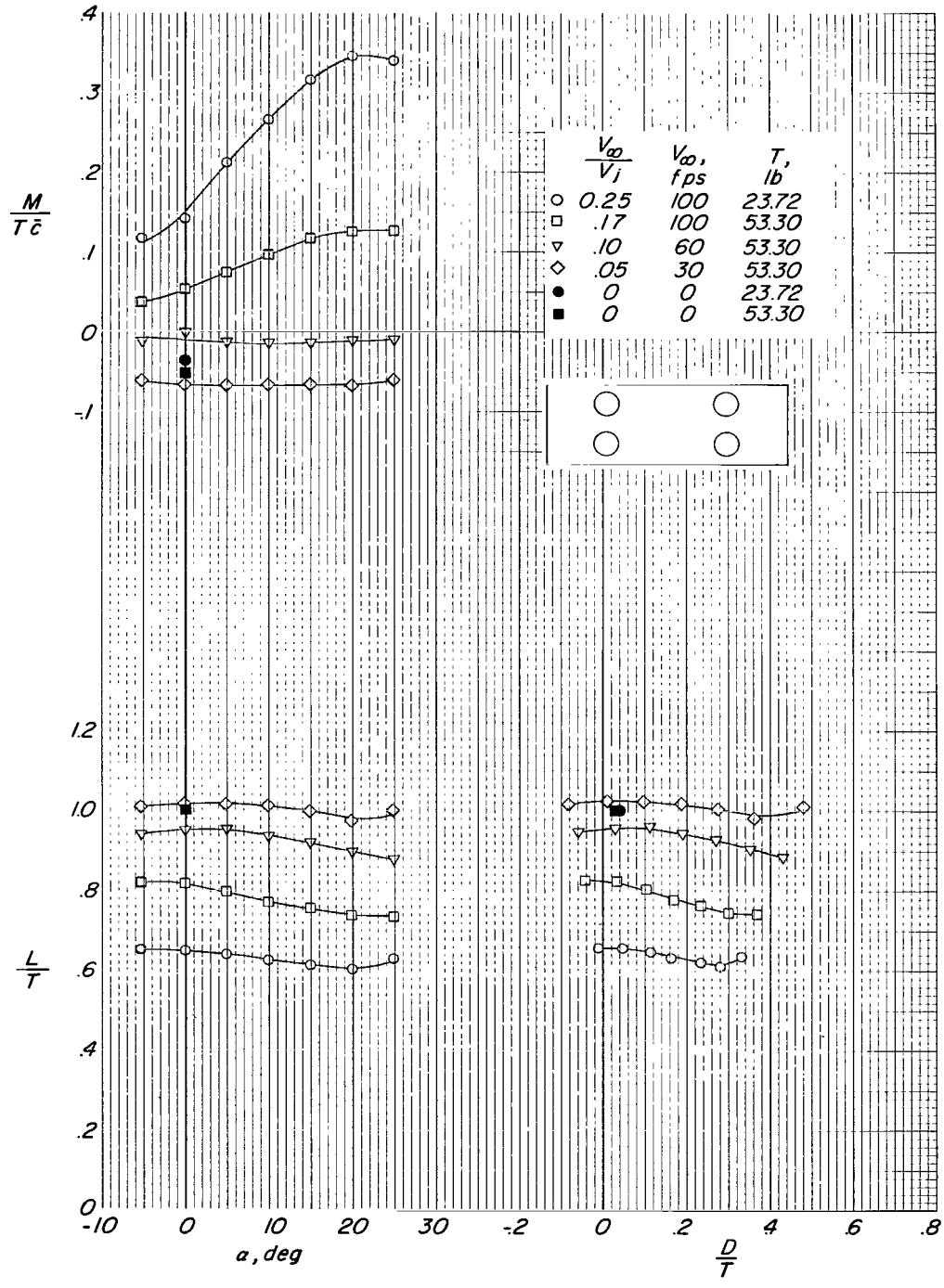

(b) Wing off.

Figure 8.- Continued.

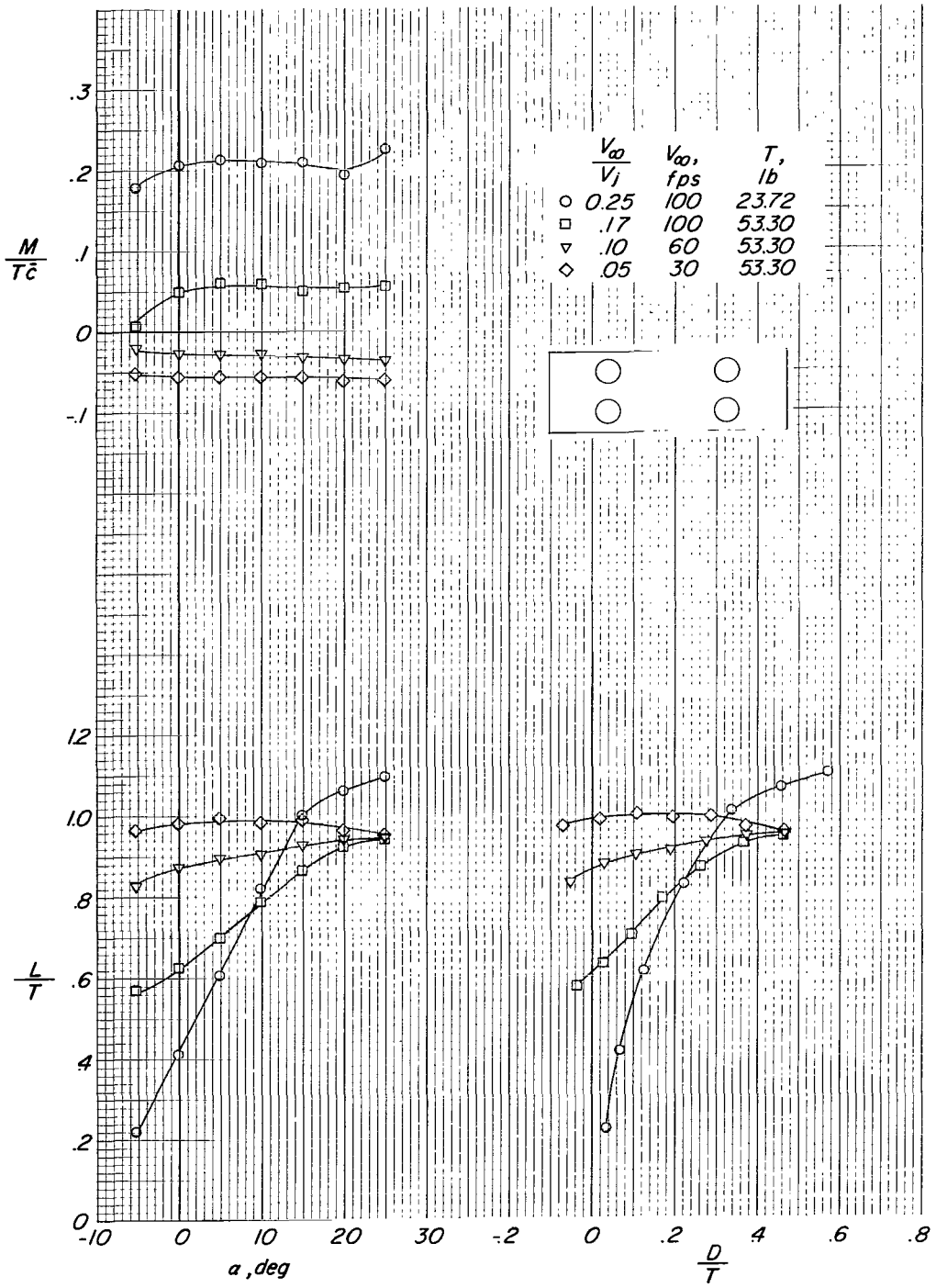

(c) Wing in low position.

Figure 8.- Concluded.

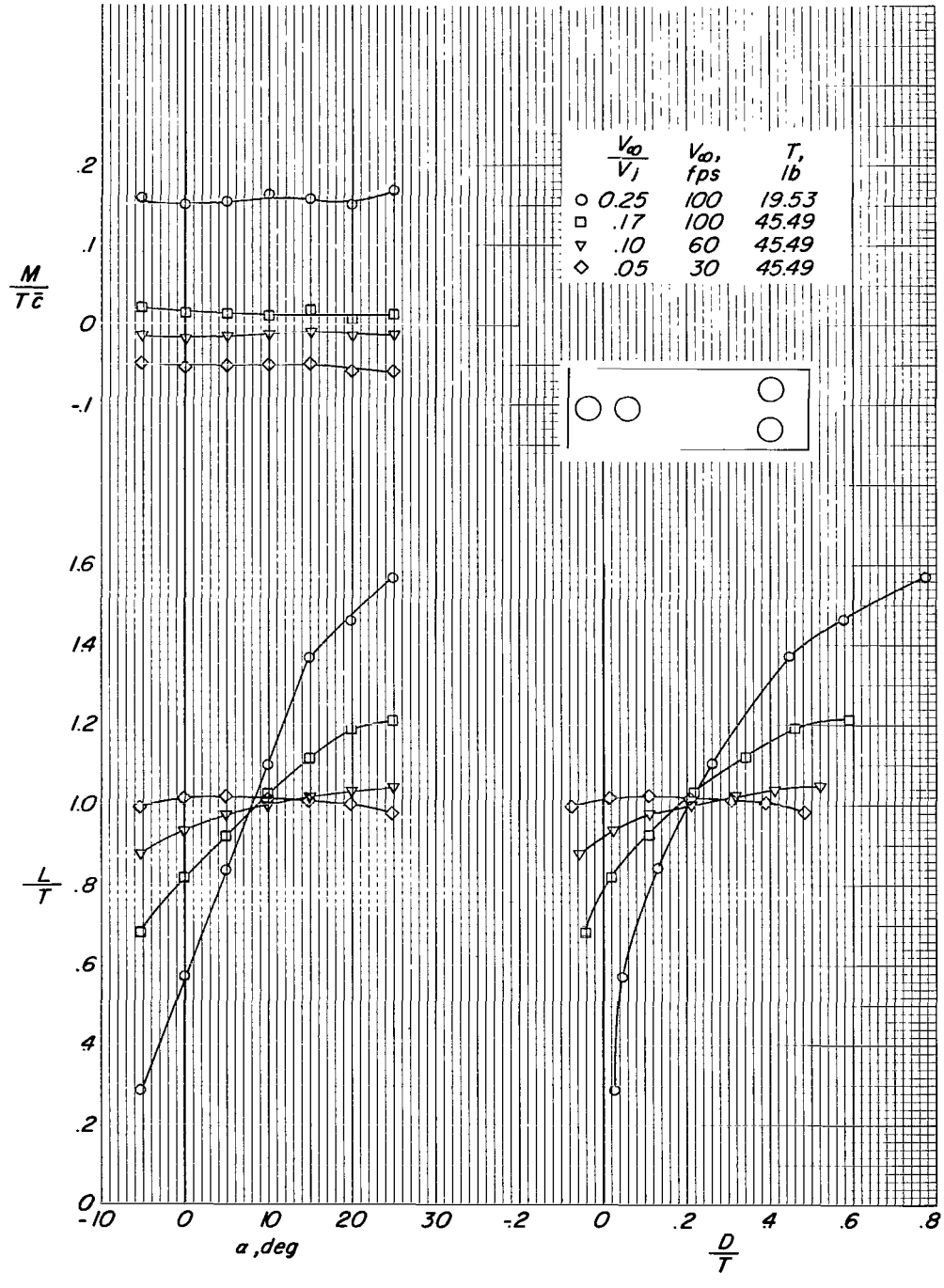

(a) Wing in high position.

Figure 9.- Jet-on aerodynamic characteristics of configuration 4. $\delta_j \approx -2^\circ$.

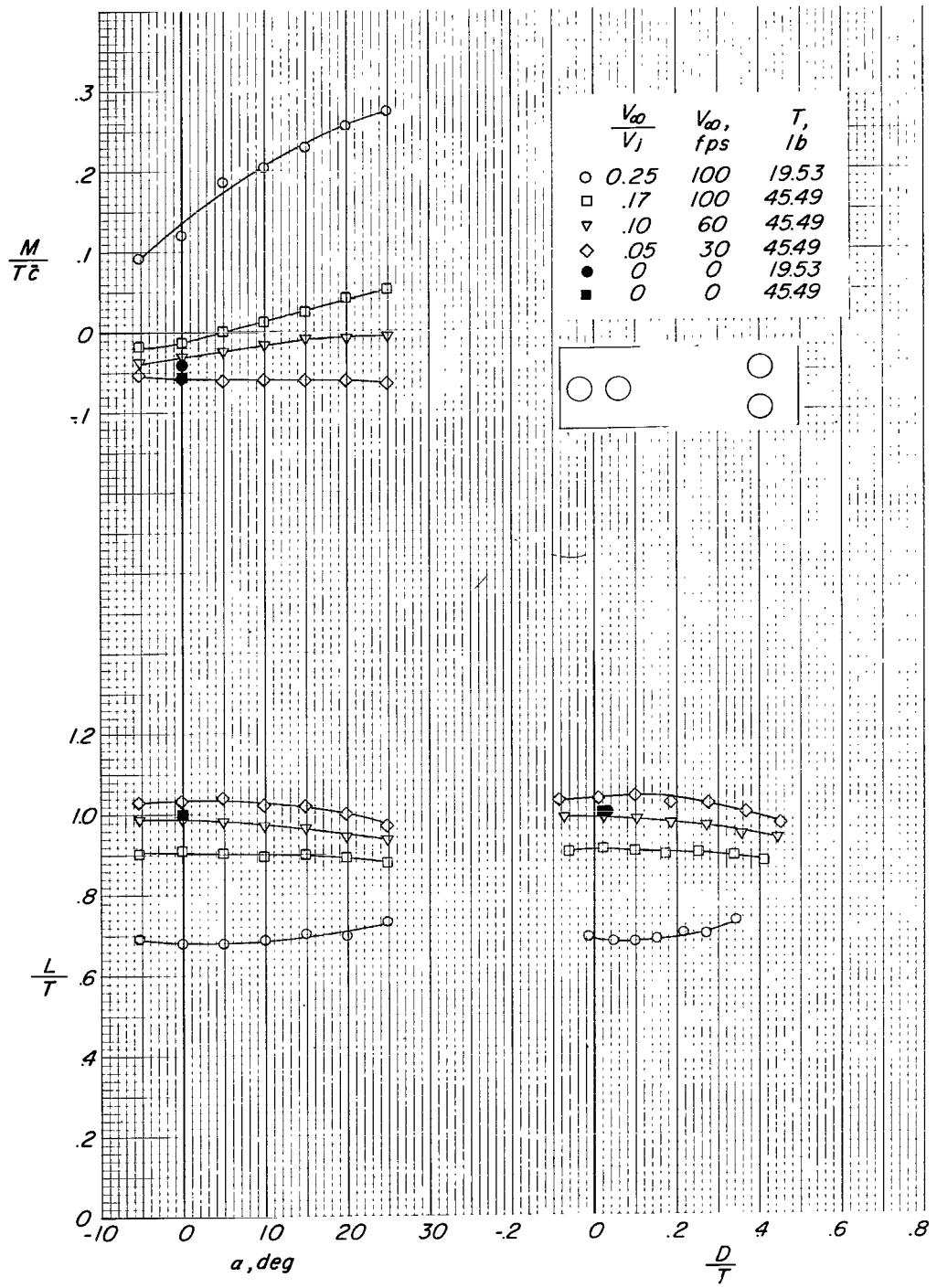

(b) Wing off.

Figure 9.- Concluded.

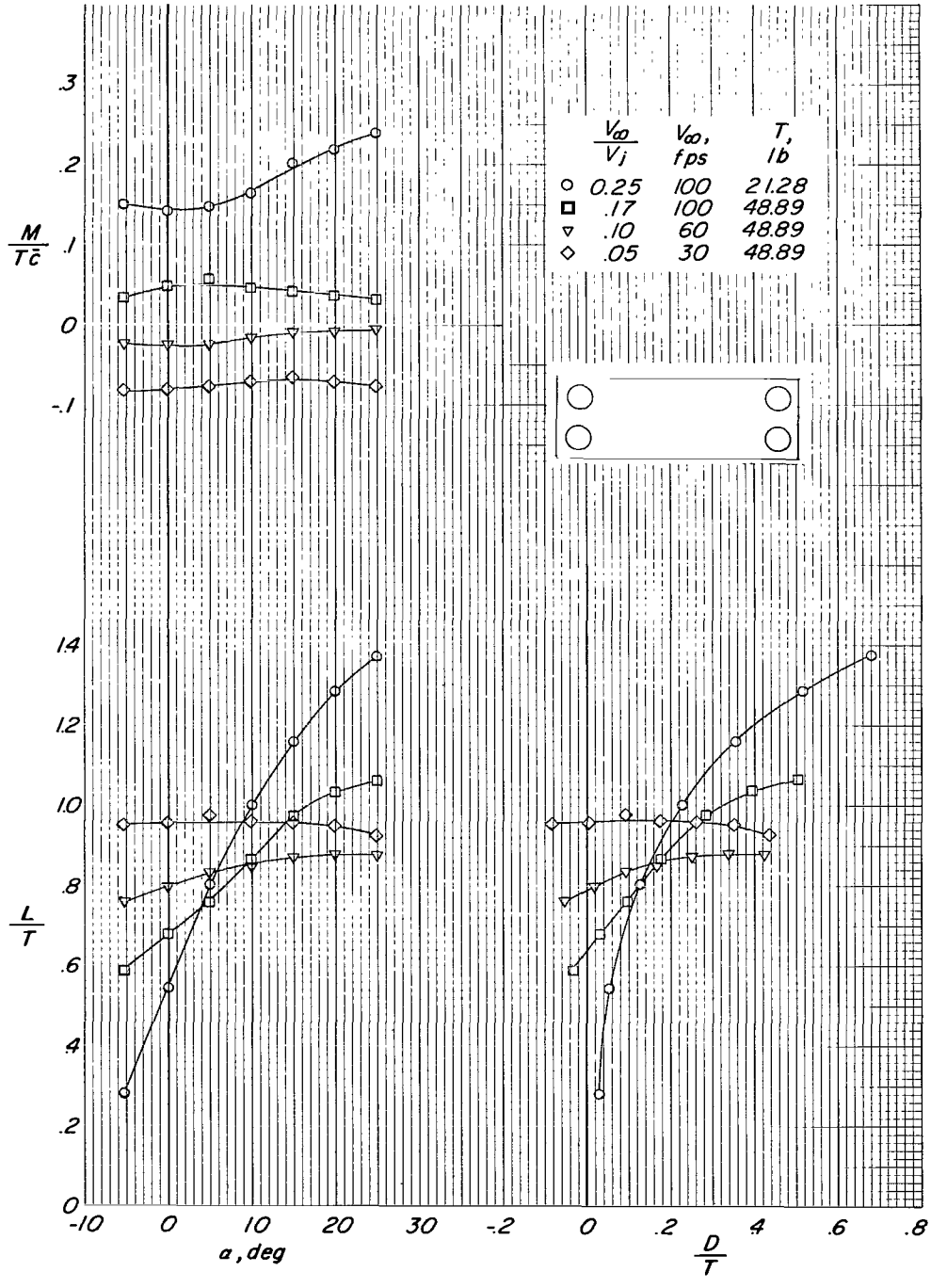

(a) Wing in high position.

Figure 10.- Jet-on aerodynamic characteristics of configuration 5. $\delta_j \approx -1^\circ$.

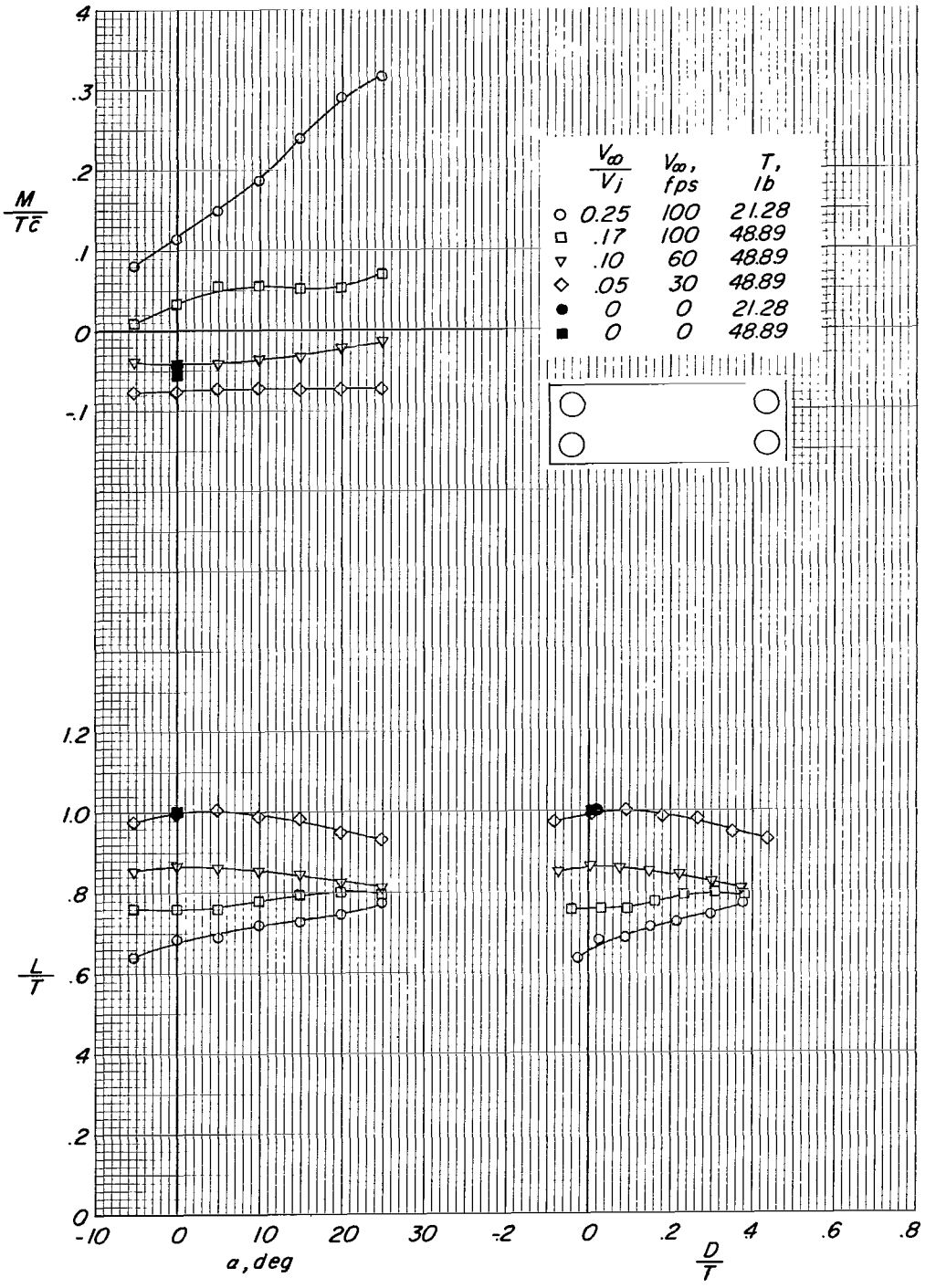

(b) Wing off.

Figure 10.- Concluded.

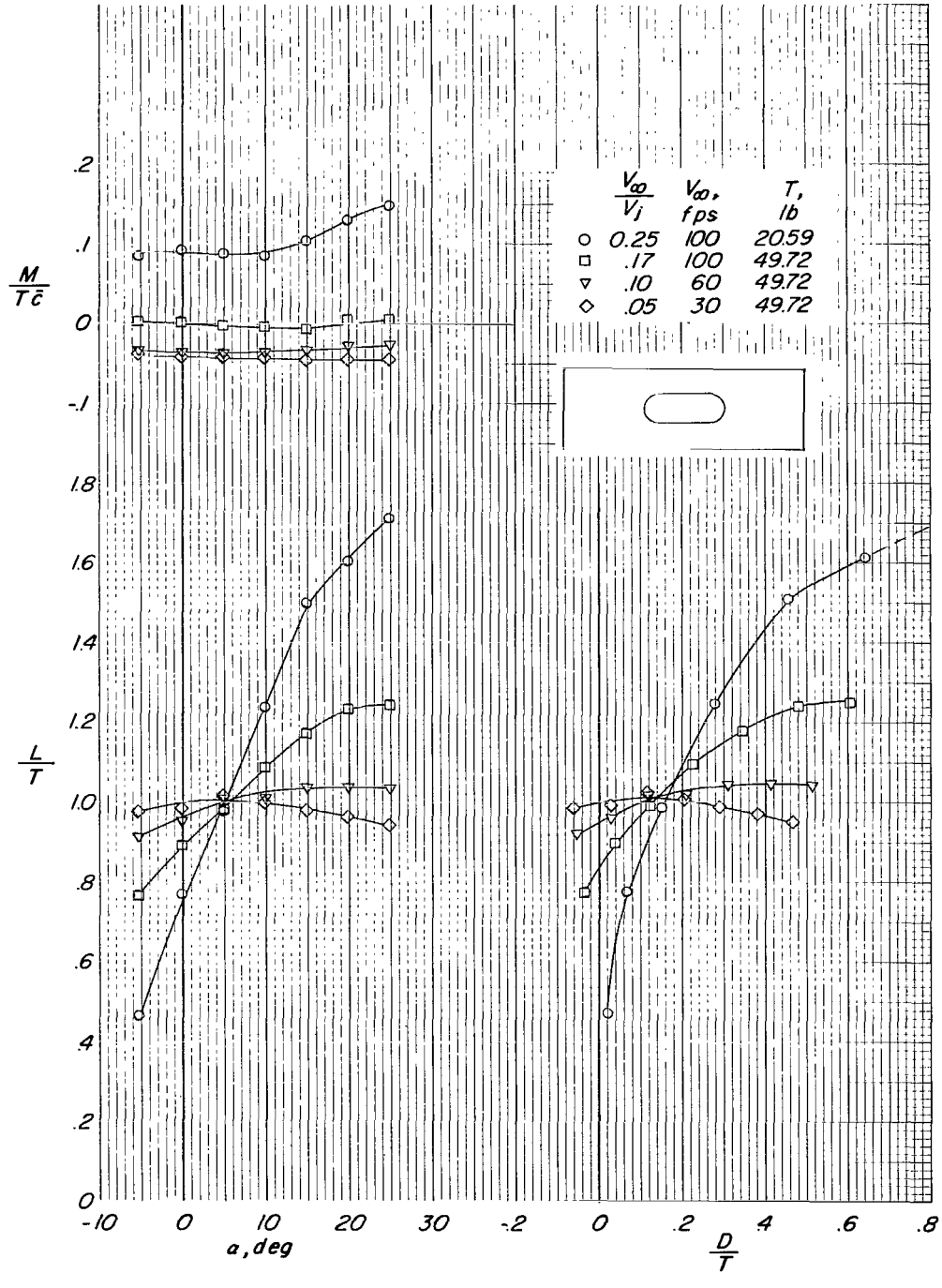

(a) Wing in high position.

Figure 11.- Jet-on aerodynamic characteristics of configuration 6. $\delta_j \approx -3^\circ$.

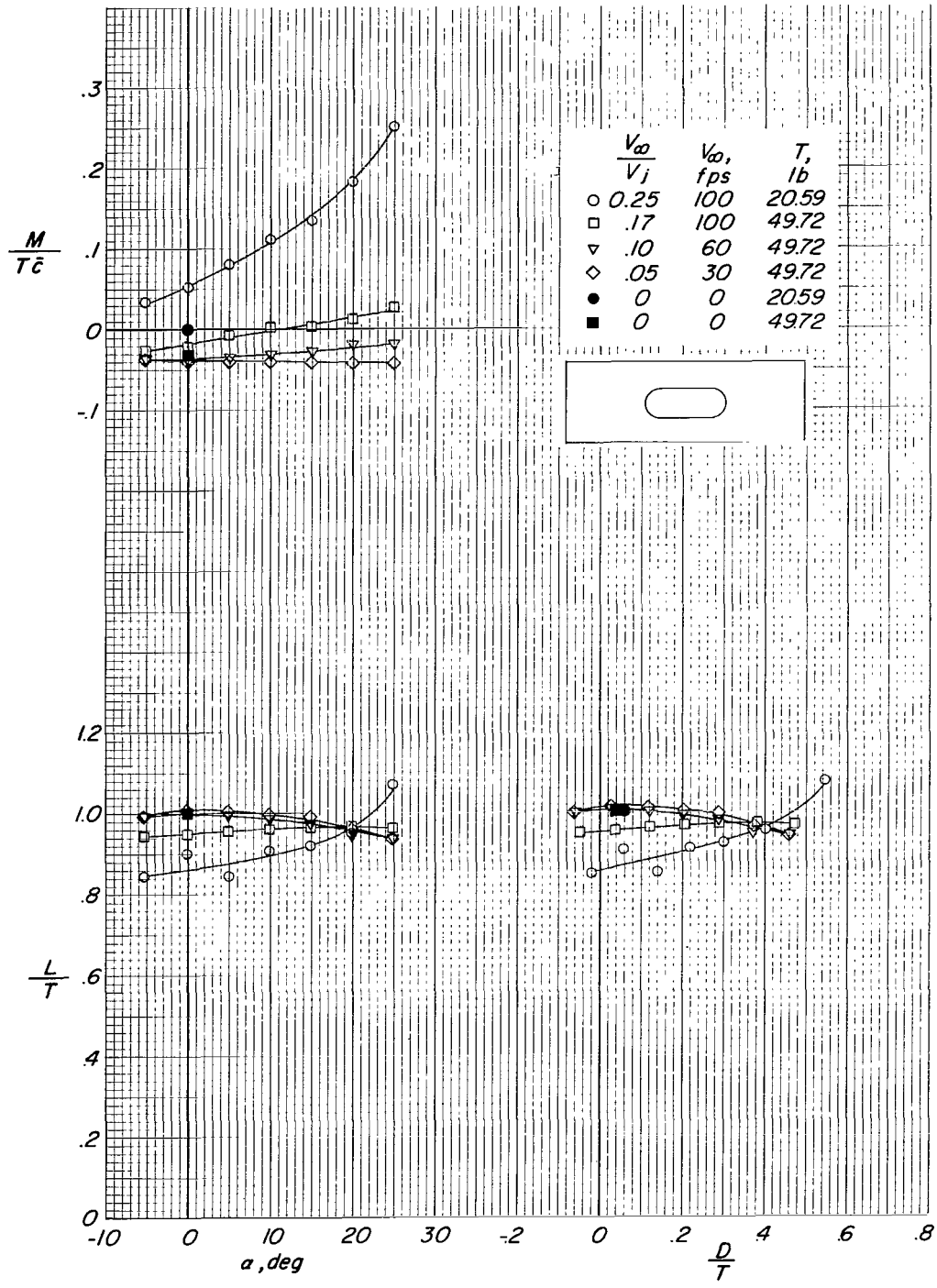

(b) Wing off.

Figure 11.- Concluded.

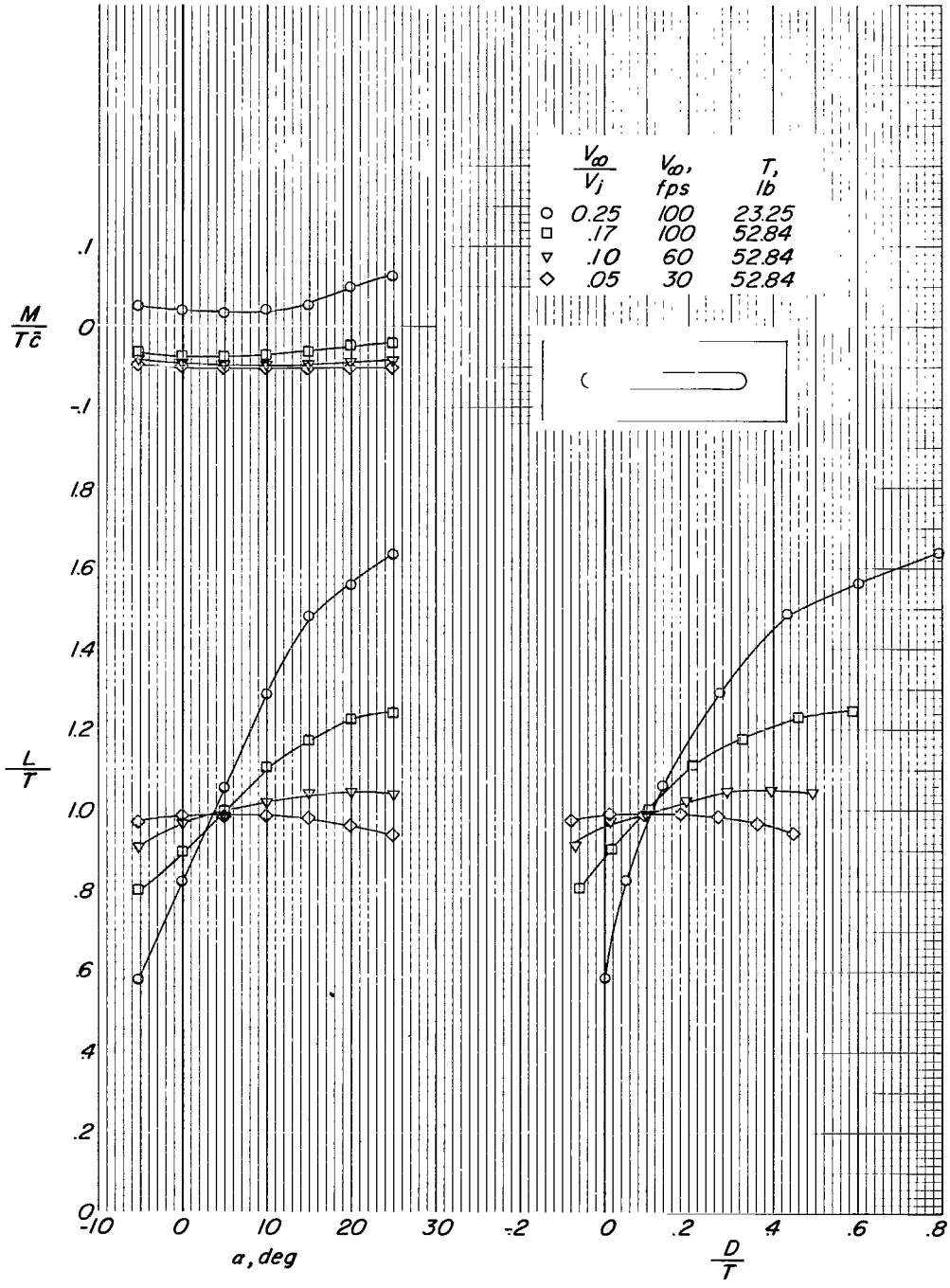

(a) Wing in high position.

Figure 12.- Jet-on aerodynamic characteristics of configuration 7. $\delta_j \approx -1^\circ$.

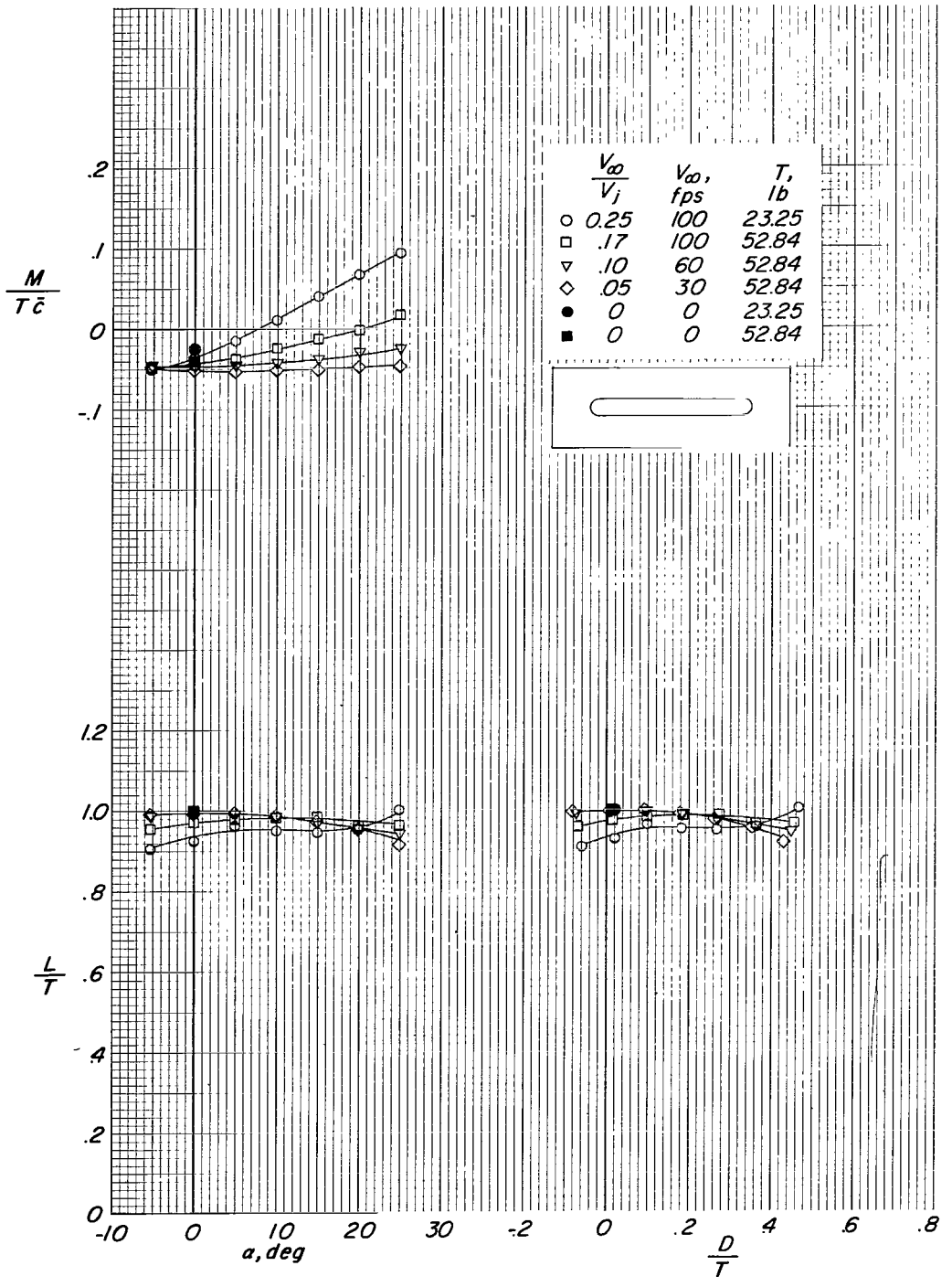

(b) Wing off.

Figure 12.- Concluded.

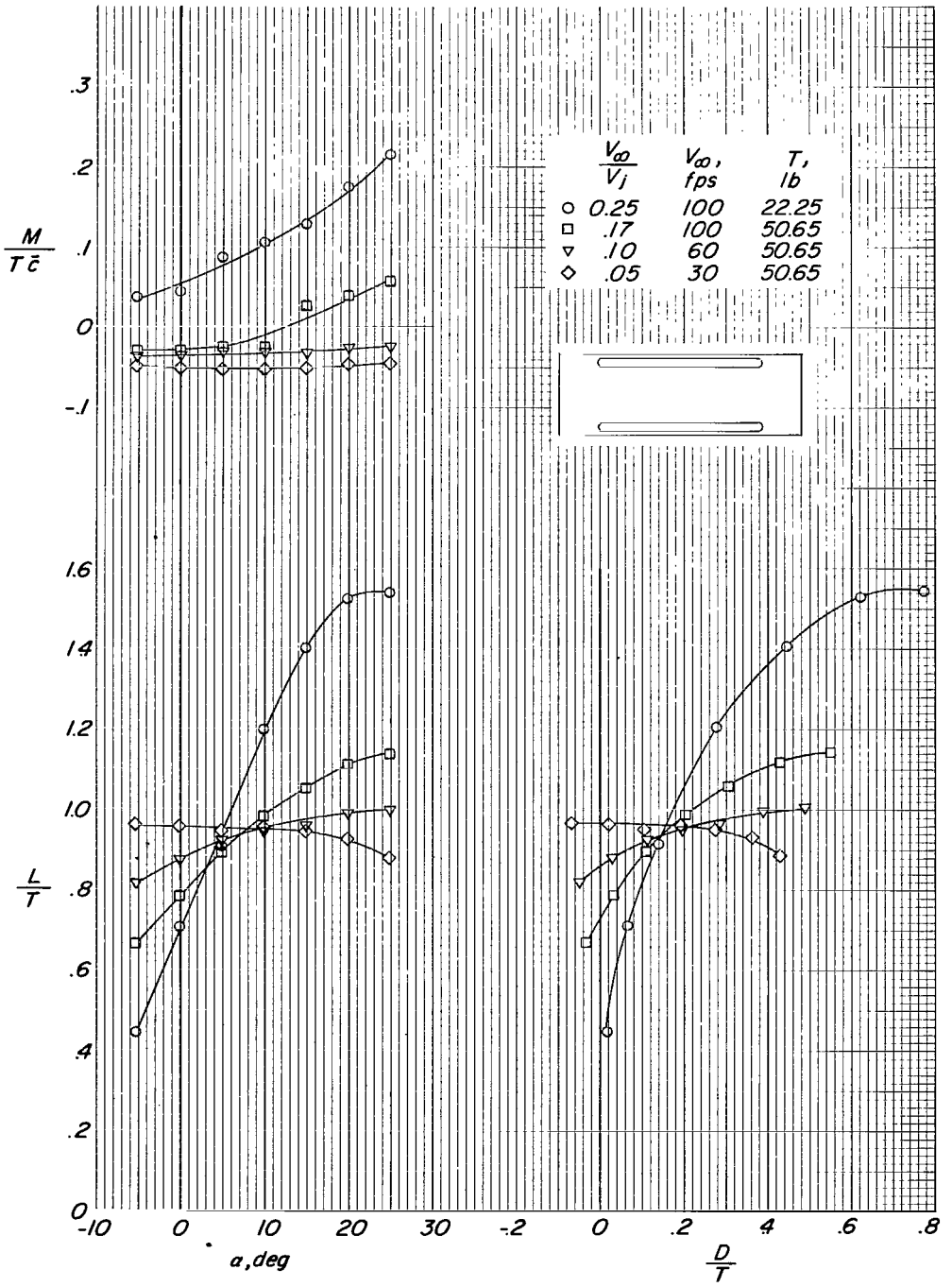

(a) Wing in high position.

Figure 13.- Jet-on aerodynamic characteristics of configuration 8. $\delta_j \approx -1^\circ$.

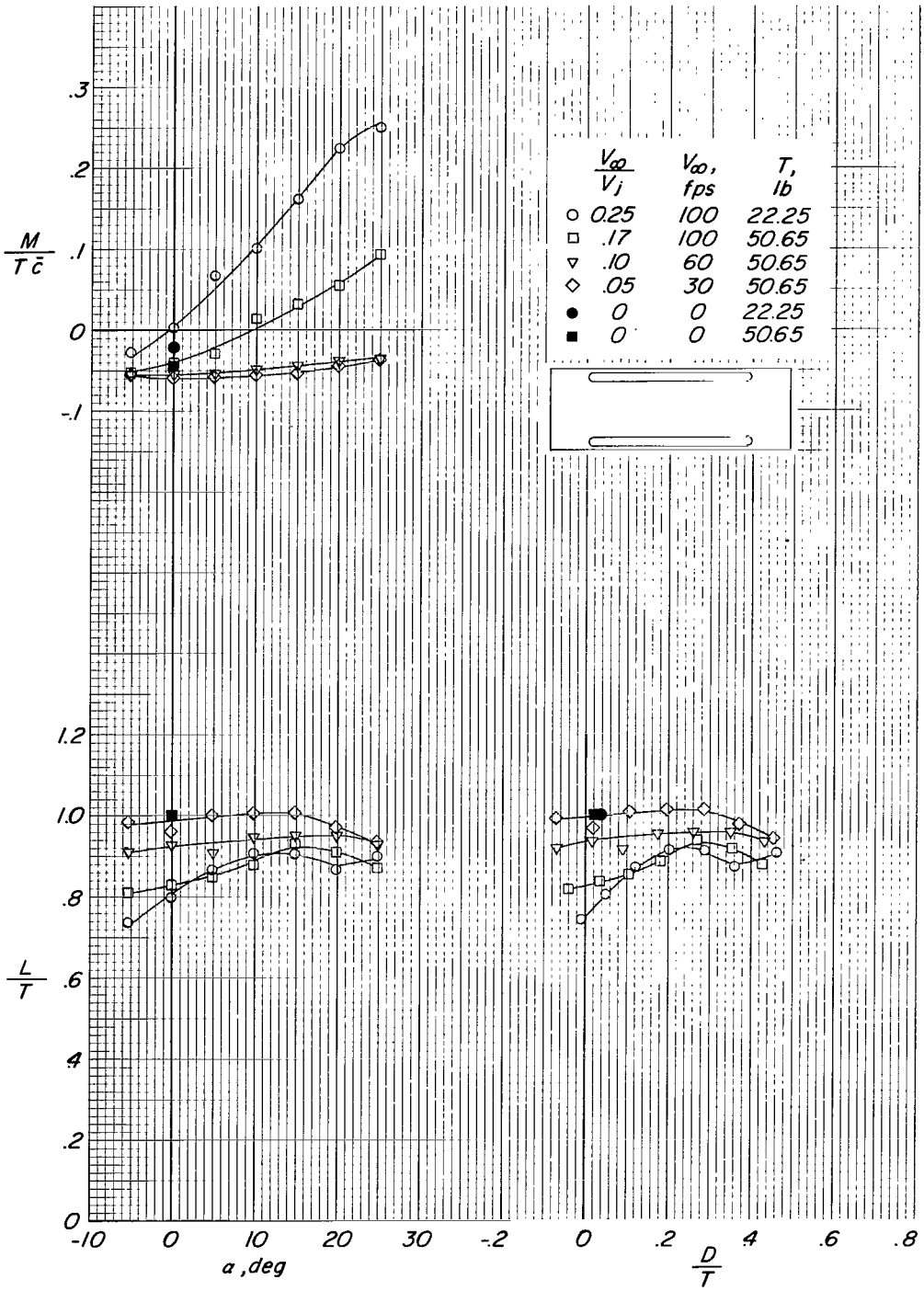

(b) Wing off.

Figure 13.- Concluded.

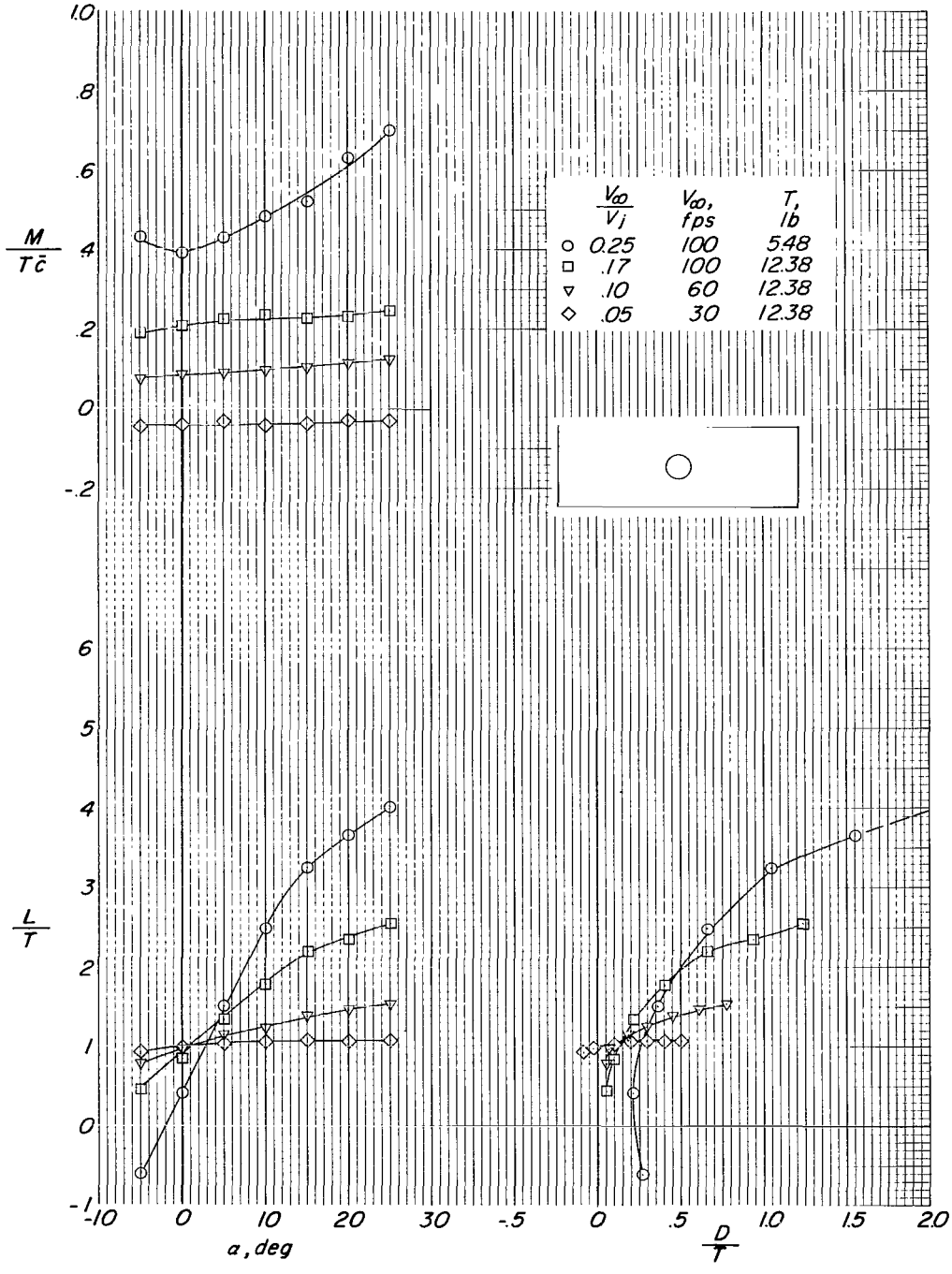

(a) Wing in high position.

Figure 14.- Jet-on aerodynamic characteristics of configuration 9. $\delta_j \approx -4^\circ$.

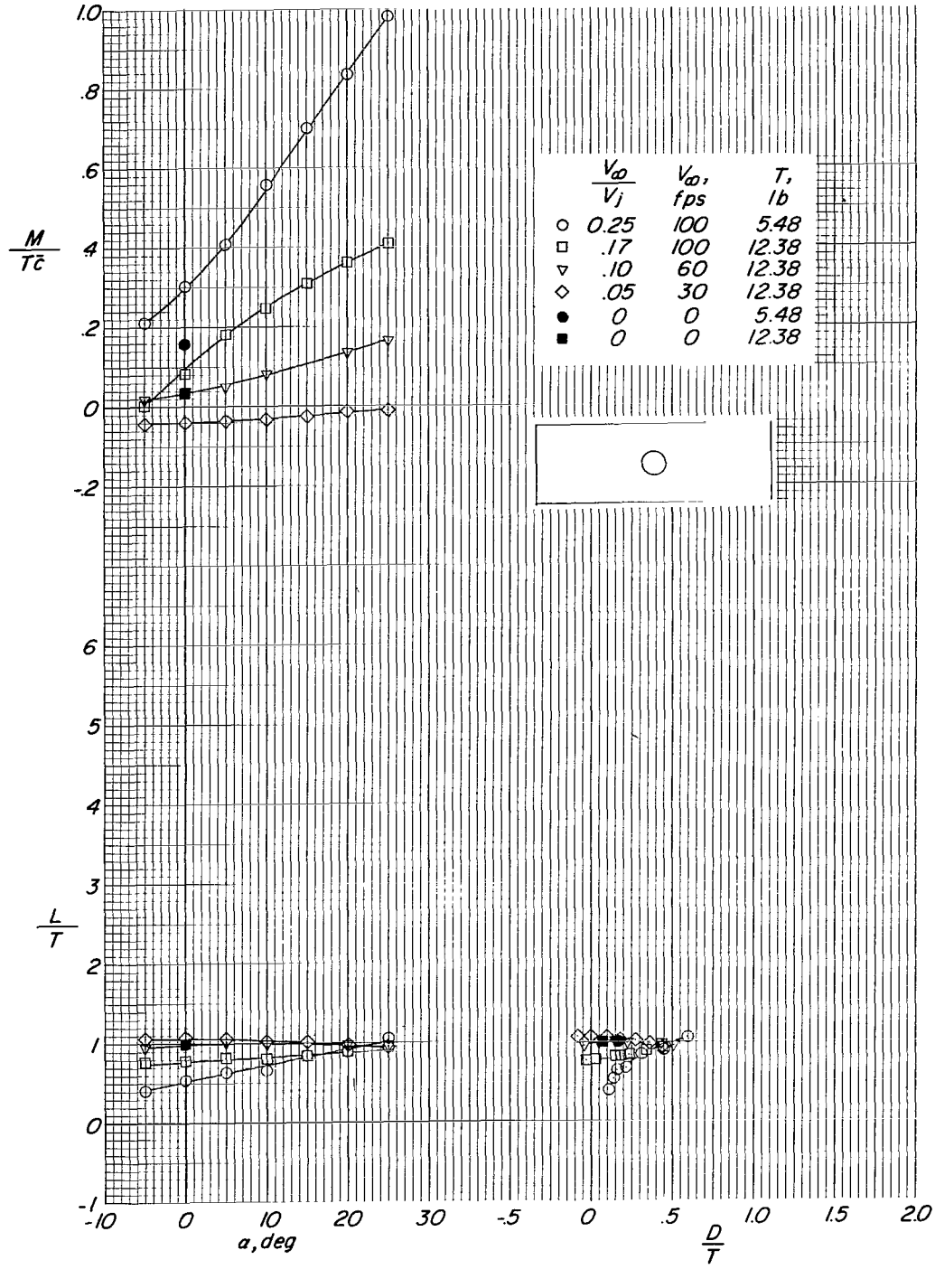

(b) Wing off.

Figure 14.- Concluded.

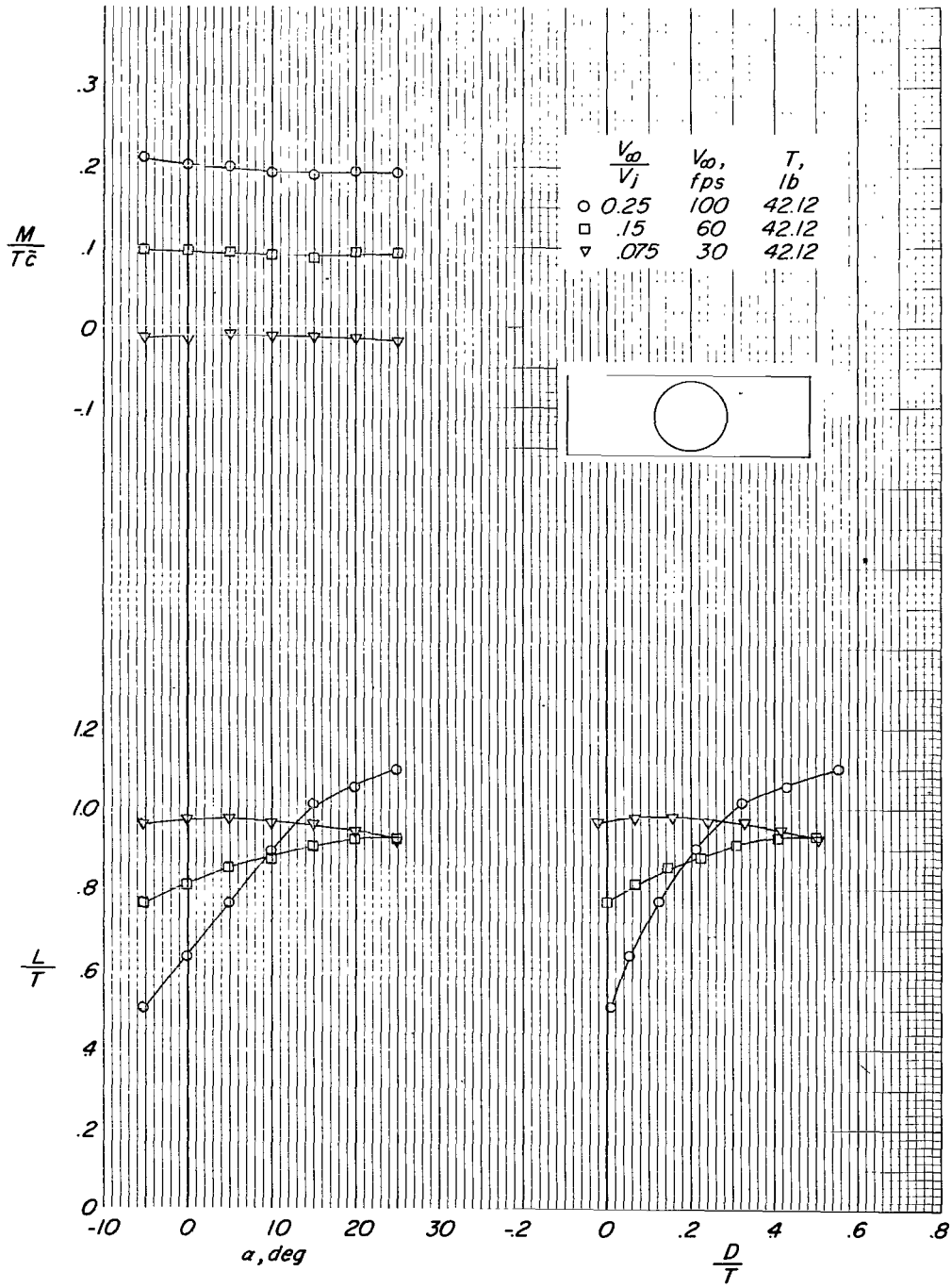

(a) Wing in high position.

Figure 15.- Jet-on aerodynamic characteristics of configuration 10. $\delta_j \approx -3^\circ$.

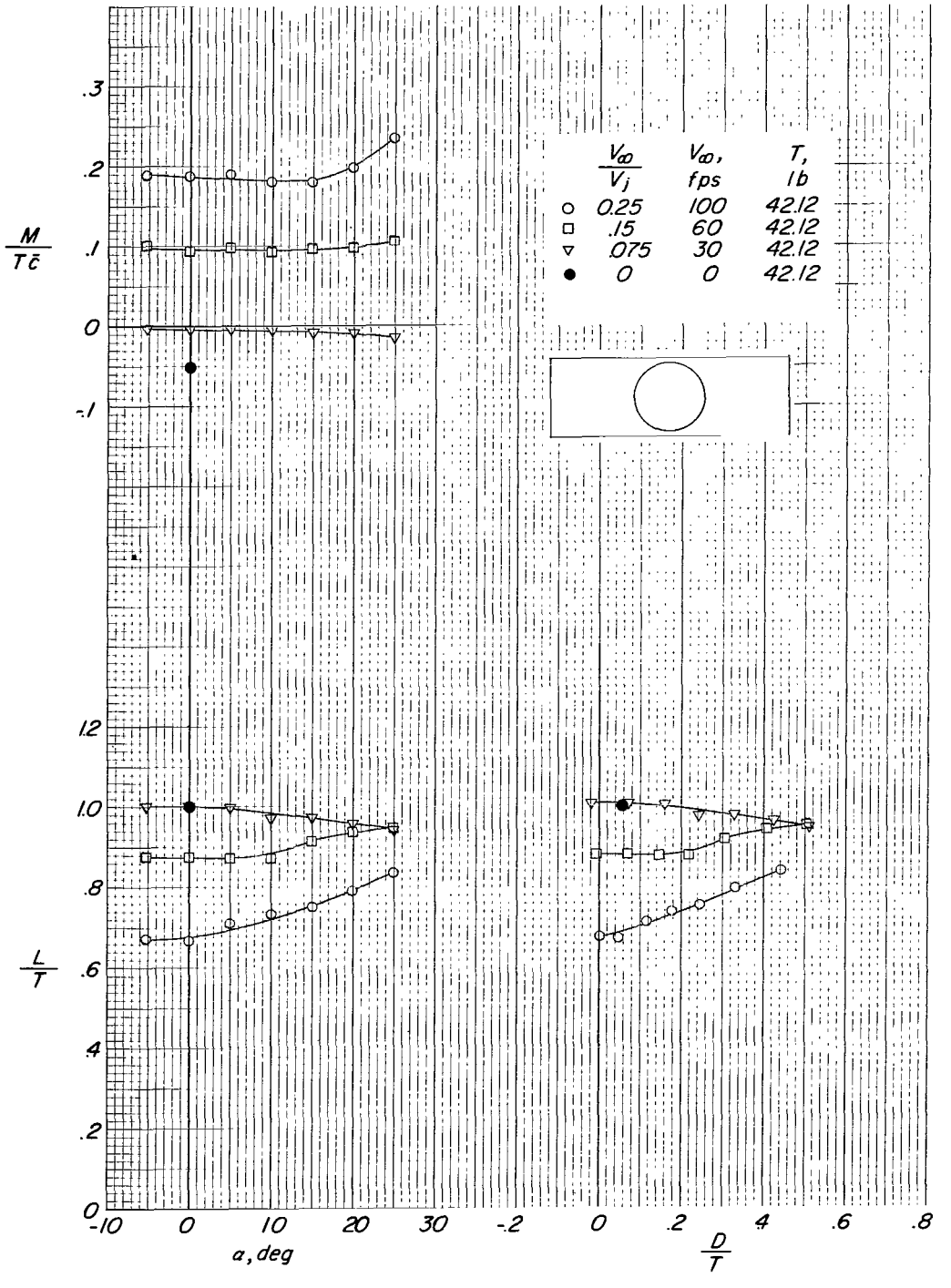

(b) Wing off.

Figure 15.- Concluded.

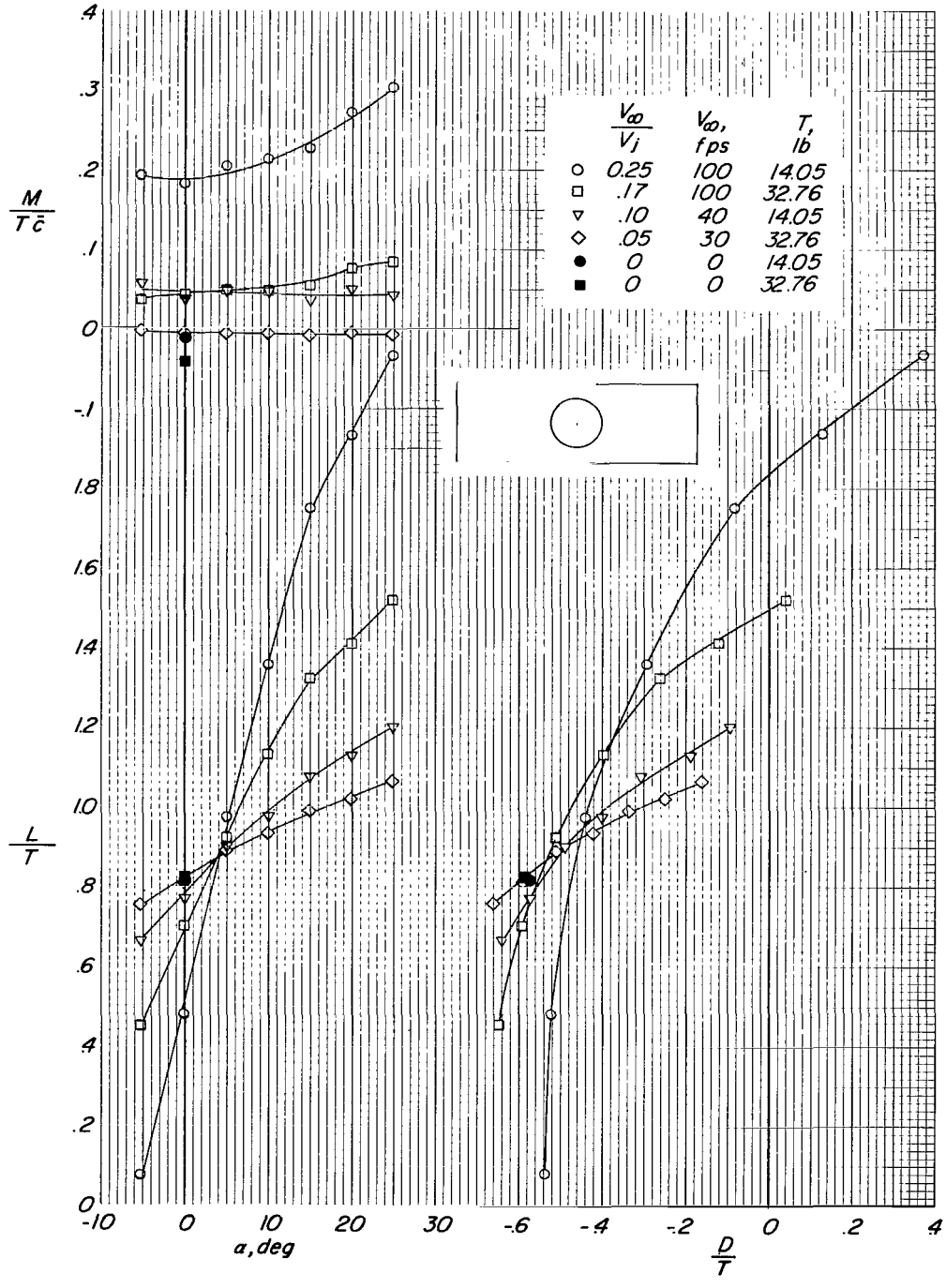

(a) Wing in high position.

Figure 16.- Jet-on aerodynamic characteristics of configuration 1. $\delta_j \approx 35^\circ$.

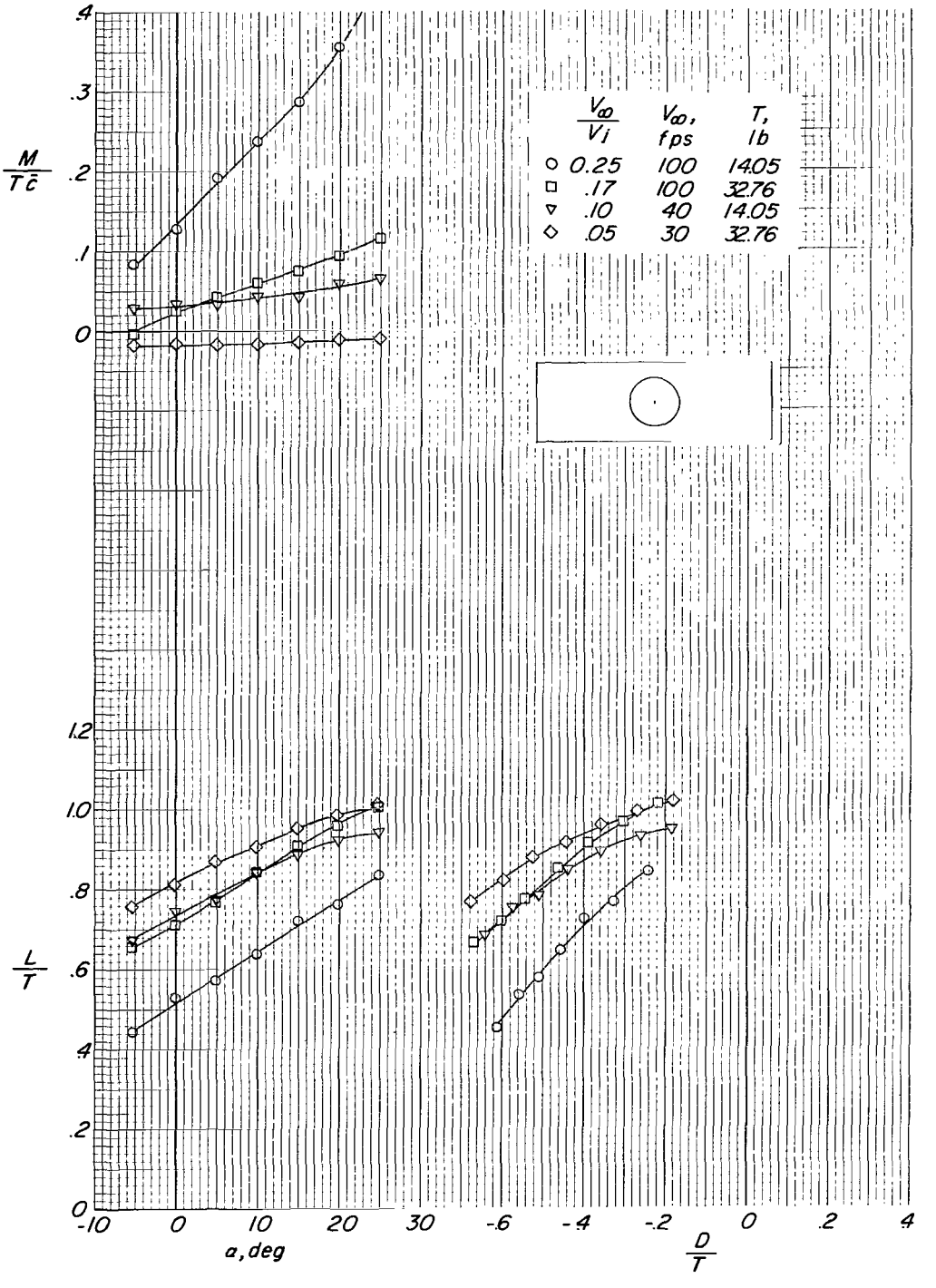

(b) Wing off.

Figure 16.- Continued.

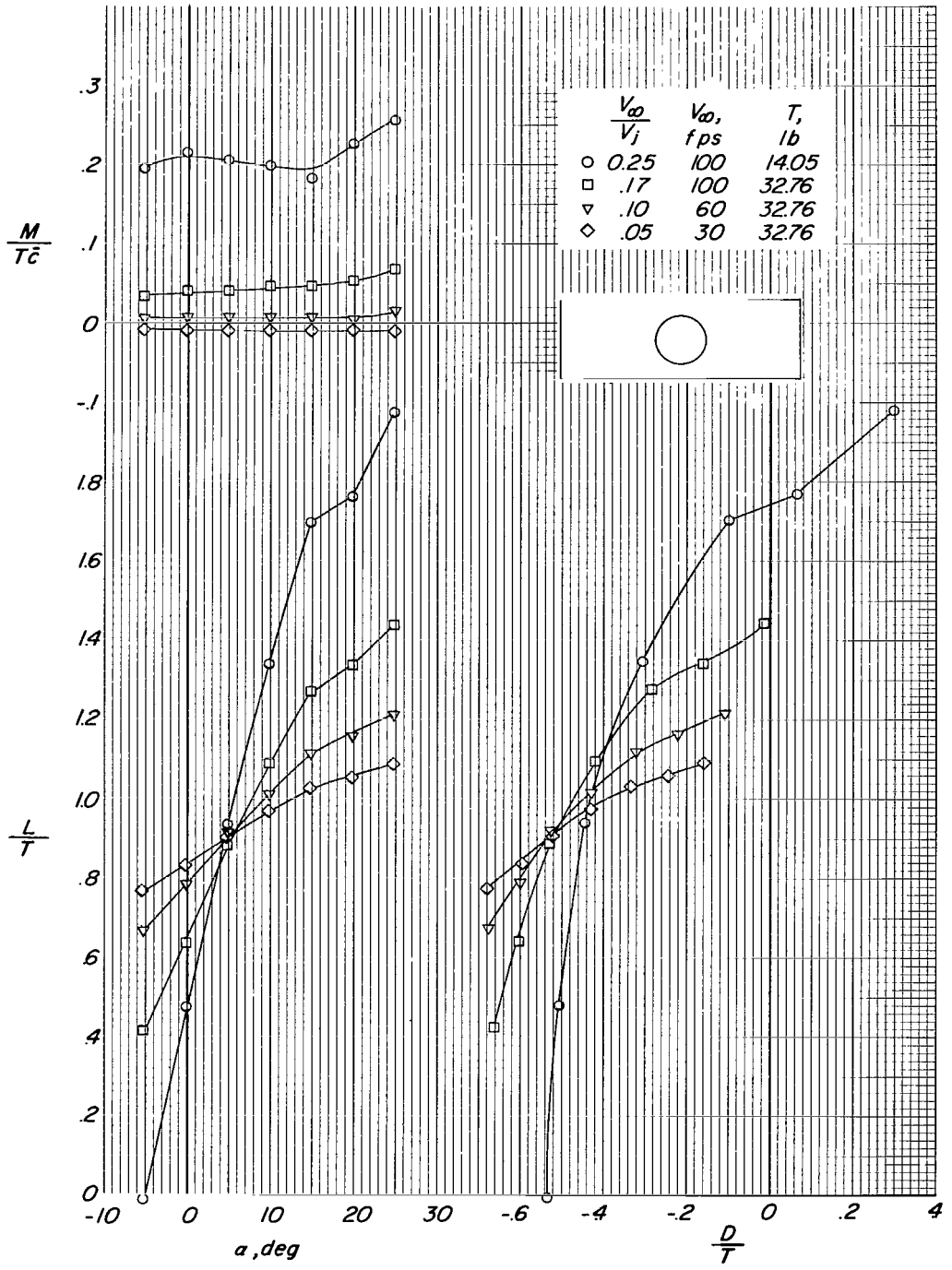

(c) Wing in low position.

Figure 16.- Concluded.

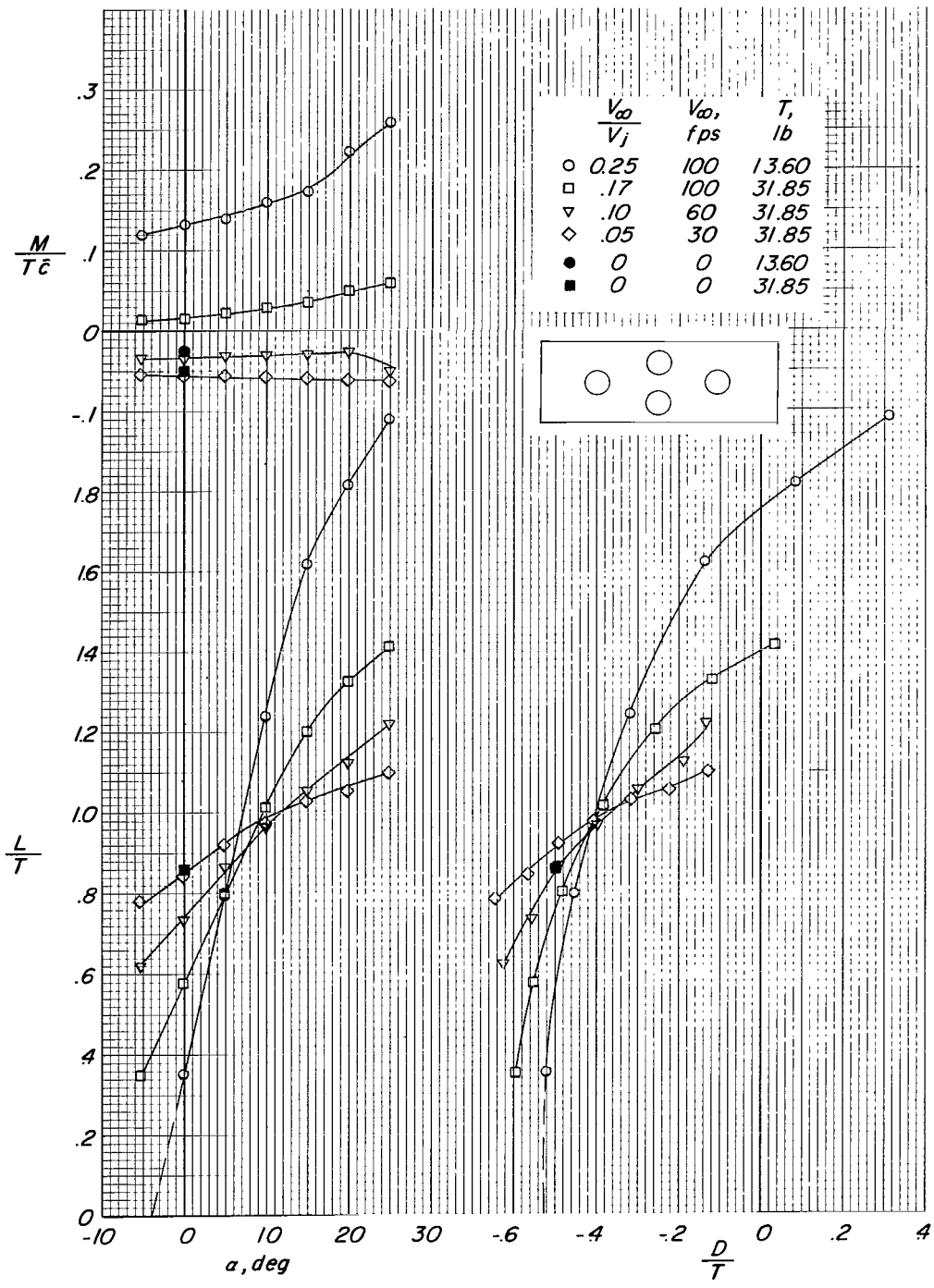

(a) Wing in high position.

Figure 17.- Jet-on aerodynamic characteristics of configuration 2. $\delta_j \approx 30^\circ$.

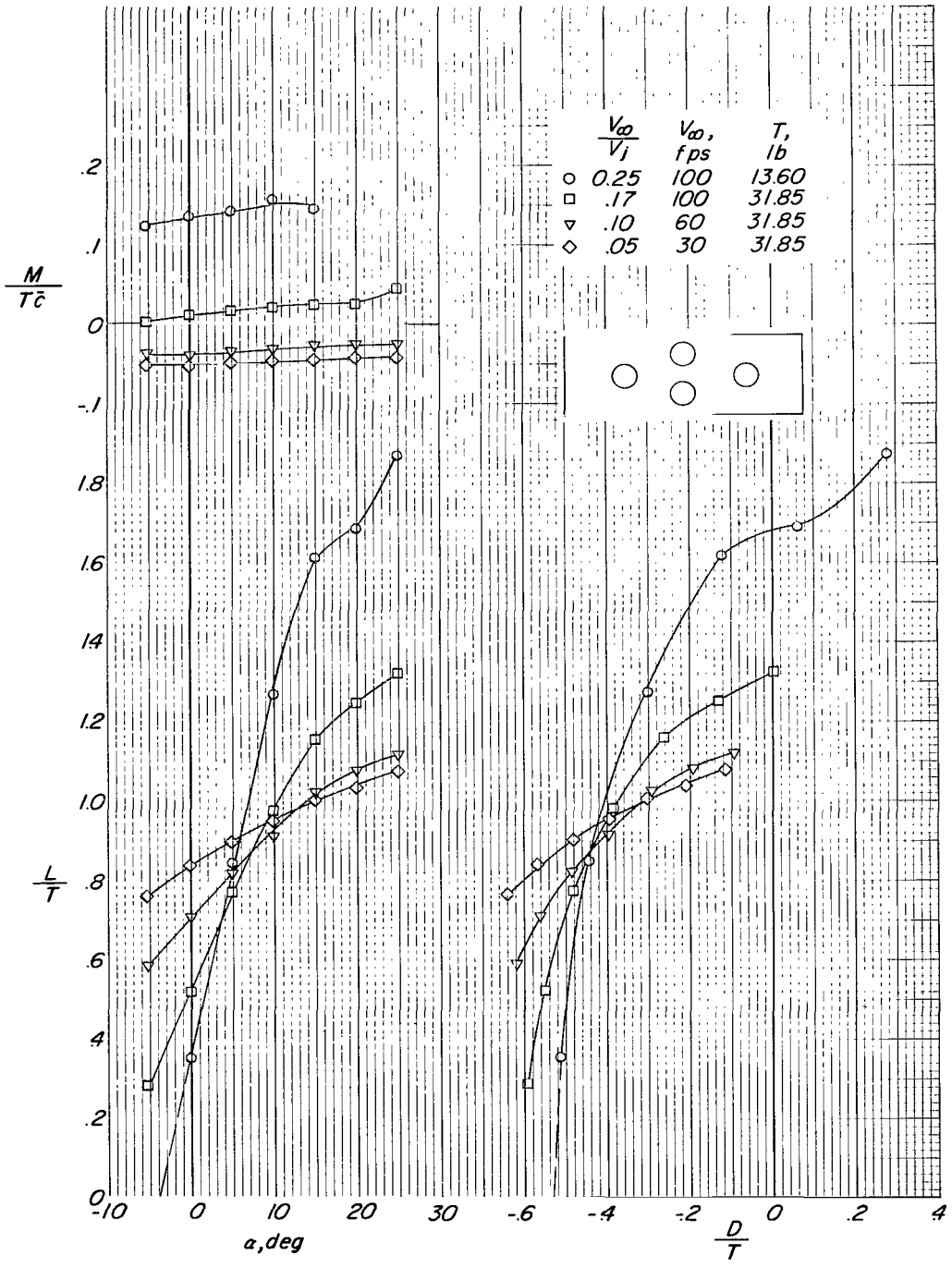

(b) Wing in low position.

Figure 17.- Concluded.

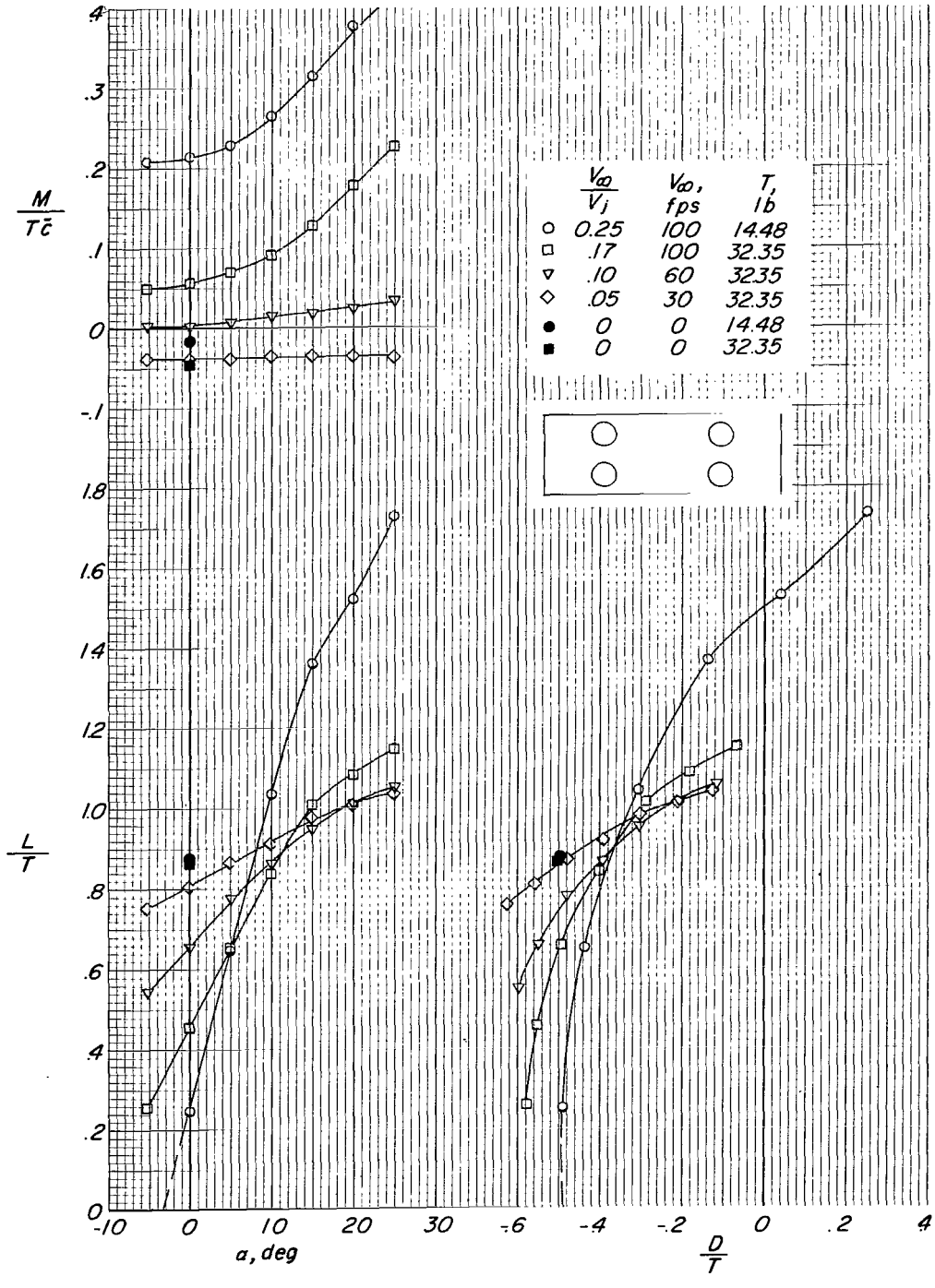

(a) Wing in high position.

Figure 18.- Jet-on aerodynamic characteristics of configuration 3. $\delta_j \approx 30^o$.

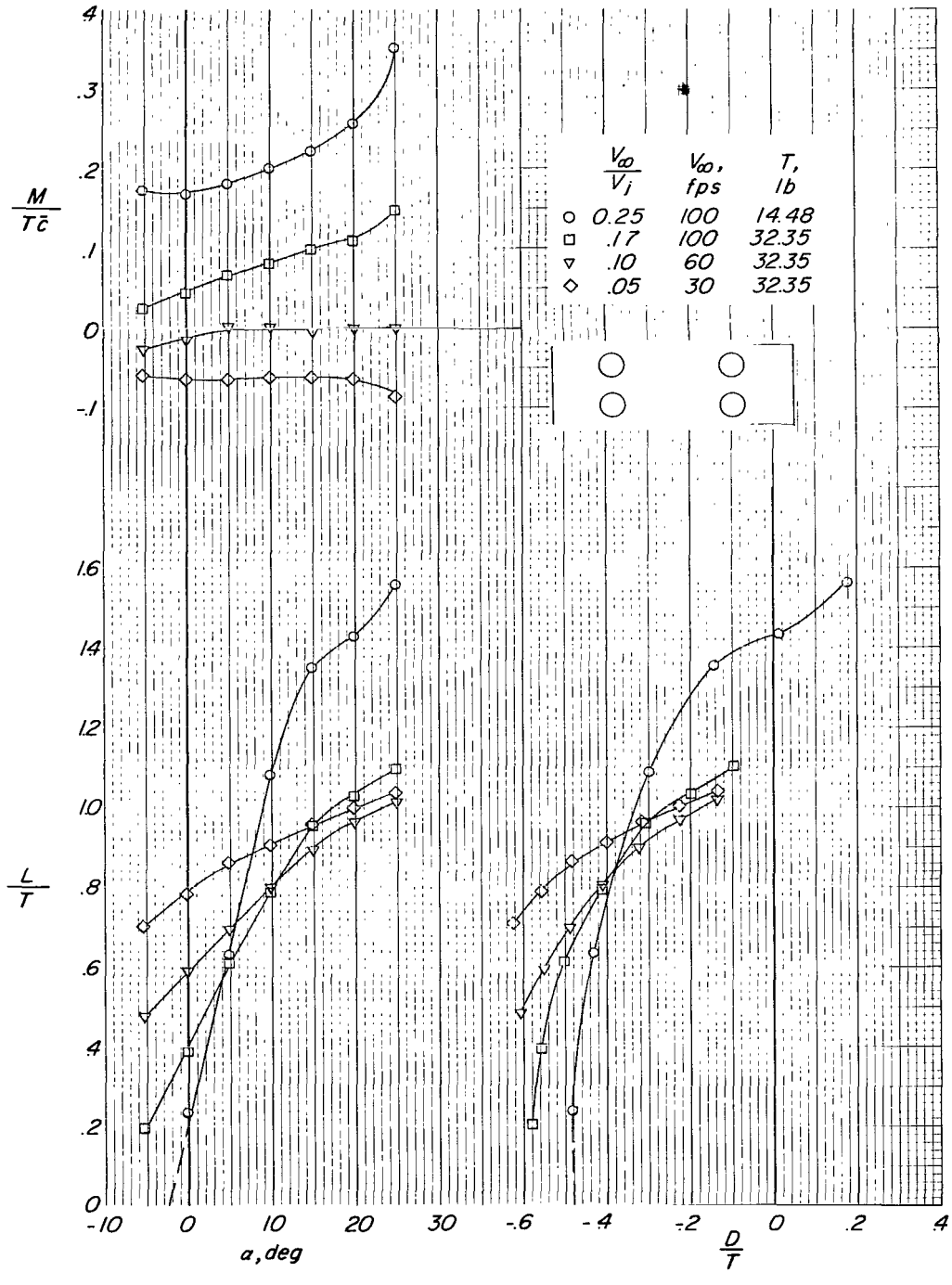

(b) Wing in low position.

Figure 18.- Concluded.

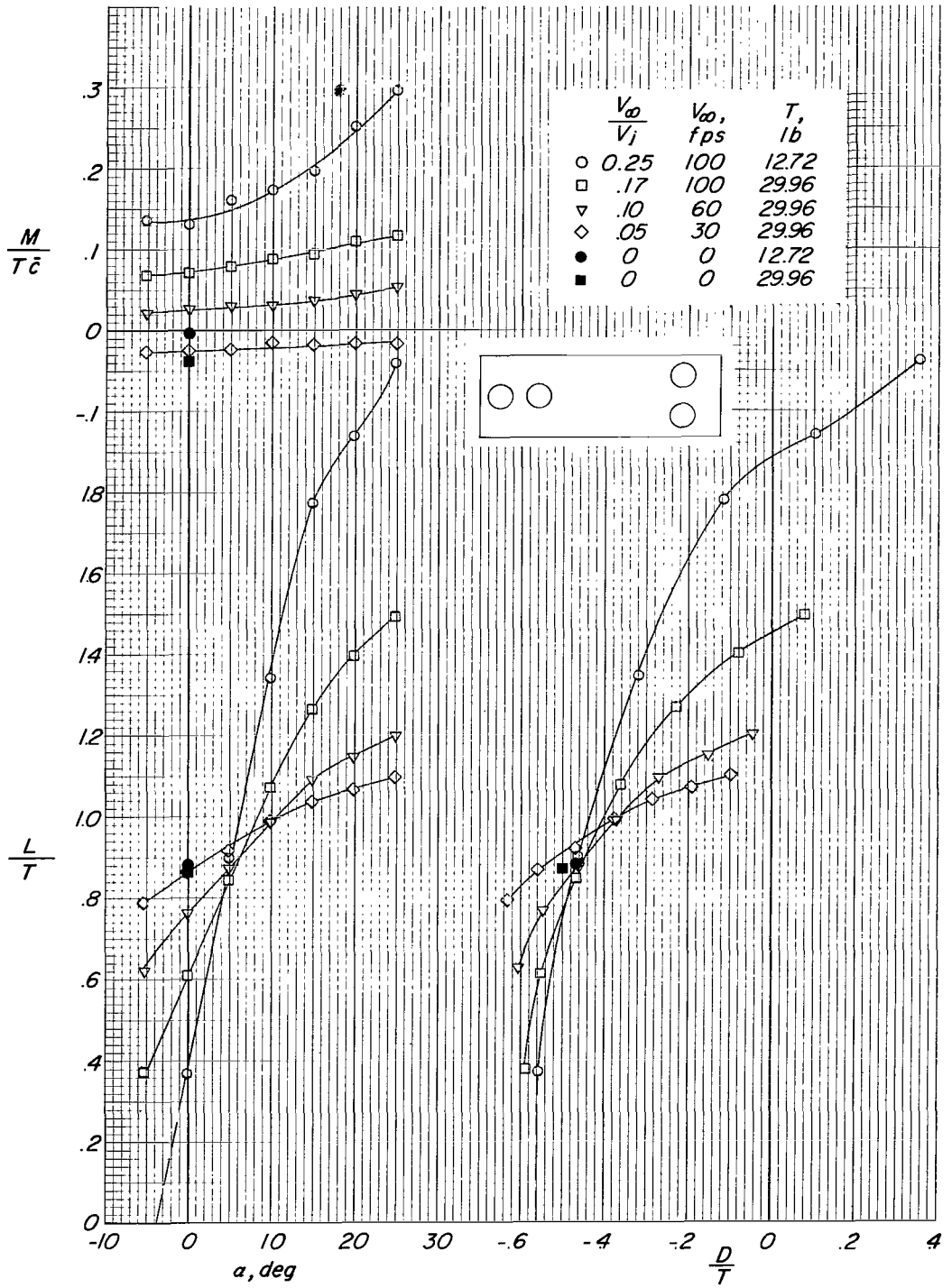

Figure 19.- Jet-on aerodynamic characteristics of configuration 4. Wing in high position; $\delta_j \approx 30^\circ$.

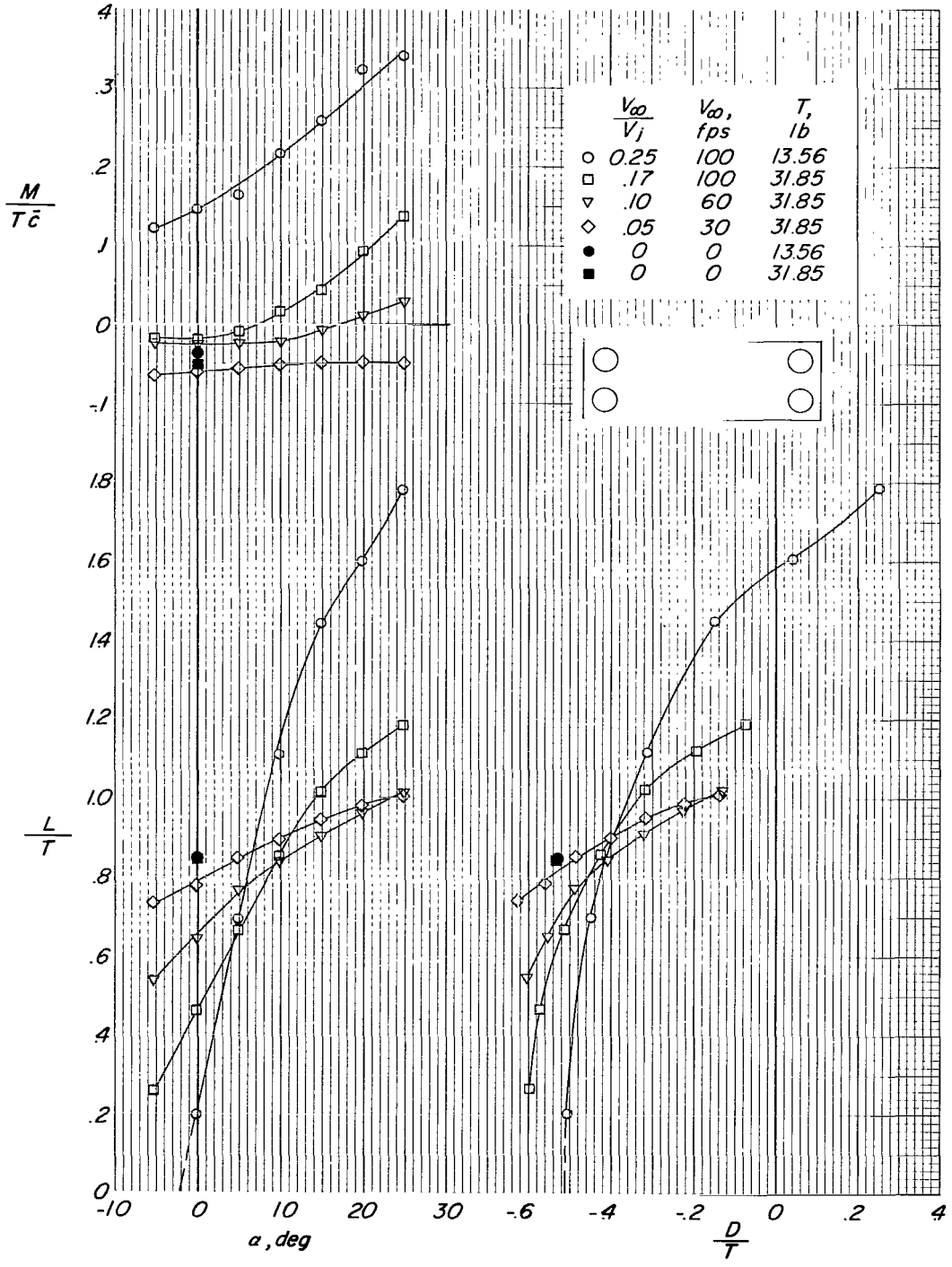

Figure 20.- Jet-on aerodynamic characteristics of configuration 5. Wing in high position; $\delta_j \approx 32^\circ$.

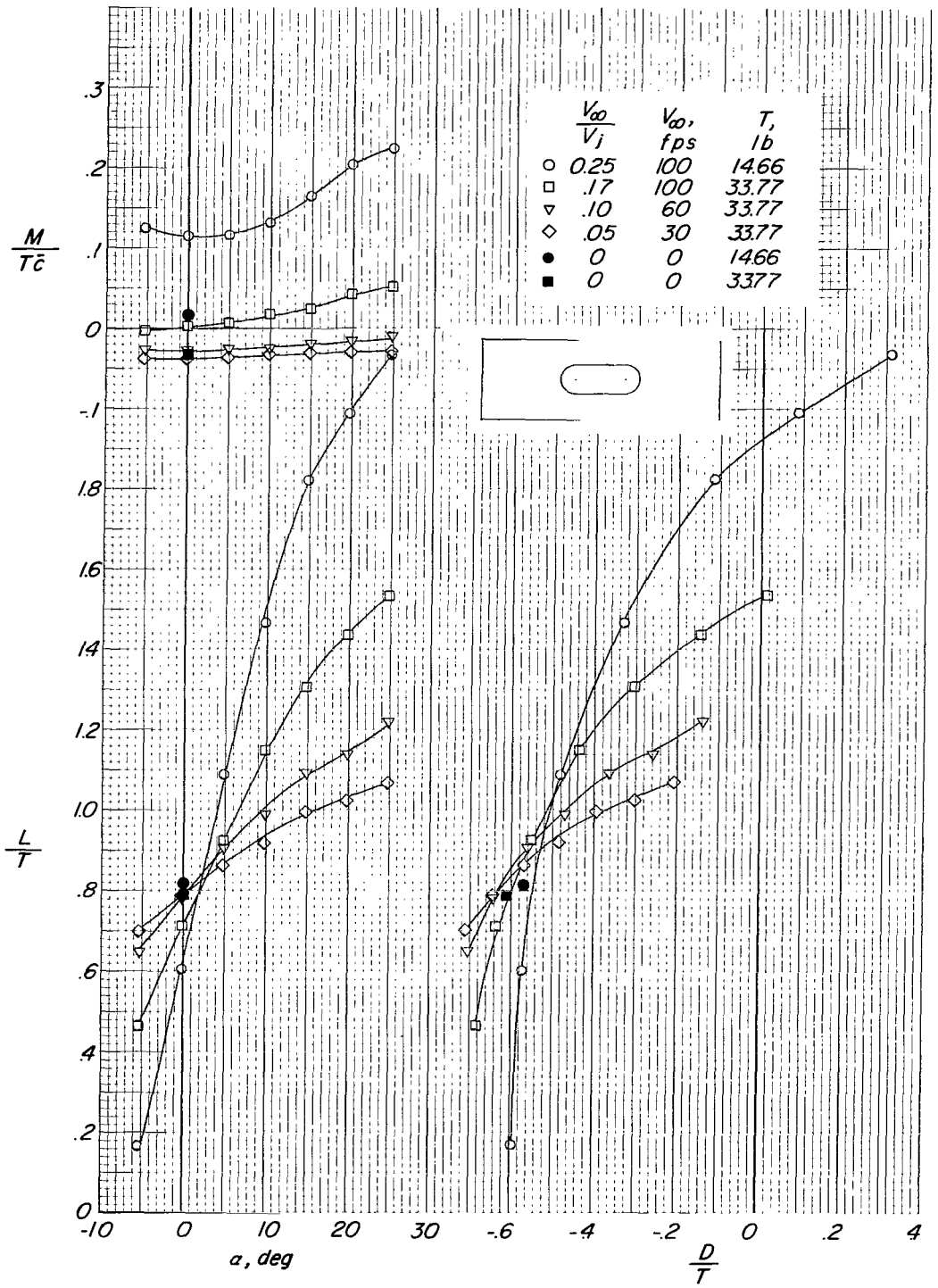

Figure 21.- Jet-on aerodynamic characteristics of configuration 6. Wing in high position; $\delta_j \approx 37^\circ$.

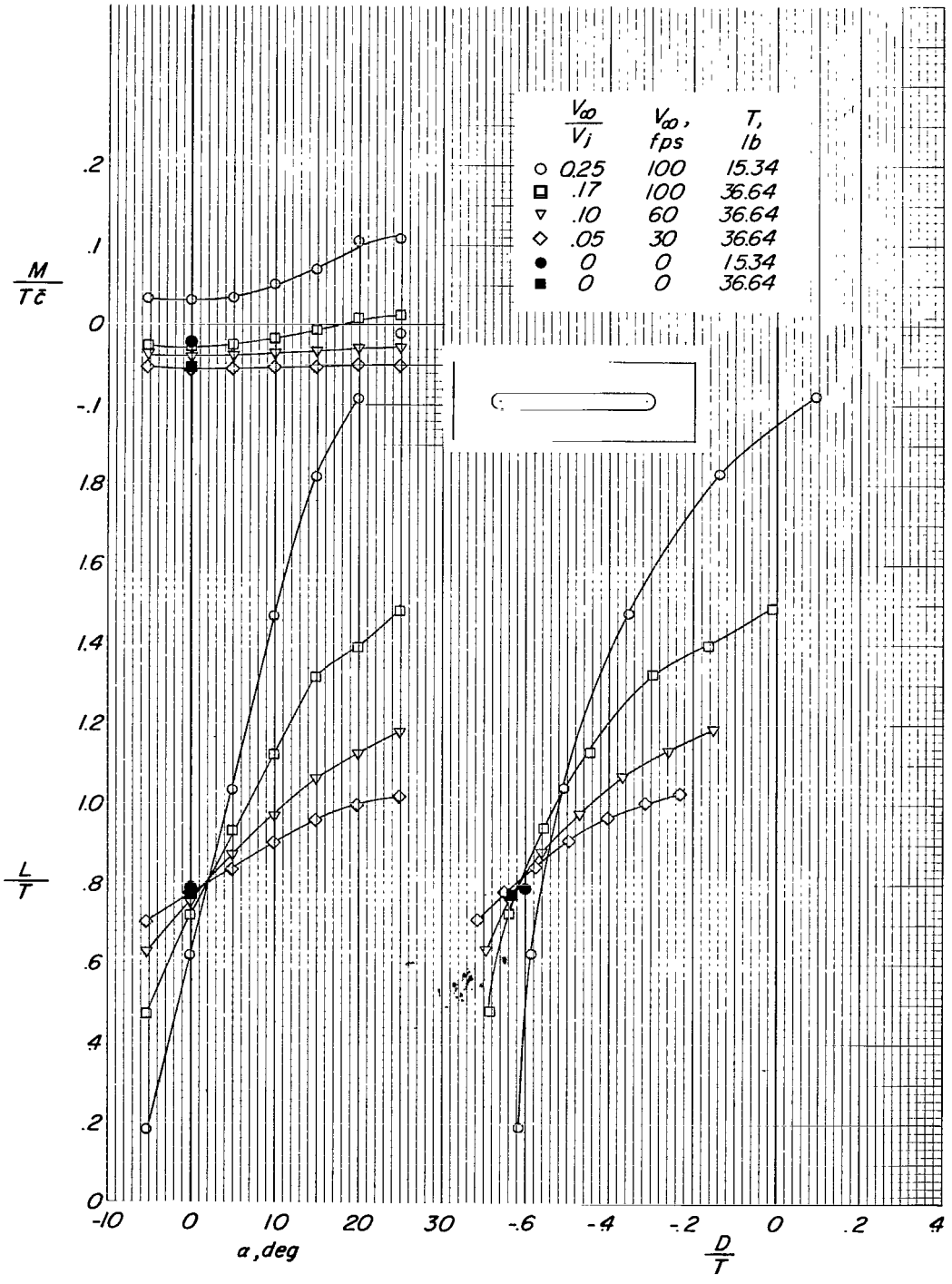

Figure 22.- Jet-on aerodynamic characteristics of configuration 7. Wing in high position; $\delta_j \approx 38^\circ$.

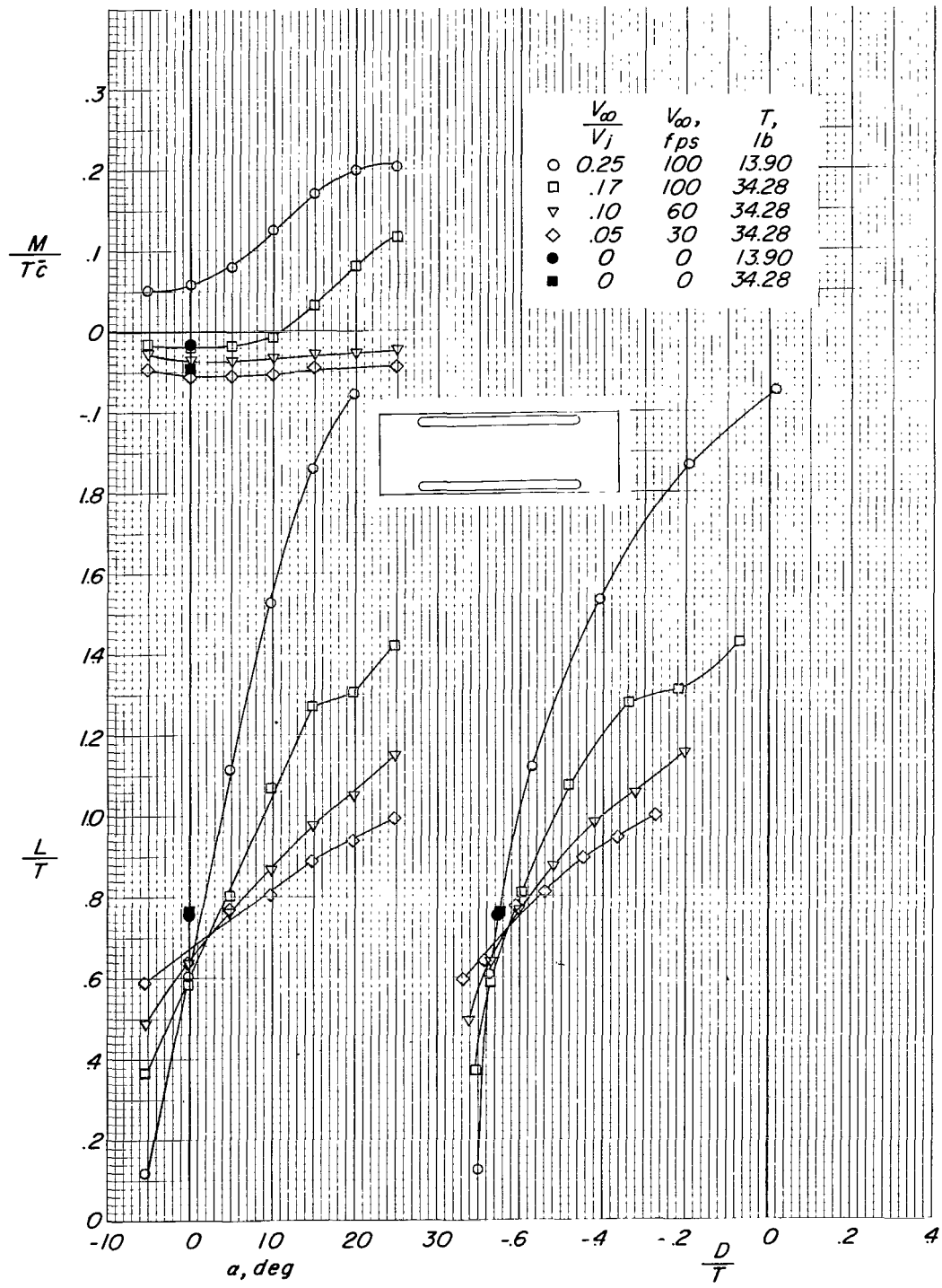

Figure 23.- Jet-on aerodynamic characteristics of configuration 8. Wing in high position; $\delta_j \approx 40°$.

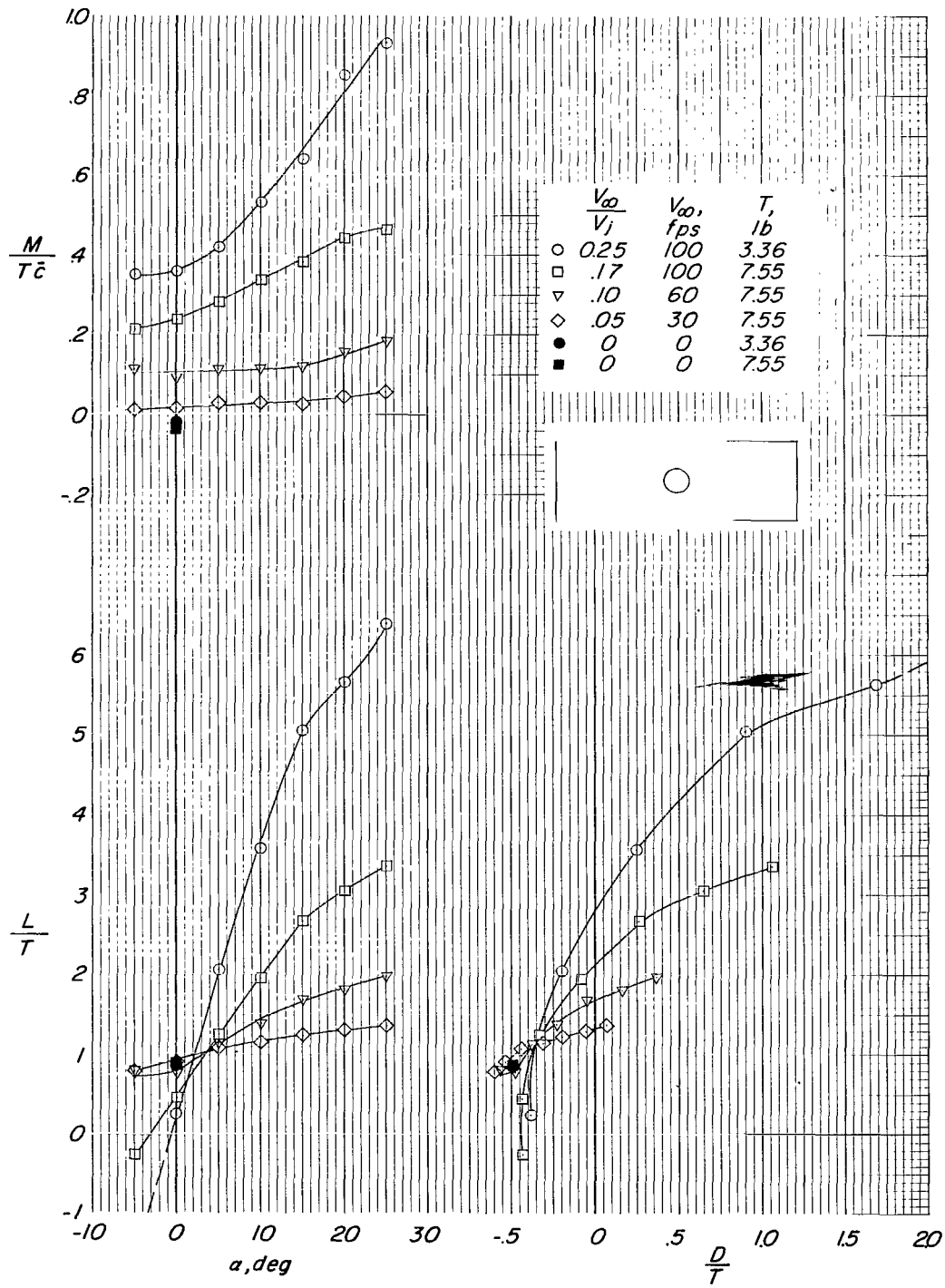

Figure 24.- Jet-on aerodynamic characteristics of configuration 9. Wing in high position; $\delta_j \approx 30^\circ$.

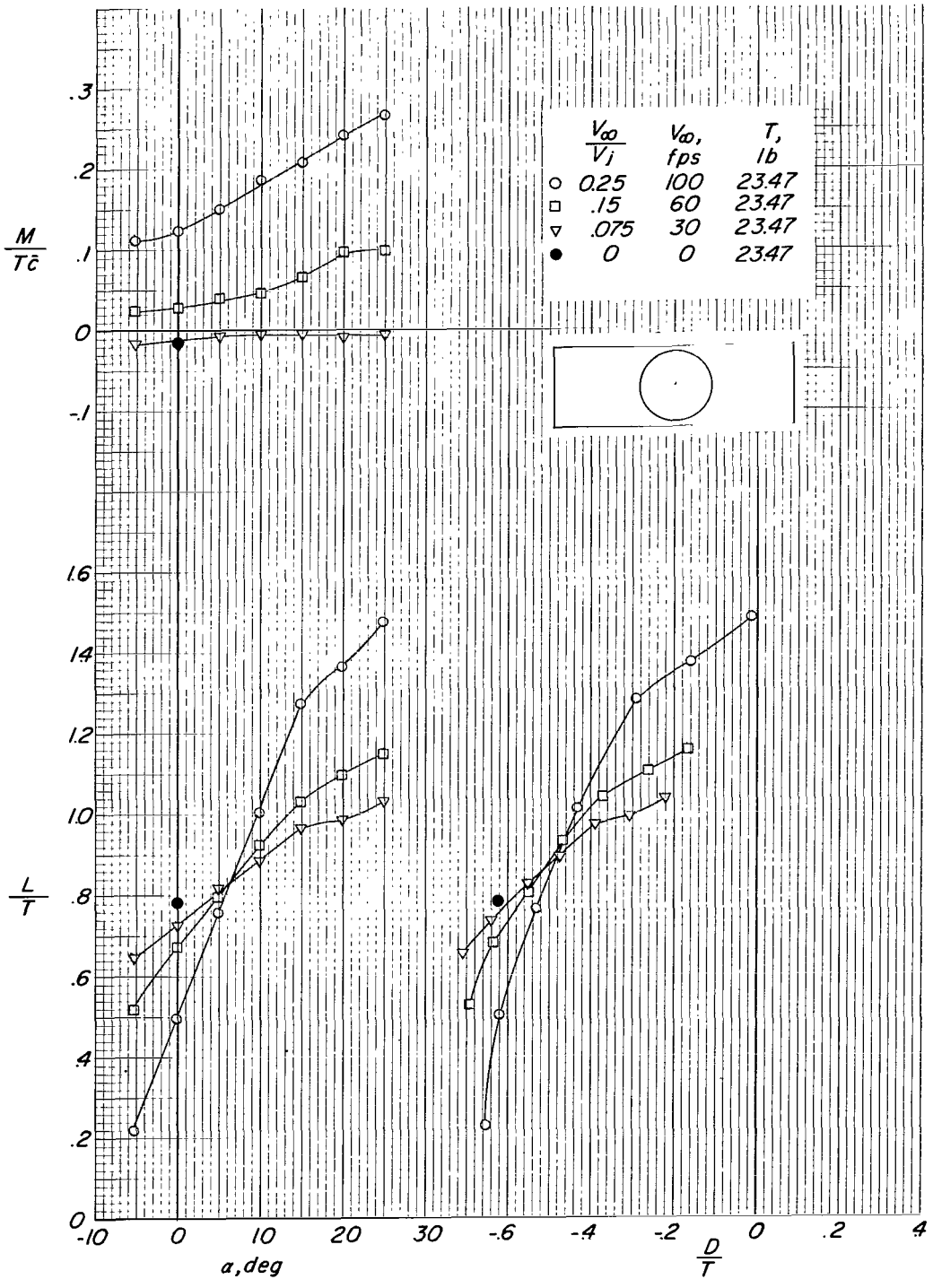

Figure 25.- Jet-on aerodynamic characteristics of configuration 10. Wing in high position; $\delta_j \approx 38^\circ$.

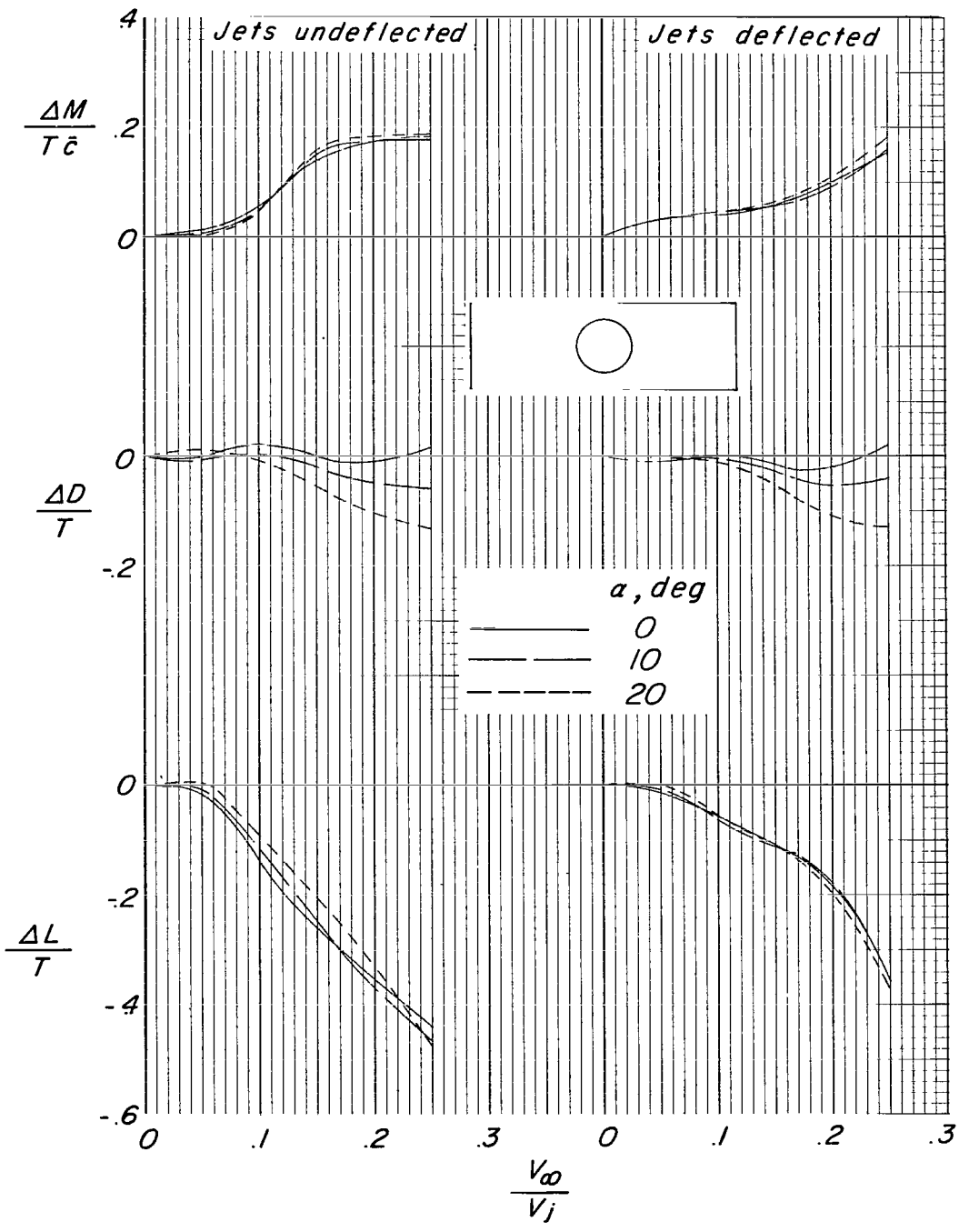

(a) Configuration 1.

Figure 26.- Effect of velocity ratio and angle of attack on the interference increments. Wing in high position.

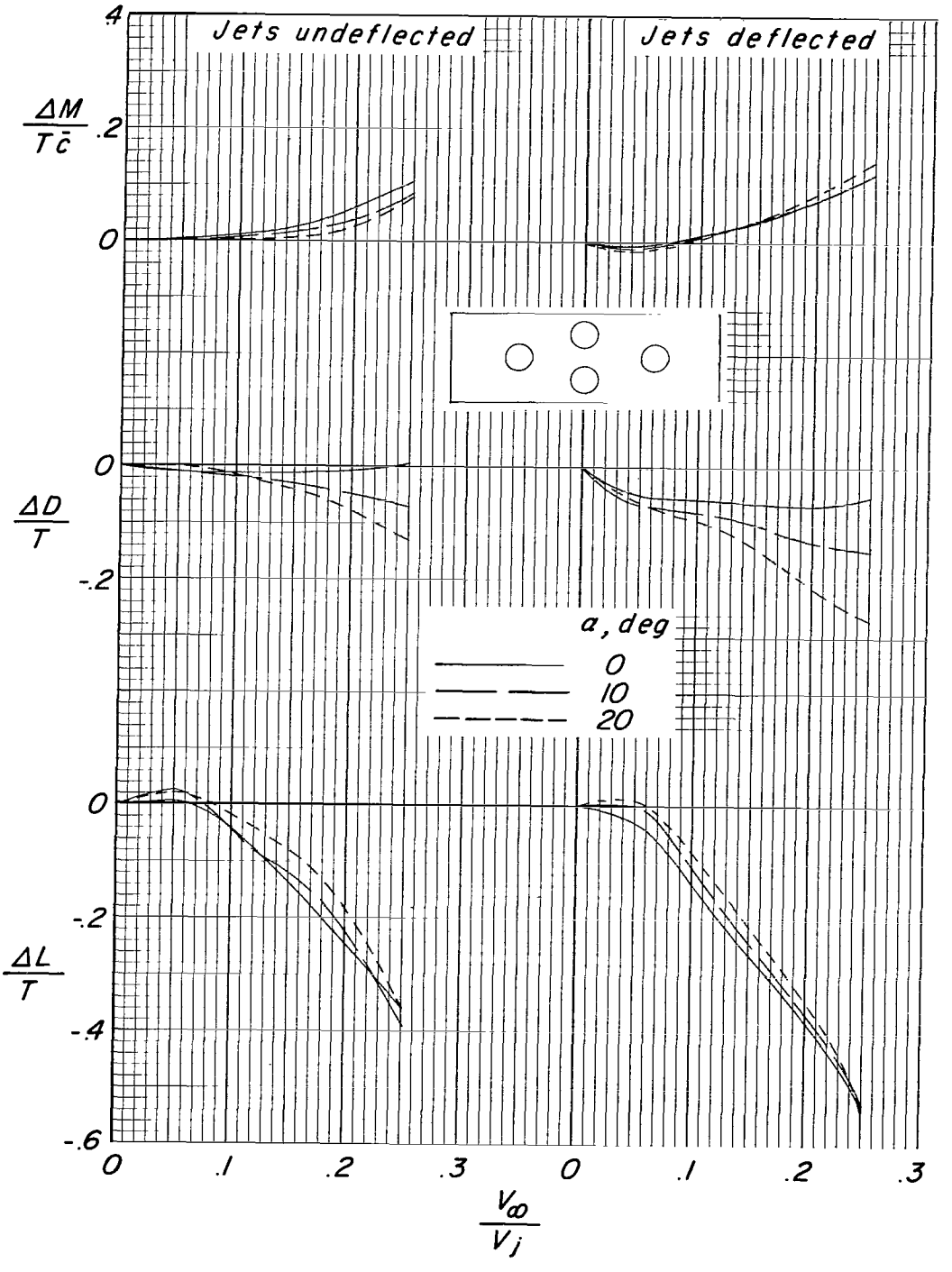

(b) Configuration 2.

Figure 26.- Continued.

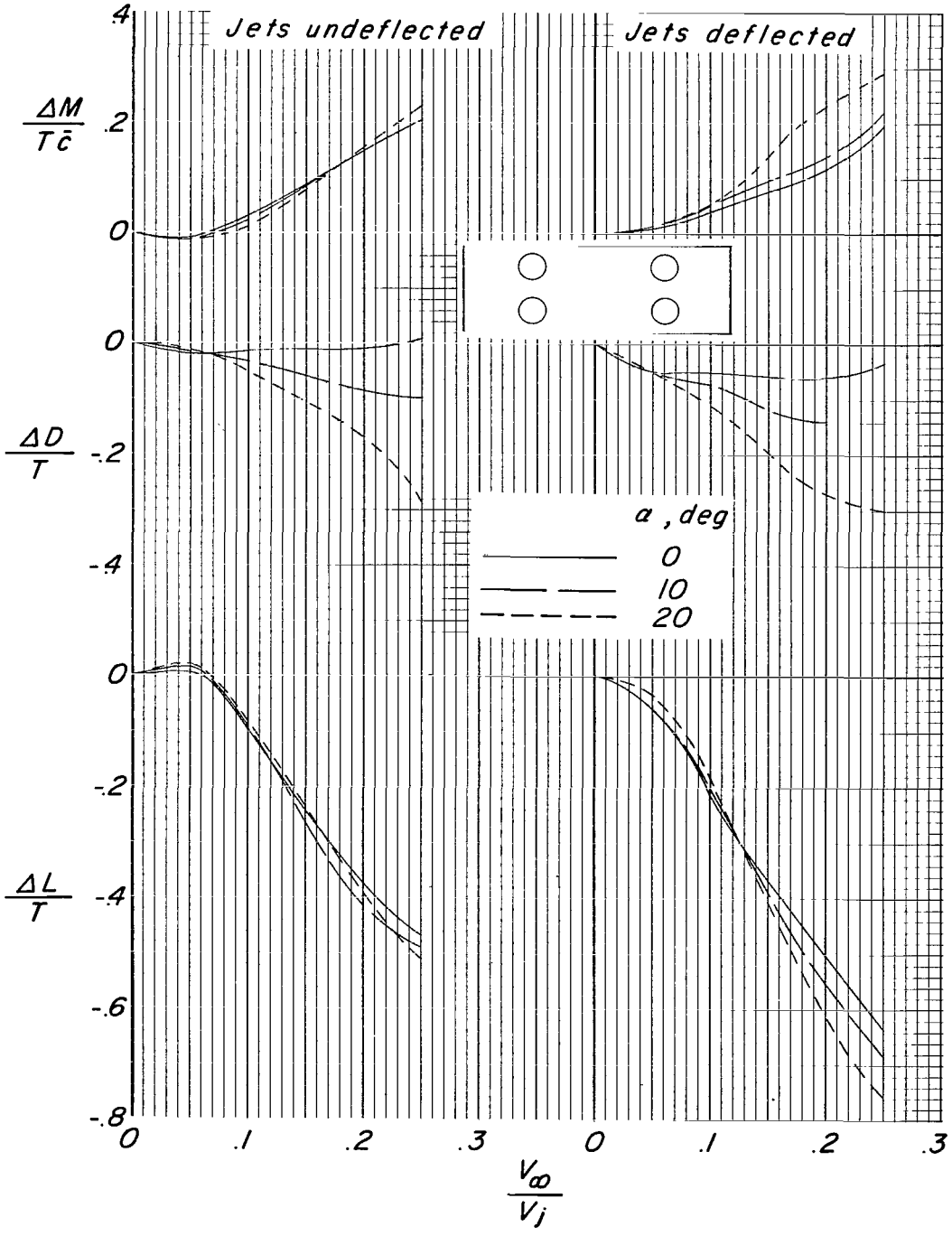

(c) Configuration 3.

Figure 26.- Continued.

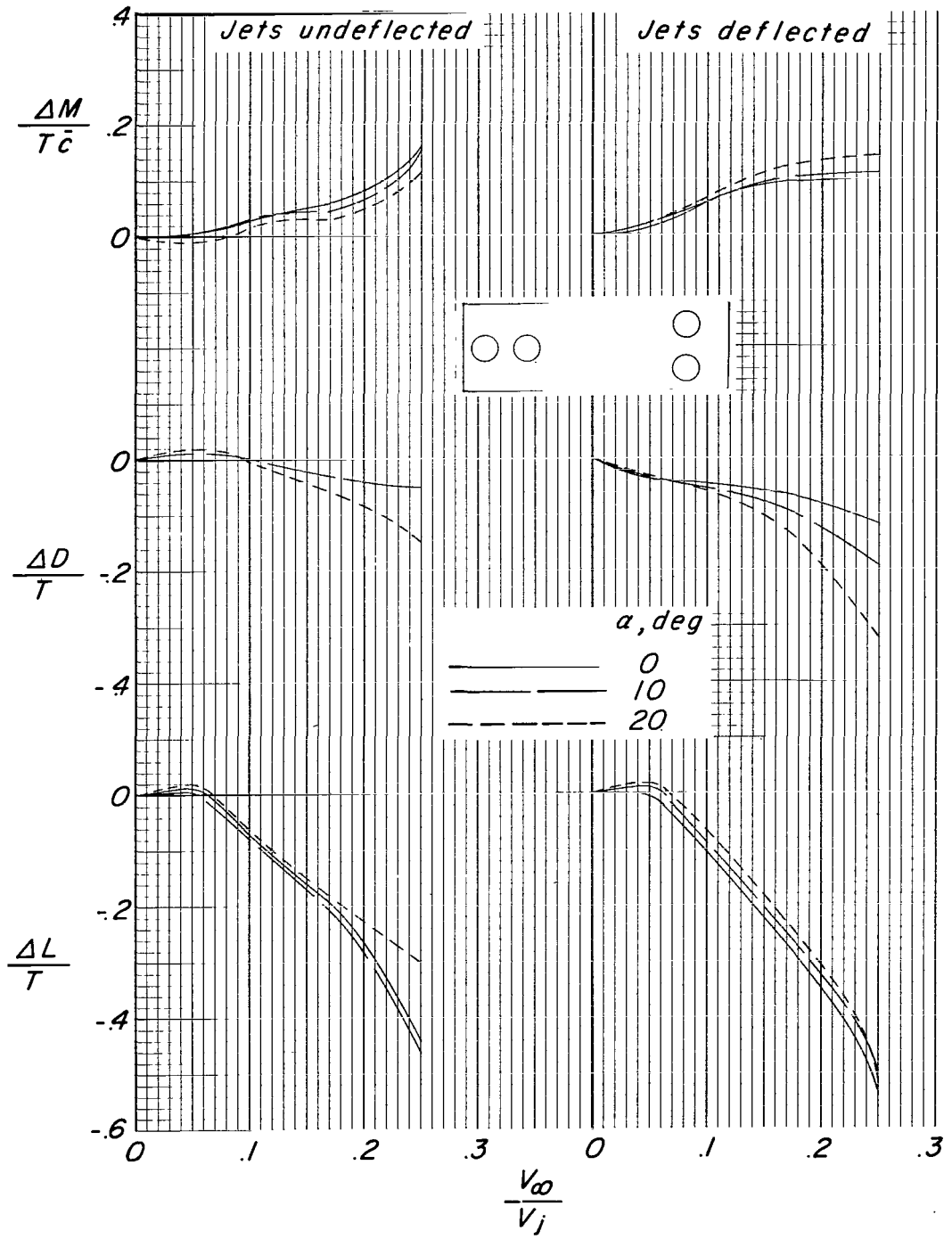

(d) Configuration 4.

Figure 26.- Continued.

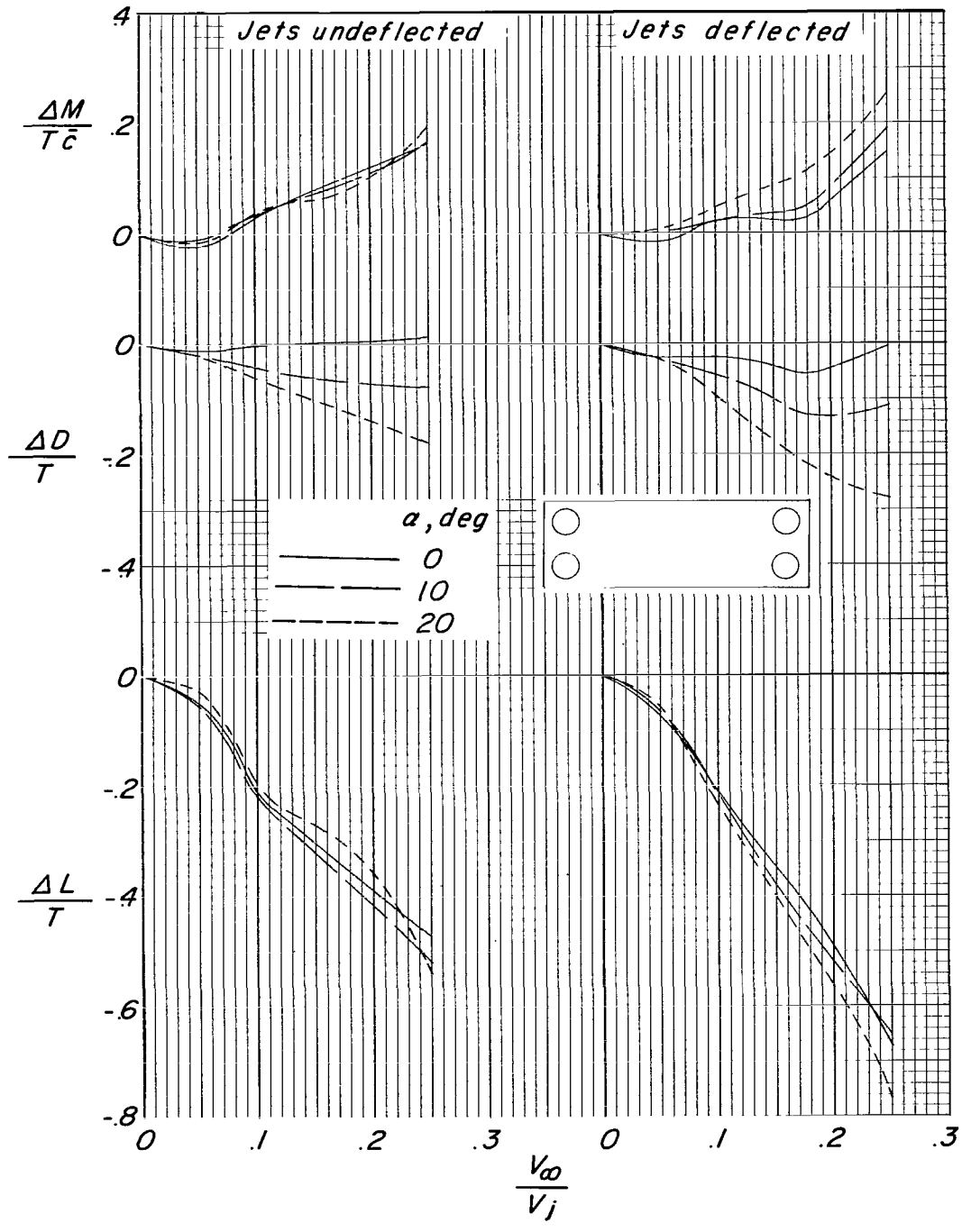

(e) Configuration 5.

Figure 26.- Continued.

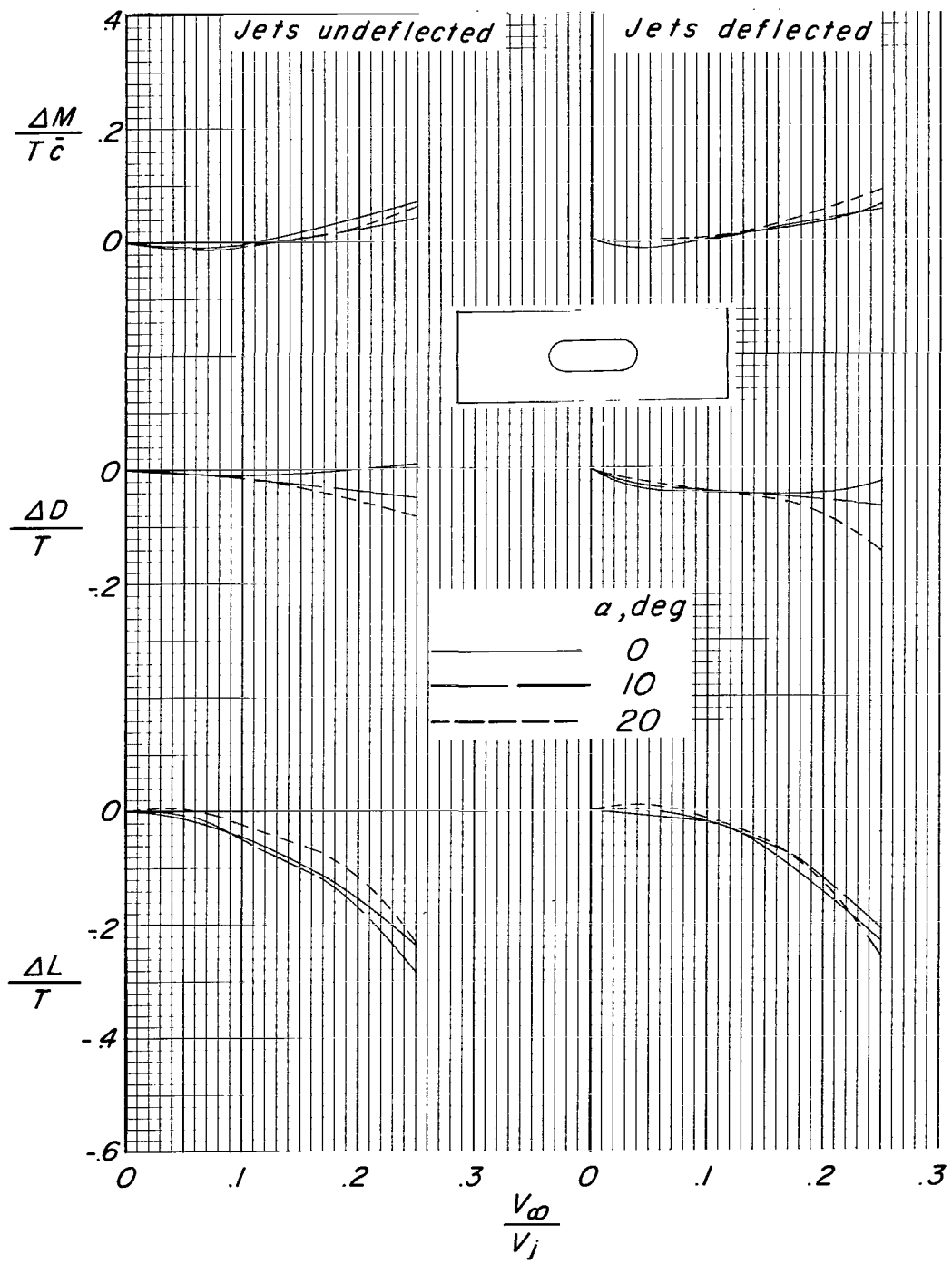

(f) Configuration 6.

Figure 26.- Continued.

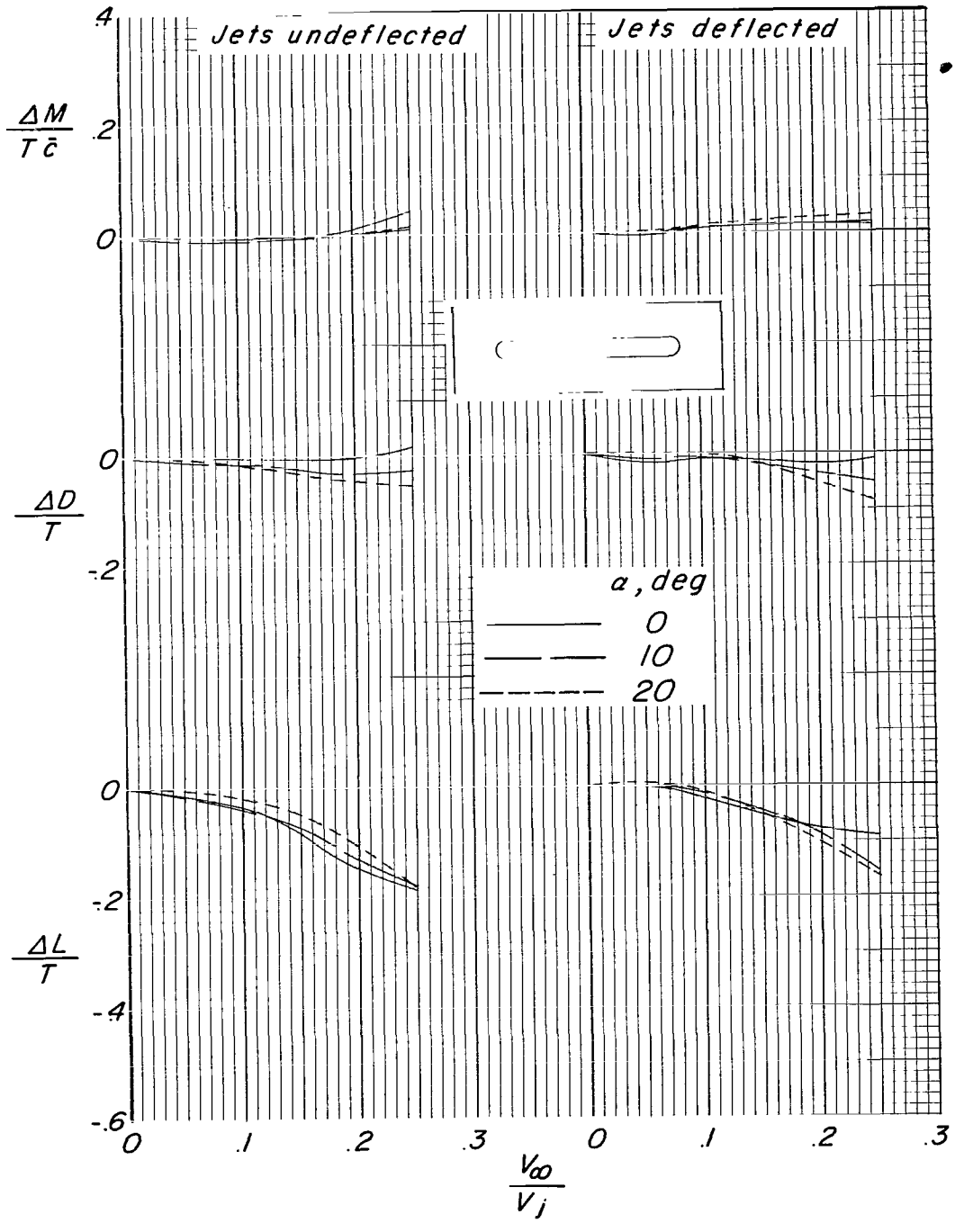

(g) Configuration 7.

Figure 26.- Continued.

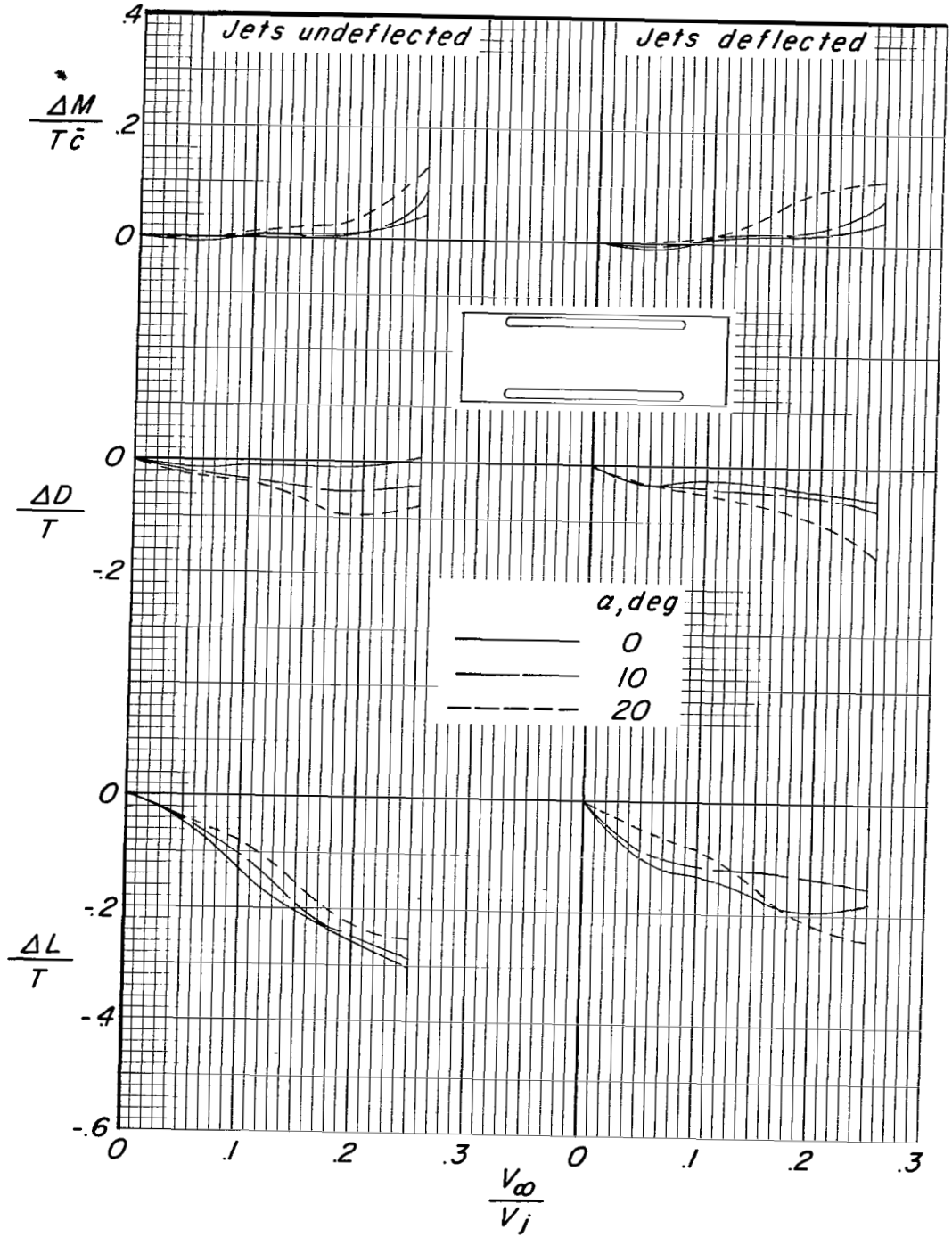

(h) Configuration 8.

Figure 26.- Continued.

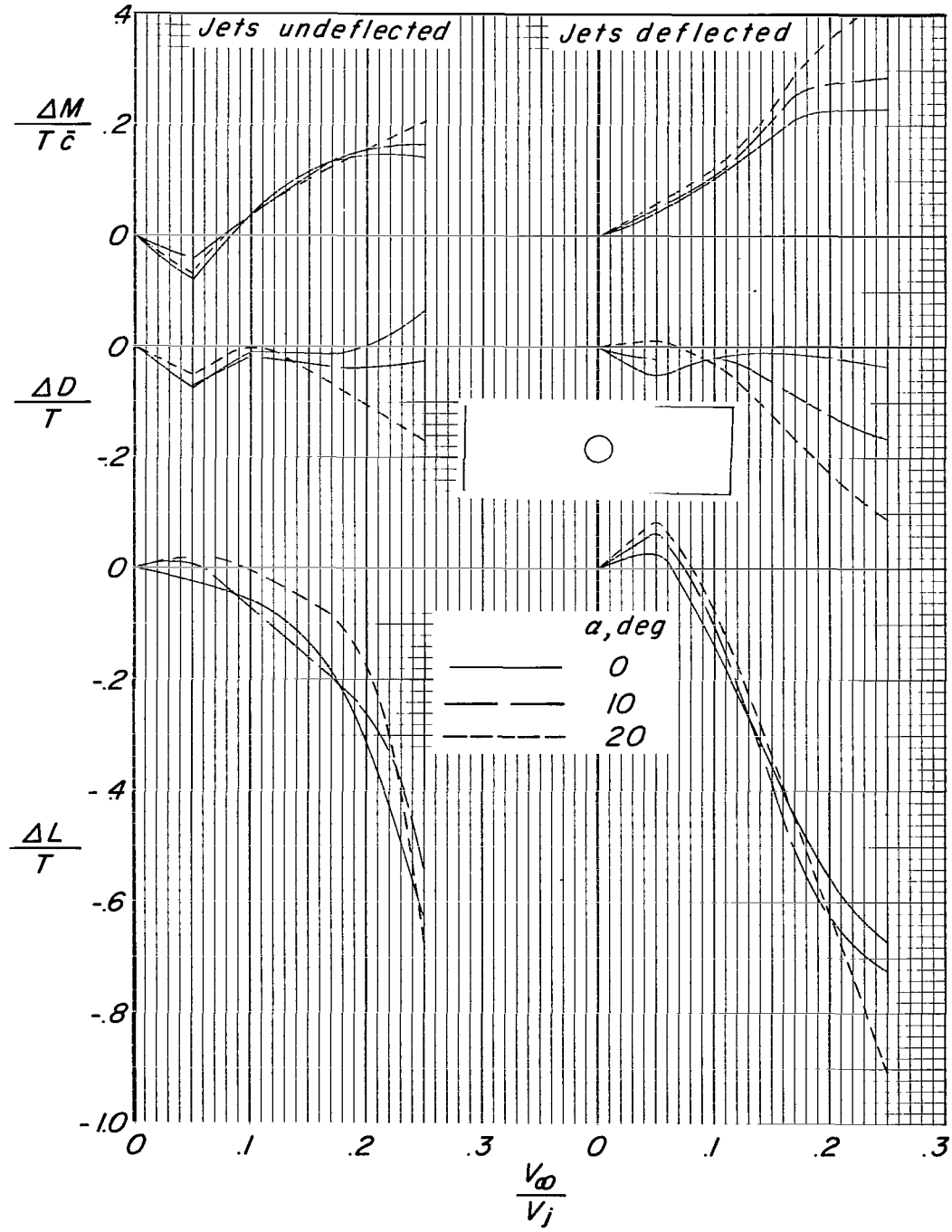

(i) Configuration 9.

Figure 26.- Continued.

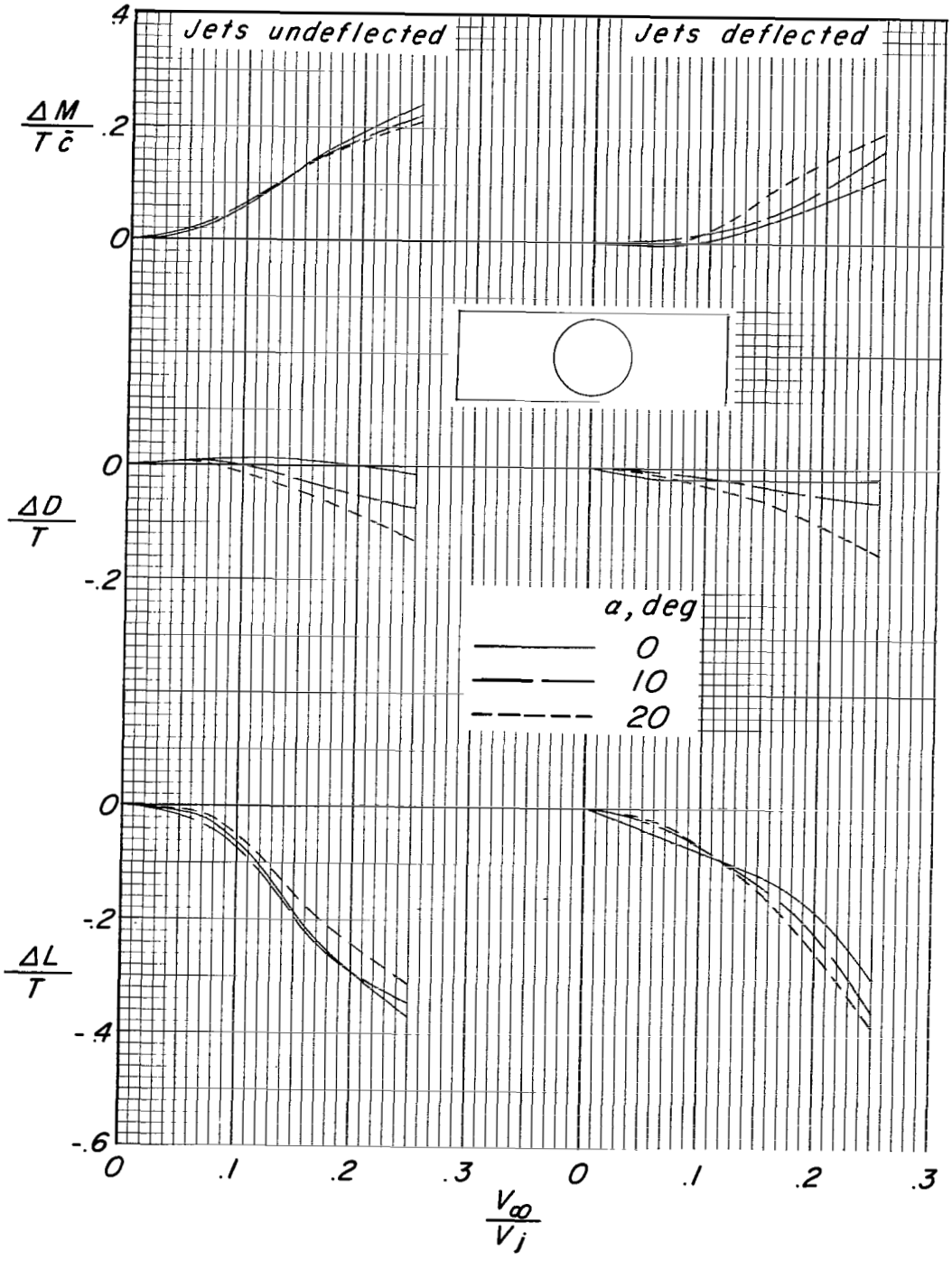

(j) Configuration 10.

Figure 26.- Concluded.

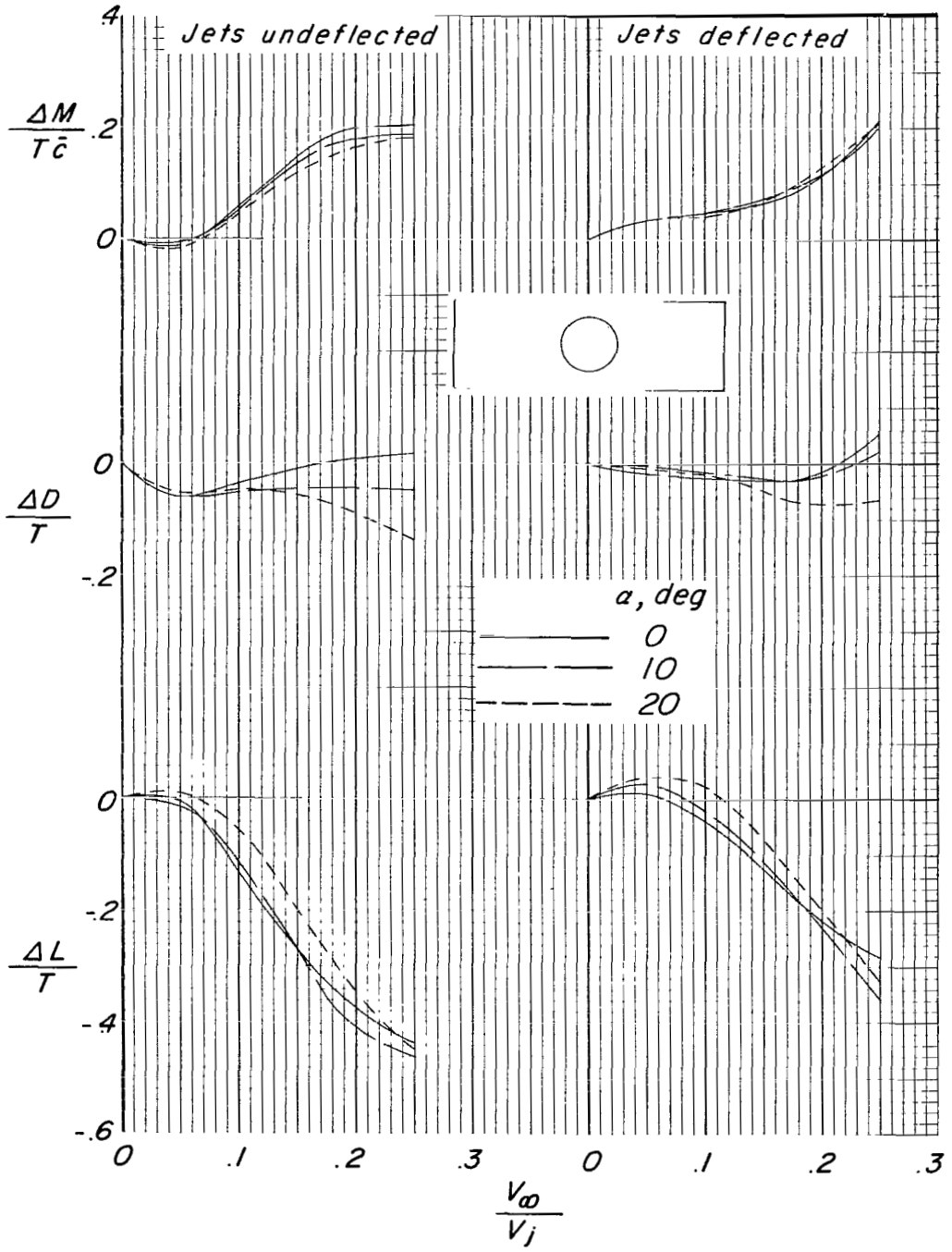

(a) Configuration 1.

Figure 27.- Effect of velocity ratio and angle of attack on the interference increments. Wing in low position.

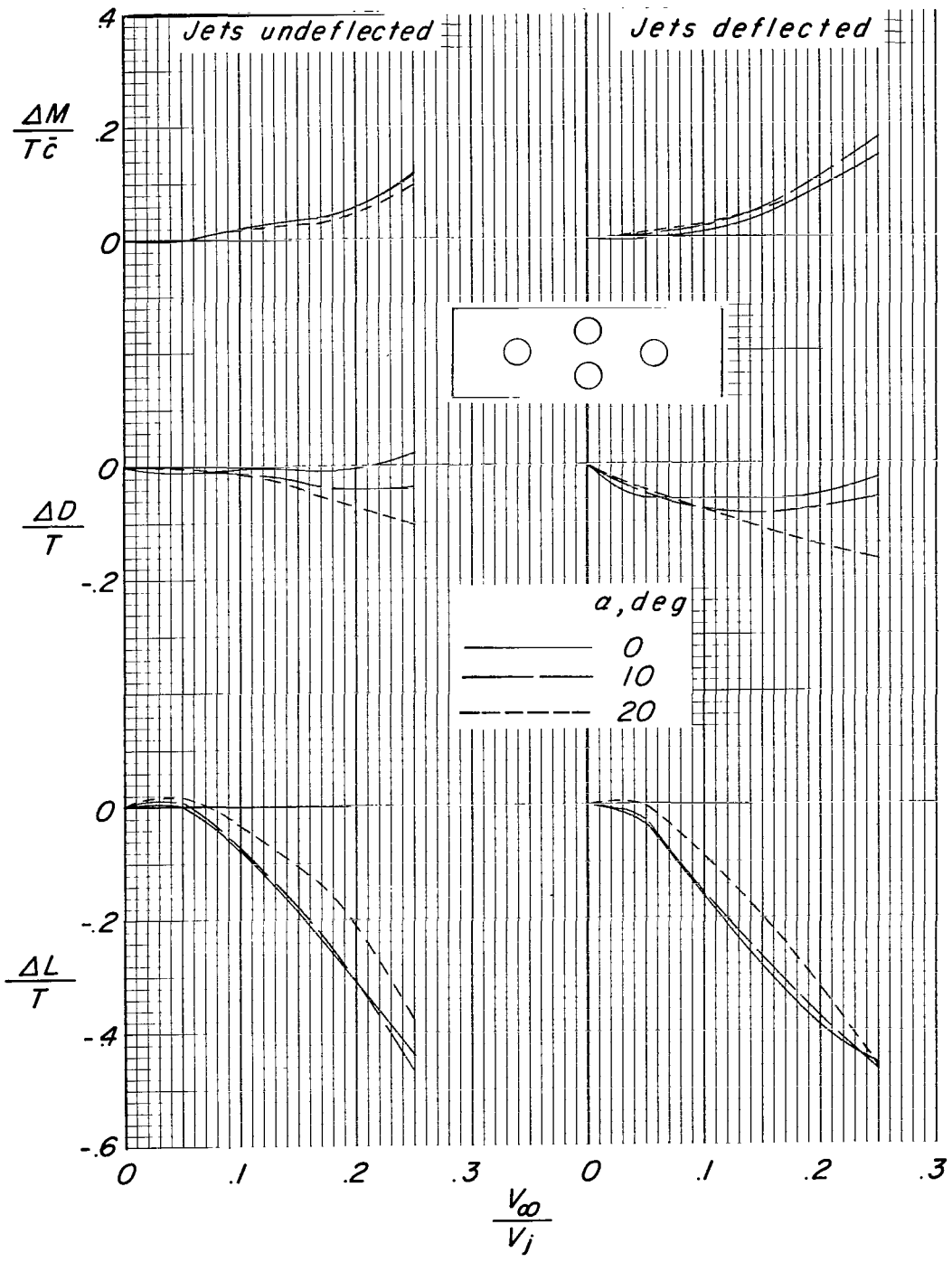

(b) Configuration 2.

Figure 27.- Continued.

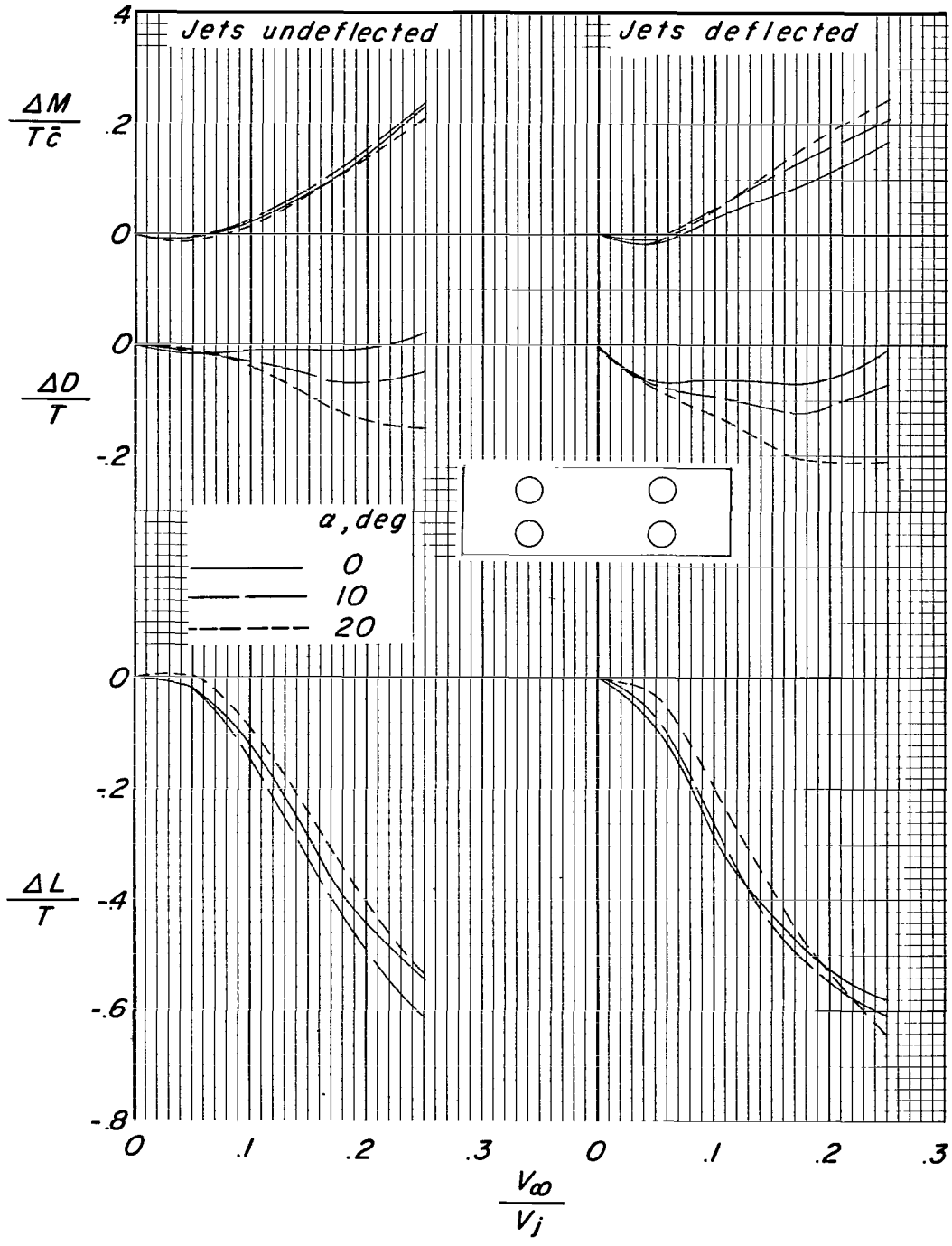

(c) Configuration 3.

Figure 27.- Concluded.

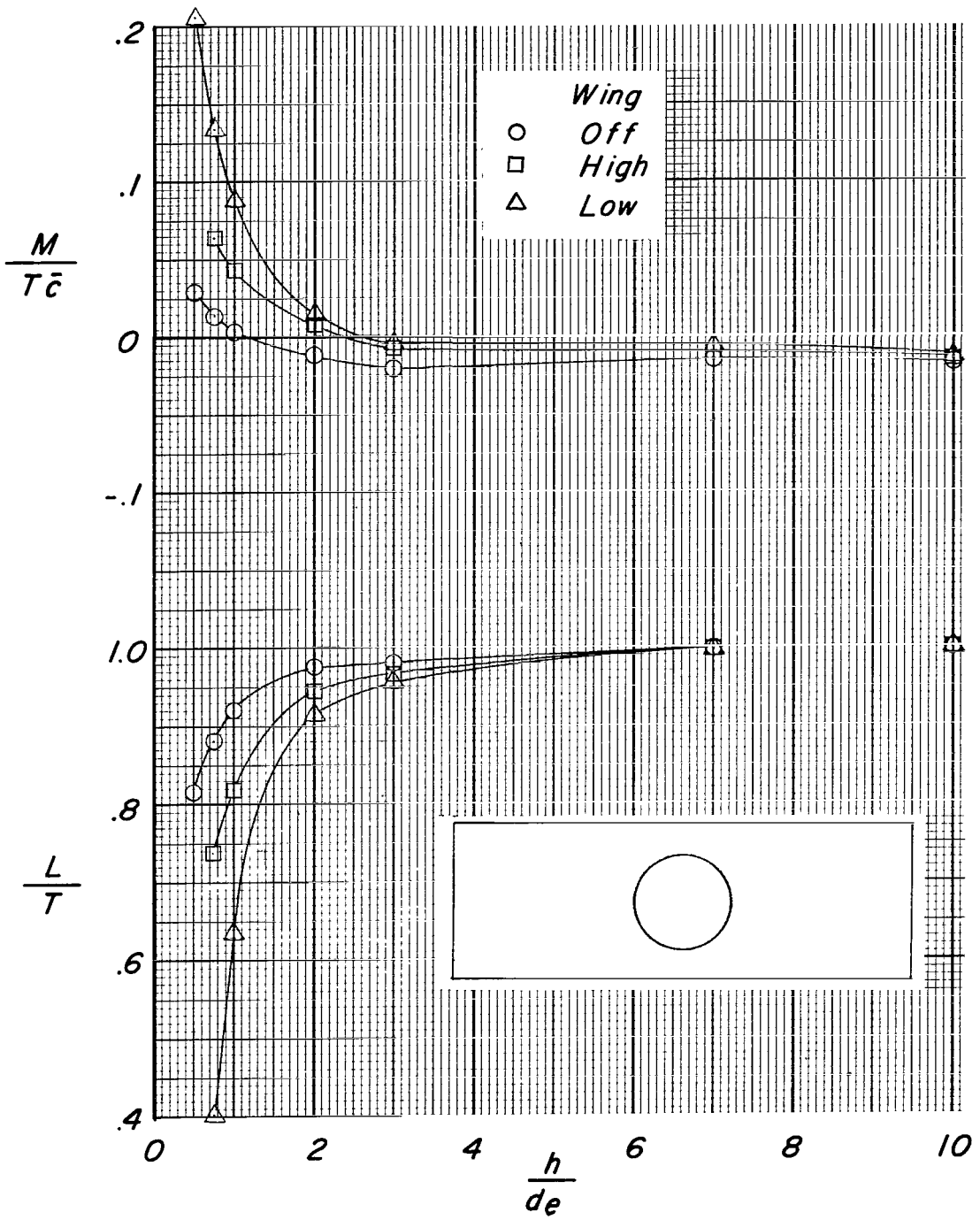

(a) Configuration 1.

Figure 28.- Effect of height above the ground on the lift and pitching moment of the model. Jets undeflected.

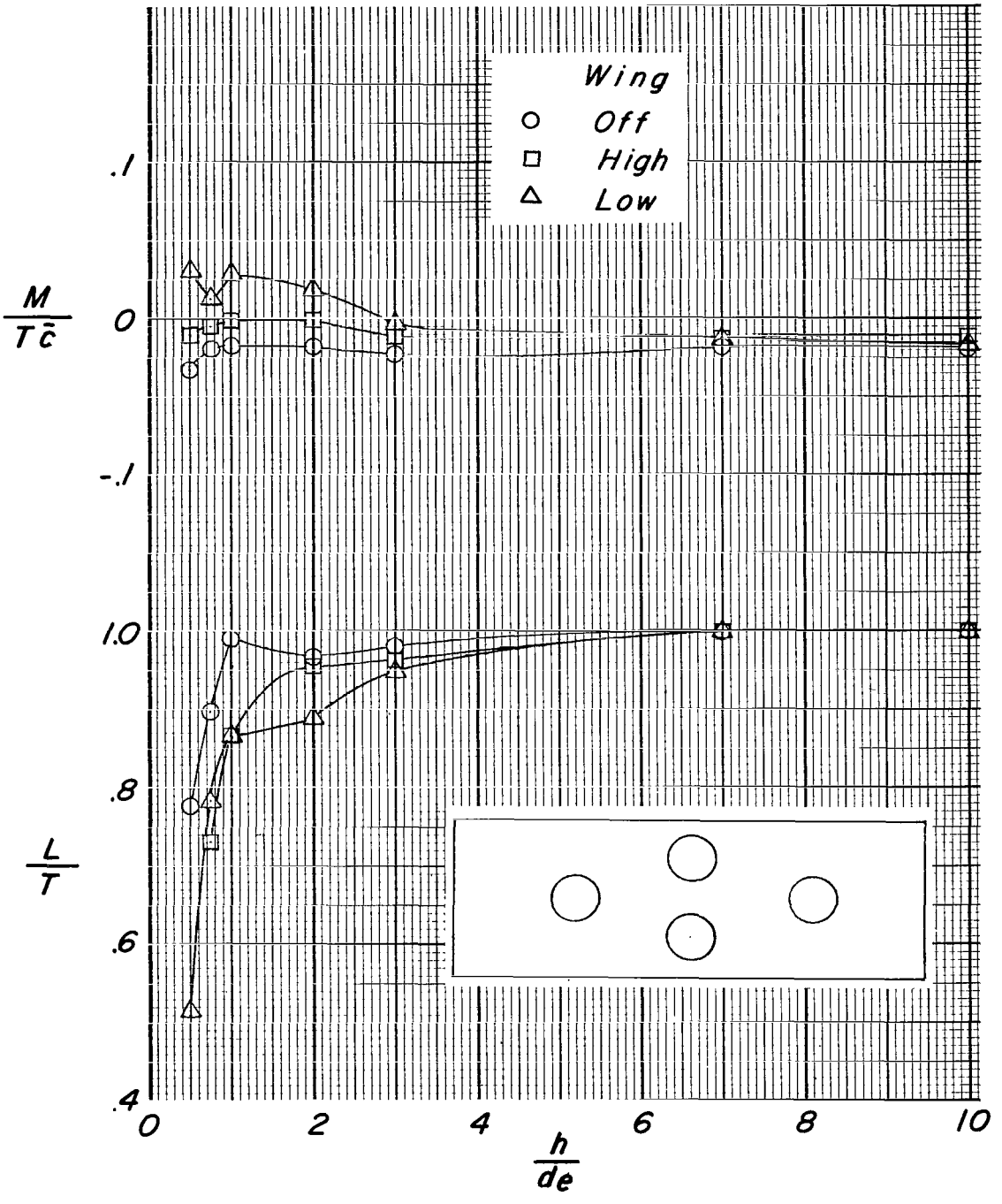

(b) Configuration 2.

Figure 28.- Continued.

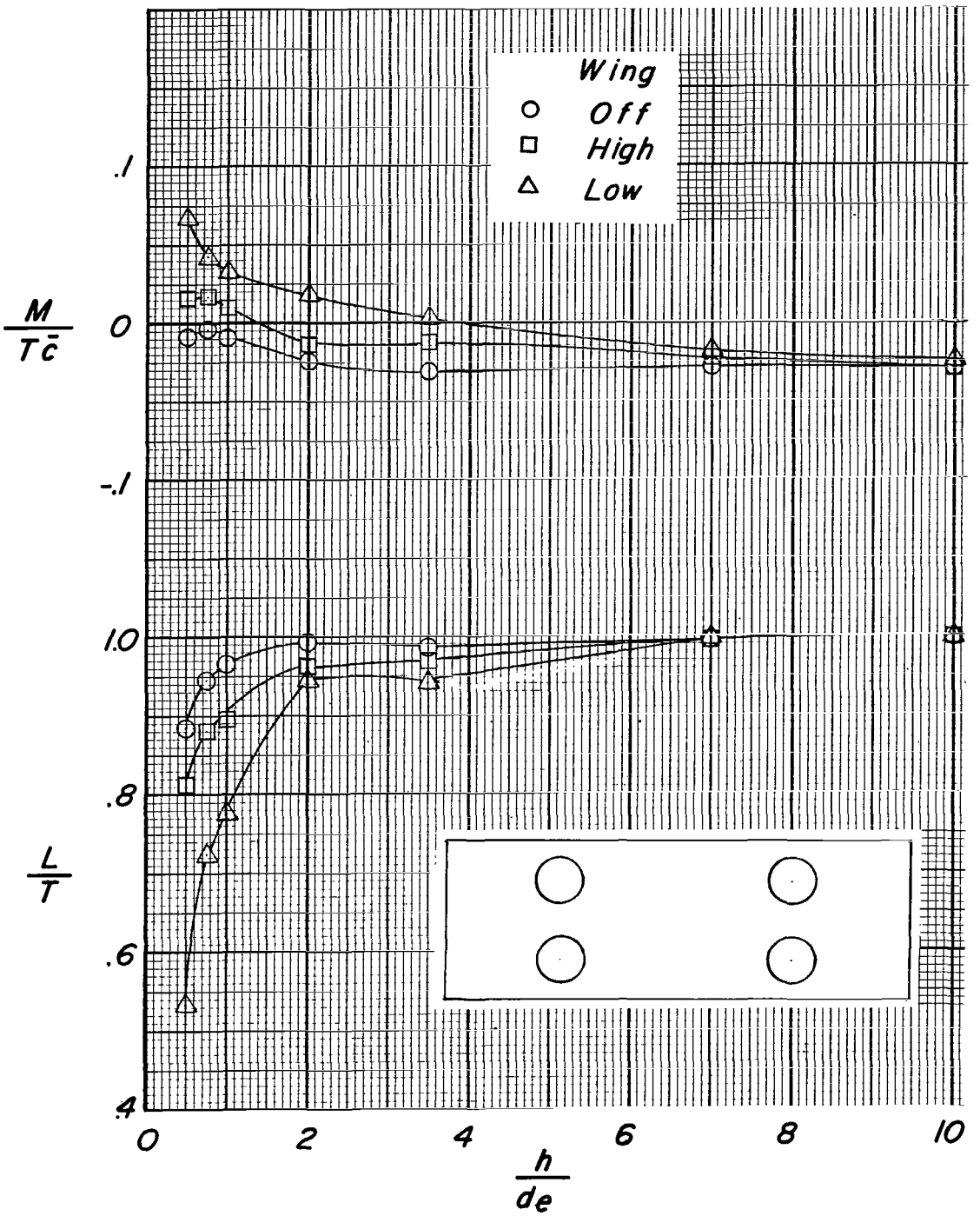

(c) Configuration 3.

Figure 28.- Continued.

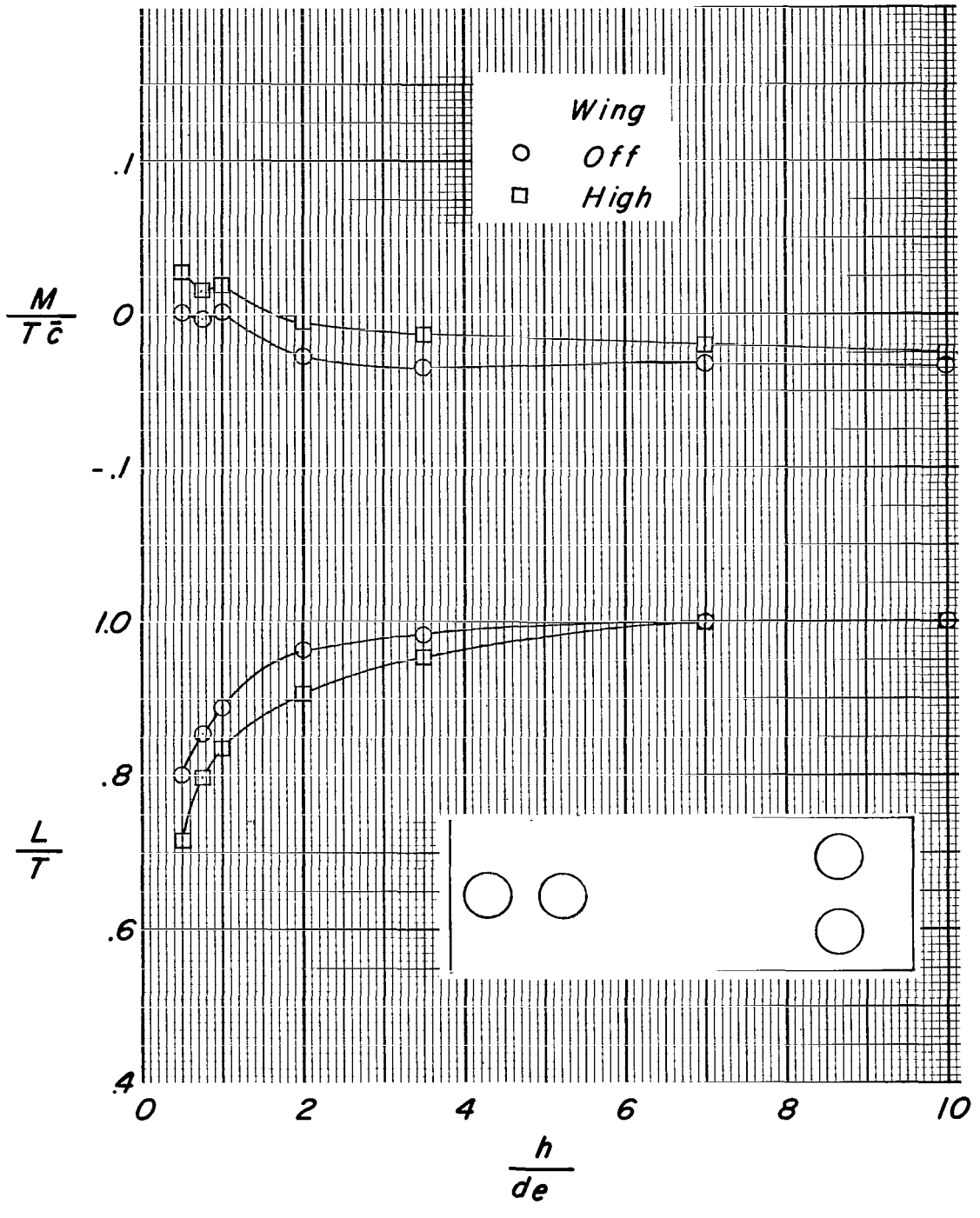

(d) Configuration 4.

Figure 28.- Continued.

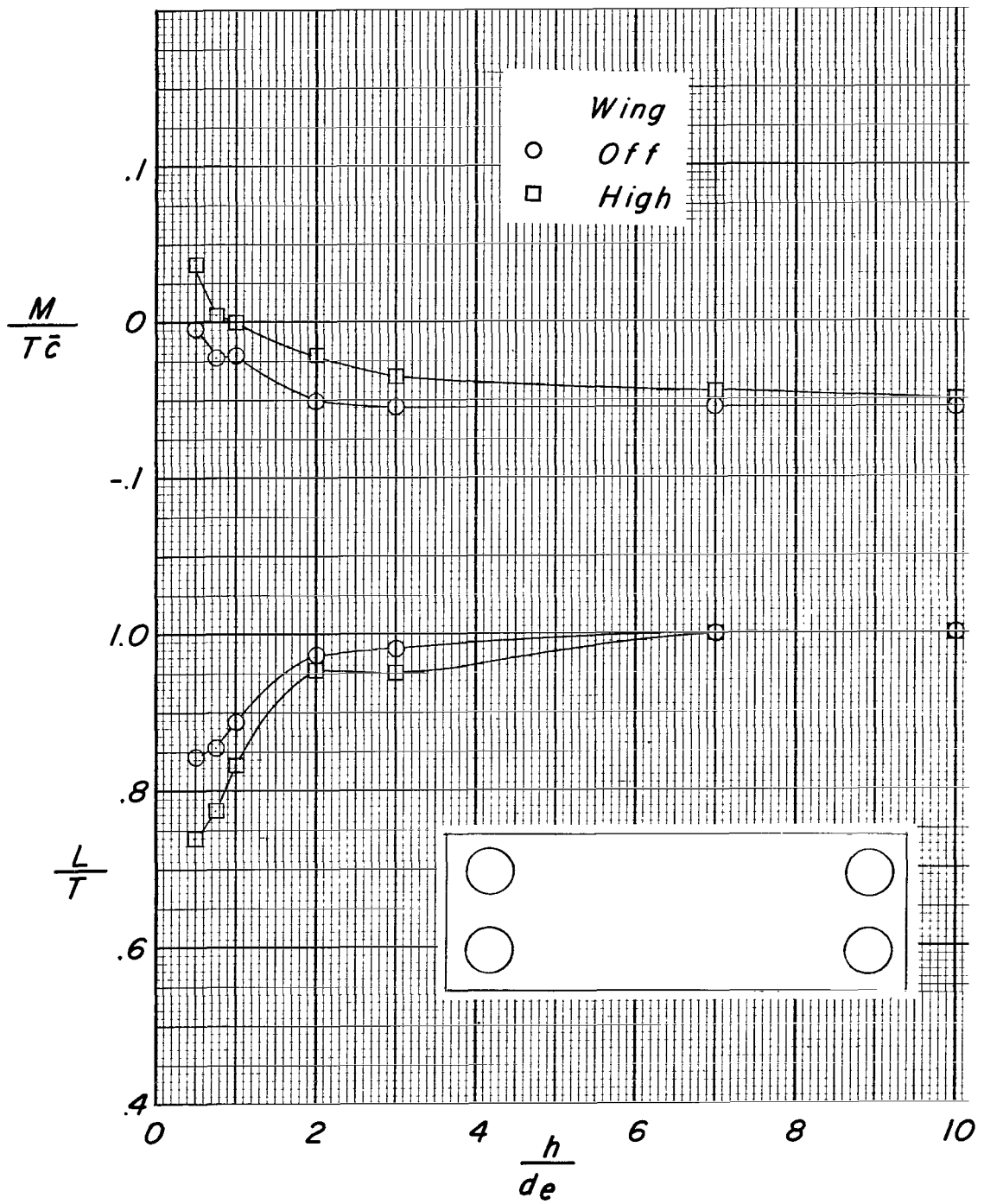

(e) Configuration 5.

Figure 28.- Continued.

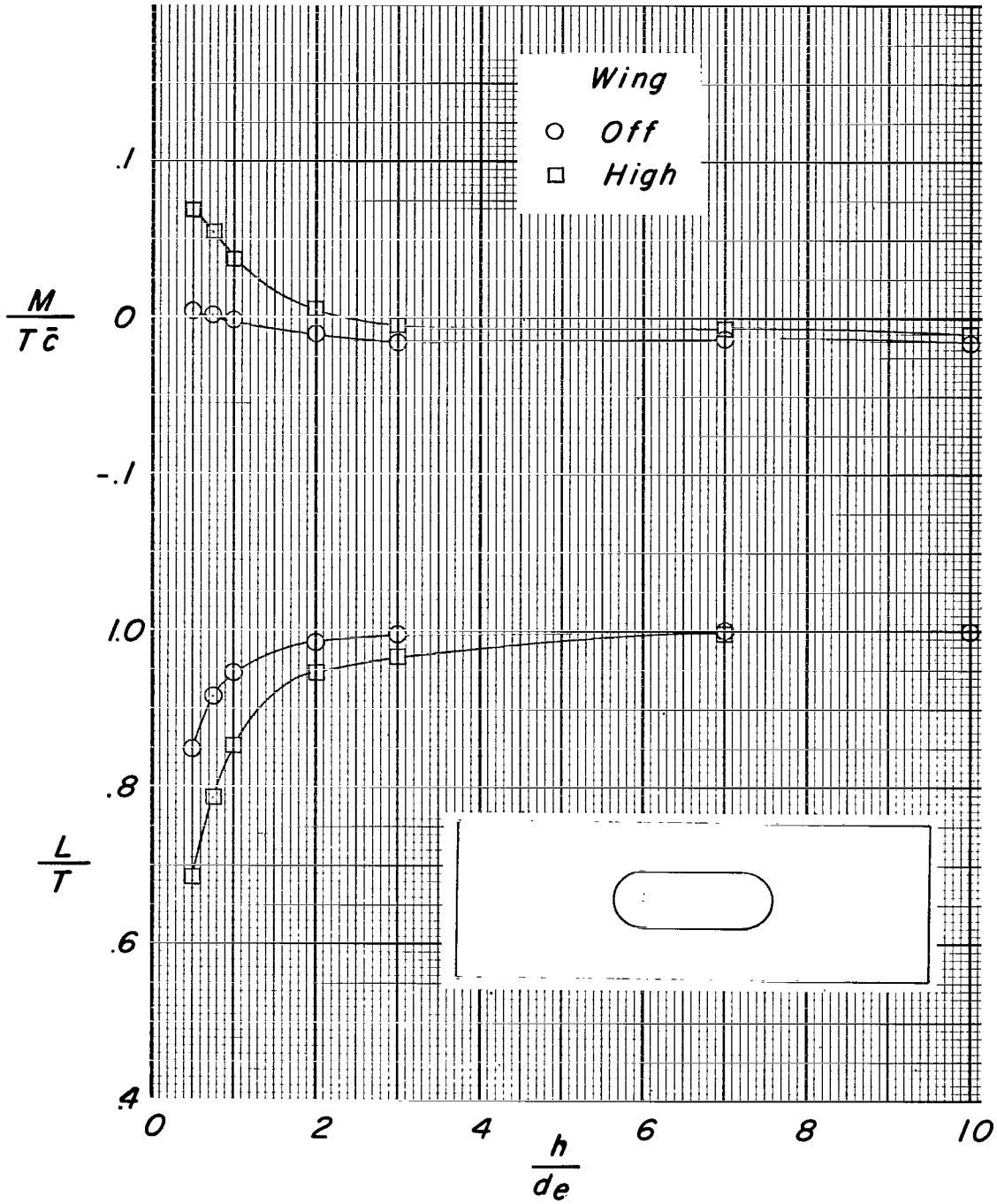

(f) Configuration 6.

Figure 28.- Continued.

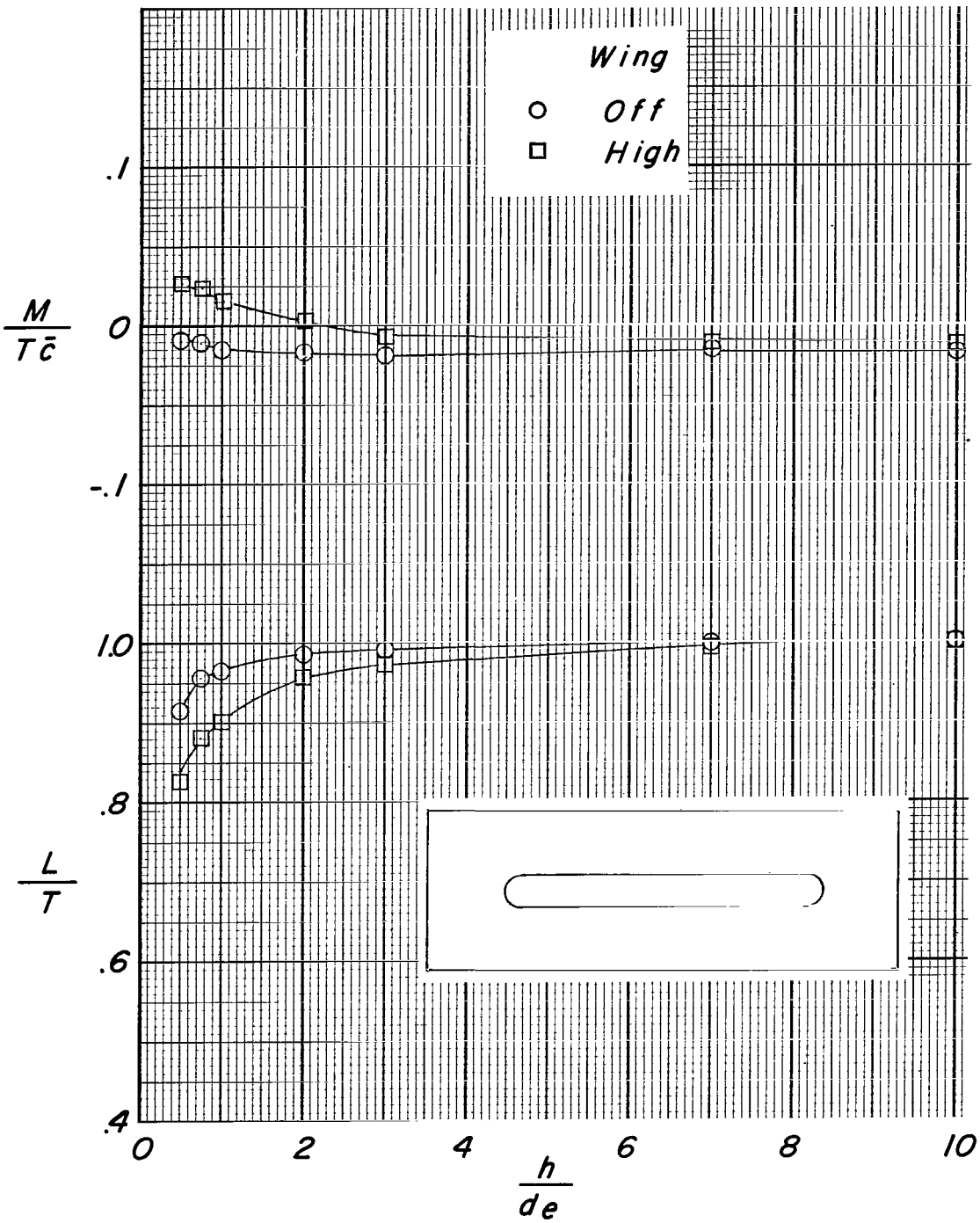

(g) Configuration 7.

Figure 28.- Continued.

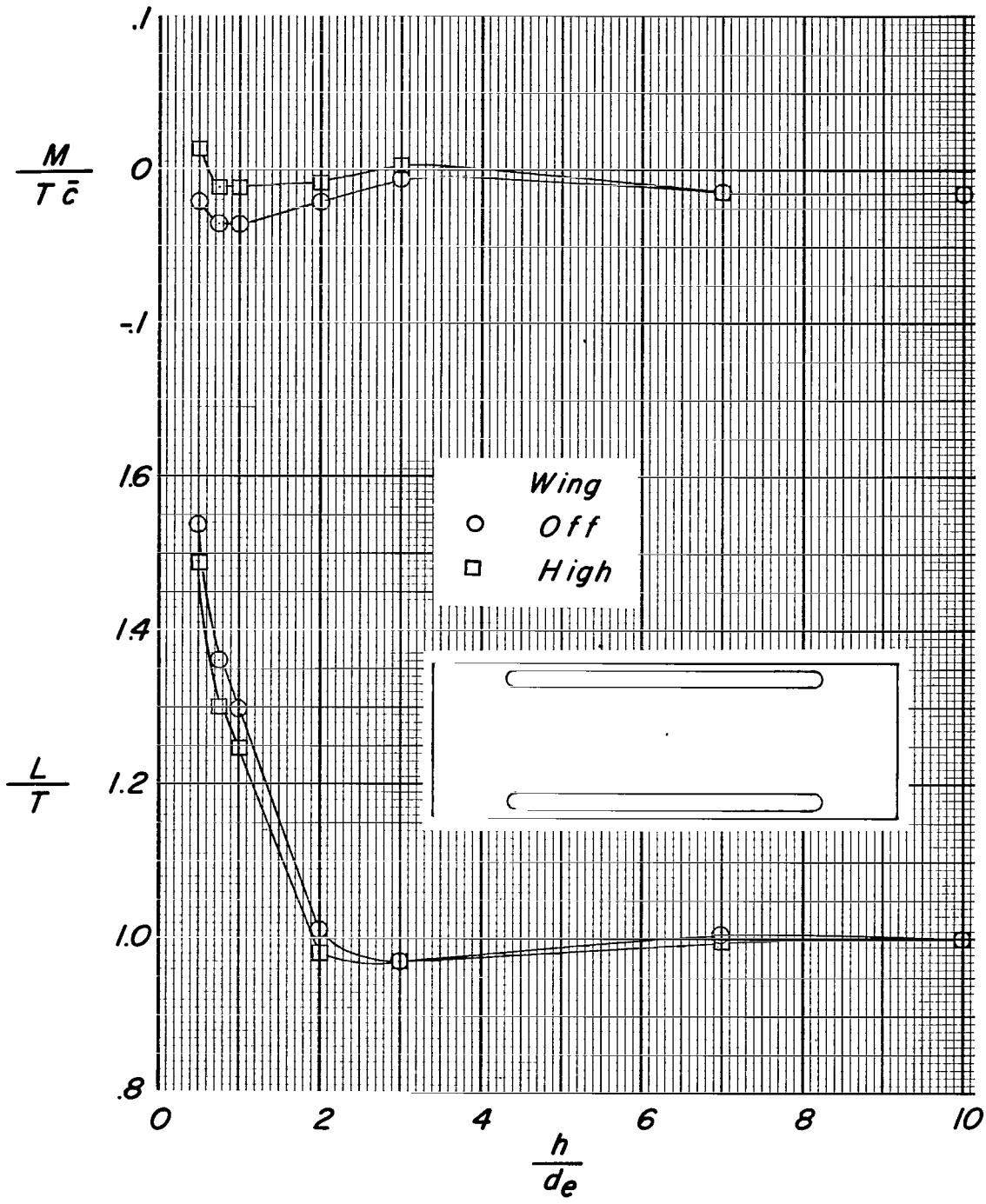

(h) Configuration 8.

Figure 28.- Continued.

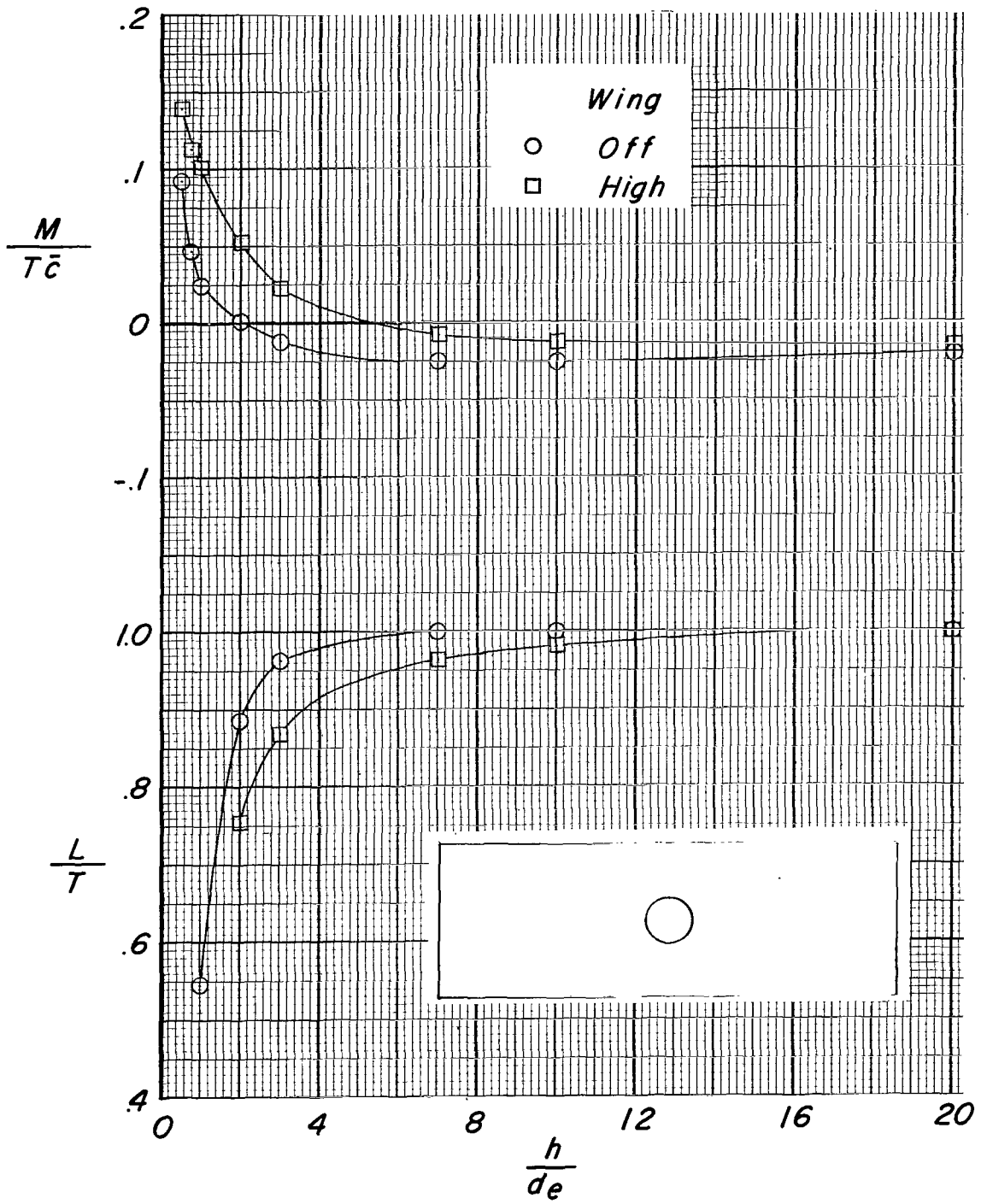

(i) Configuration 9.

Figure 28.- Continued.

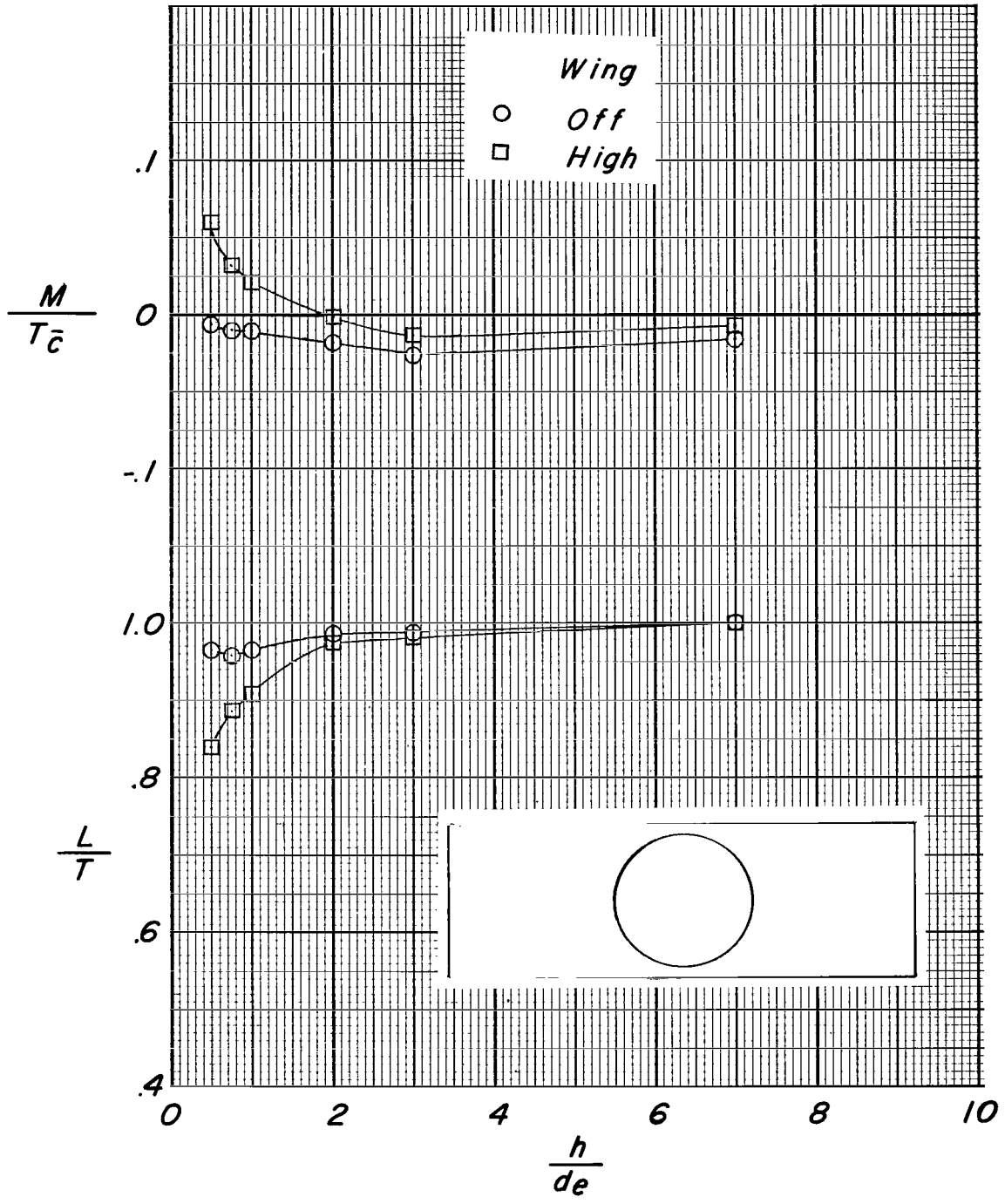

(j) Configuration 10.

Figure 28.- Concluded.

2 17 05

"The aeronautical and space activities of the United States shall be conducted so as to contribute . . . to the expansion of human knowledge of phenomena in the atmosphere and space. The Administration shall provide for the widest practicable and appropriate dissemination of information concerning its activities and the results thereof."

—NATIONAL AERONAUTICS AND SPACE ACT OF 1958

NASA SCIENTIFIC AND TECHNICAL PUBLICATIONS

TECHNICAL REPORTS: Scientific and technical information considered important, complete, and a lasting contribution to existing knowledge.

TECHNICAL NOTES: Information less broad in scope but nevertheless of importance as a contribution to existing knowledge.

TECHNICAL MEMORANDUMS: Information receiving limited distribution because of preliminary data, security classification, or other reasons.

CONTRACTOR REPORTS: Technical information generated in connection with a NASA contract or grant and released under NASA auspices.

TECHNICAL TRANSLATIONS: Information published in a foreign language considered to merit NASA distribution in English.

TECHNICAL REPRINTS: Information derived from NASA activities and initially published in the form of journal articles.

SPECIAL PUBLICATIONS: Information derived from or of value to NASA activities but not necessarily reporting the results of individual NASA-programmed scientific efforts. Publications include conference proceedings, monographs, data compilations, handbooks, sourcebooks, and special bibliographies.

Details on the availability of these publications may be obtained from:

SCIENTIFIC AND TECHNICAL INFORMATION DIVISION

NATIONAL AERONAUTICS AND SPACE ADMINISTRATION

Washington, D.C. 20546